Applications of Metal-Organic Frameworks in Catalysis and Separations

by

Bryant Ross James

A dissertation submitted in partial fulfillment
of the requirements for the degree of
Doctor of Philosophy
(Chemistry)
in The University of Michigan
2018

Doctoral Committee:

Professor Melanie S. Sanford, Chair
Professor Adam J. Matzger
Professor Levi T. Thompson
Professor John P. Wolfe

Bryant Ross James

bryjames@umich.edu

ORCID iD : 0000-0001-6229-4161

"*ipsa scientia potestas est*" ('knowledge itself is power')

— Sir Francis Bacon

Acknowledgements

I would first like to thank my advisor, Professor Melanie Sanford. She has believed and supported me since I first stepped into her lab as a REU student. We didn't always see eye to eye but she was always kind and understanding. She helped to push me forward and see the light at the end of the tunnel. I would also like to thank Professor Adam Matzger. Matzger was always available and willing to answer questions, whether it be about MOF structure or which vacuum to buy. I would also like to thank my remaining committee members, Professor Levi Thompson and John Wolfe, for valuable insight and varied perspectives on my research. I would like to thank the Sanford lab, especially Prof. Doug Genna, who mentored me when I was just starting grad school.

I have to acknowledge all of the teacher who have contributed to my success thus far from high school chemistry (Mr. Matia and Mr. Leuschner) through college (Prof. Anna, Prof. Hill, Prof. Turchi, and Prof. Rajaseelan) without their guidance and motivation I would never have been able to accomplish my dreams. Lastly, I would like to thank my family. While not the closest family they have always supported me in my educational journey and allowed me to become the chemist I am today.

Table of Contents

List of Tables

List of Figures

Abstract

Metal-organic frameworks (MOFs) are a class of porous coordination polymers that has been the subject of intense investigation since there discovery almost 30 years ago. The combination of organic linker and metal node in a 3-dimensional framework leads to materials that are tunable, have high surface area and in most cases are highly porous. The applications of these materials spans from gas storage to catalysis. Chapter 2 describes the utilization of MOFs to catalyze the carbonation of propylene oxide to propylene carbonate. The design and construction of a packed-bed flow reactor was undertaken to allow systematic investigation. This systematic investigation of co-catalyst, catalyst synthesis, catalyst activation, node metal and node geometry resulted in high yielding conditions with low CO_2 pressure (1-10 bar) and no added co-catalyst, conditions that previously, under batch conditions, lead to poor yields. These studies eventually resulted in the identification of a new catalyst, MIL-100(Sc), for this reaction. Chapter 3 investigates post-synthetic modification of MIL-101-SO_3X through cation exchange. MIL-101-SO_3X was treated with various potassium salts resulting in substitution at the sulfonate and establishing a relationship between conjugate acid pKa and MOF degradation. The exchange process demonstrated allow for rapid and complete conversion between protonated (–SO_3H) and alkali metal exchanged (–SO_3X) through brief (10 min) treatment with bicarbonate base followed by alkali chloride salt treatment for 1 h or by the utilization of high equivalents of alkali chloride salt relative to incorporated sulfonate. The exchange process was successful in generating previously unreported MIL-101-SO_3X loaded with K, Rb, and Cs. Chapter 4 expands upon post-synthetic modification by investigating the conversion of aminated MOFs (IRMOF-3, UMCM-1-

NH_2, MIL-53(Al)-NH_2, and UiO-66-NH_2) into sulfonated MOFs by reaction with 1,3-propanesultone. This process can be performed both neat and in solvent leading to 26 and 61% loading of sulfonate. This mild procedure was used on a wide variety of aminated MOFs containing different node metals (Zn, Zr, Al) and organic linkers (2-aminoterephtalic acid and benzene tribenzoic acid) to generate sulfonates that would otherwise be difficult to access. Loading of Ir, Pd and Rh cationic catalyst was attempted resulting in improved loading in sulfonated MOFs. Further evaluation of cationic loading into post-synthetically modified MOFs is necessary to elucidate the primary contributed factors for exchange in these materials.

Chapter 1

Introduction

1.1 Porous Materials

1.1.1 Activated Carbon

Porous materials have been used industrially for decades, with activated carbonaceous materials being among the most common. These materials are composed of charcoal that has been specifically synthesized to maximize surface area, pore accessibility, and pore volume. Applications for charcoal date back to as early as ancient Egypt where it was used for drying wounds.[1] Greeks and Romans also report utilizing charcoal for purifications.[1] Use of charcoal as an industrial sorbent was known as early as the eighteenth century when it was used as a decolorizing agent in sugar refining.[5] Due to its high surface area and porosity, activated carbon continues to find a wide range of applications including in liquid[6-8] and gas purification[9-11] and as catalyst supports.[12-14]

Activated carbon is largely amorphous. While models are available to approximate its structure, there is no single definition to describe the molecular architecture.[15] This lack of specific structural detail is partially derived from the diverse range of starting materials used to synthesize activated carbon. Materials ranging from bamboo[16] and coconut shells[17] to waste polyester[18] have all been used to synthesize activated carbonaceous materials. Therefore, specific interactions that lead to catalysis or separations are difficult to determine in this type of heterogeneous system.

1.1.2 Metal-Oxides: Zeolites, Silica, Alumina

Porous alternatives to activated carbon include metal oxides, specifically those formed from some combination of aluminium, silicon and oxygen. Porous silicates (e.g., silica gel) have been known for centuries. During World War I, silica gel found use as a sorbent in gas masks because of its function as a selective filter.[19] Differences in preparation from sodium silicate starting materials can result in different particle sizes with a variety of uses. Commonly used as a stationary phase for column chromatography, silica allows for the separation of diverse organic substrates with high resolution.[20] Being relatively inexpensive and widely available, silica has become one of the most common sorbents used in industrial and laboratory settings,[21, 22] and has also found commercial use as a desiccant contained in packaging of products ranging from food to clothing.

Alumina, a metal oxide with the formula Al_2O_3, is a naturally occurring and crystalline material. In the early 1900s, synthetic methods were developed to synthesize porous alumina.[23, 24] Primarily formed during the production of aluminium metal, alumina is predominantly used for purification. Alumina has also been applied as a catalyst support, and tandem catalysis between the installed catalyst and acidic sites on alumina can occur.[25, 26] Aluminium also forms naturally occurring microporous structures with phosphorous, though the structures and subsequent uses of these materials were not reported until the early 1980's.[27] A portion of the aluminium atoms in aluminophosphates can also be replaced with silicon, generating a charged framework that can be used for catalysis[28] and to increase sorption properties.[29]

Materials containing both aluminium and silicon are commonly referred to as aluminosilicates or zeolites. While these materials are naturally occurring, they didn't become a topic of intense research until the end of the 1700's.[30] These metal oxide materials experienced a

massive growth in popularity when Richard Barrer demonstrated the hydrothermal synthesis of both naturally occurring[31] and previously unreported zeolite architectures.[32] Zeolite structures, like many other porous materials, have found industrial applications as sorbants and as catalysts. However, they are superior to materials like activated carbon because of their highly predictable structures that enable size sieving of substrates.[33] For example, the alkylation of toluene can generate *ortho*, *meta*, and *para* isomers of xylene. By utilizing the ZSM-5-class of zeolites, the *para* isomer can be generated selectively inside the pore.[34] This selectivity is attributed to the reduced pore size sterically inhibiting the formation of the *meta* and *ortho* isomers. Zeolites, like activated carbon, have also been used as solid supports for heterogeneous catalysis.[35]

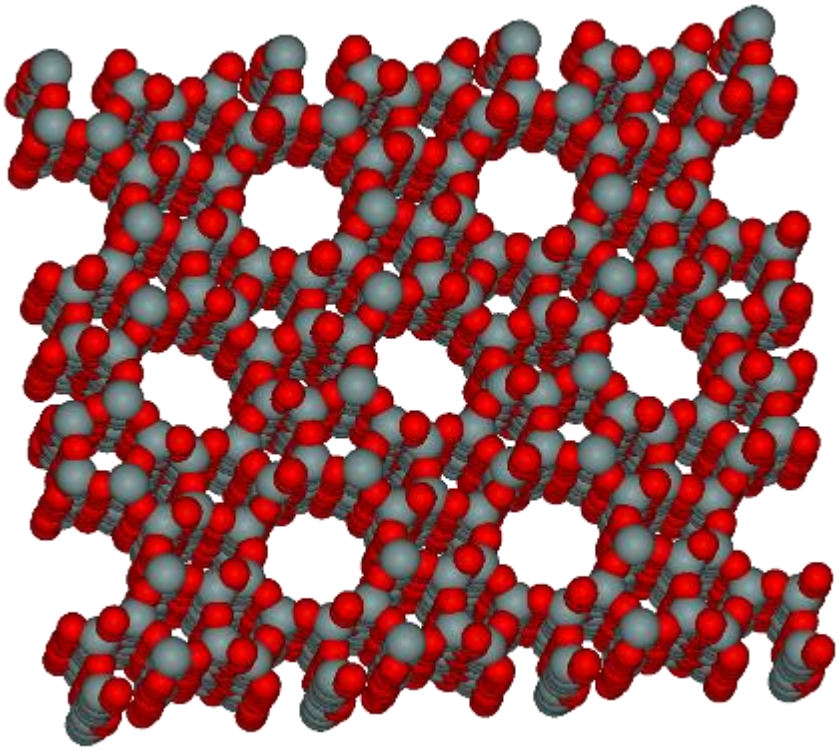

Figure 1.1 Example structure of a Zeolite (ZSM–5 = $Na_nAl_nSi_{96-n}O_{192}\cdot 16H_2O$ ($0<n<27$)) red = oxygen, grey = aluminum or silicon. Sodium and water have been excluded for clarity.

1.2 Metal-Organic Frameworks (MOFs)

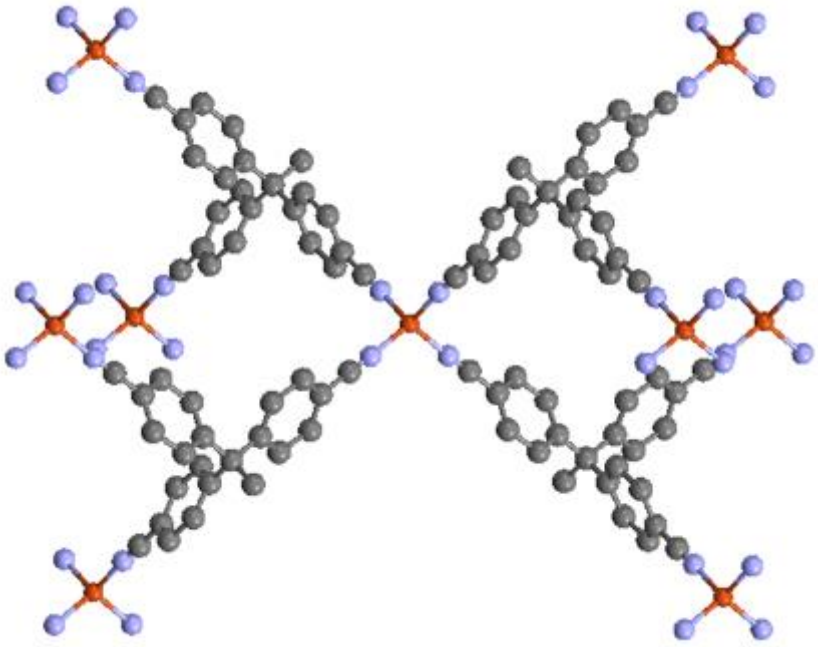

Figure 1.2 Early example of a MOF containing copper nodes linked by organic 4,4´,4´´,4´´´-tetracyanotetraphenylmethane moities[3] Orange = Copper, Grey = Carbon, Blue = Nitrogen

MOFs are "a class of CPs (coordination polymers) comprising organic linkers wherein metal−ligand interaction/bonding leads to a 2D or 3D crystalline network."[36] Early discoveries in this area were based on the hypothesis that rigid, tetrahedral, organic linkers could be used to coordinate metals and provide porous 3D networks. Hoskins showed that this approach could be used to synthesize porous materials by assembling 4,4´,4´´,4´´´-tetracyanotetraphenylmethane and Cu^{+} into a 3D framework using a solvent evaporation technique (**Figure 1.2**).[3] Major progress in the field was made when materials by Yaghi[37] (**Figure 1.3**) and Williams[38] exhibited high permanent surface area previously only seen in activated carbon and aluminosilicates. The structures of these materials are diverse, allowing for isolation of traits ideal for specific applications.

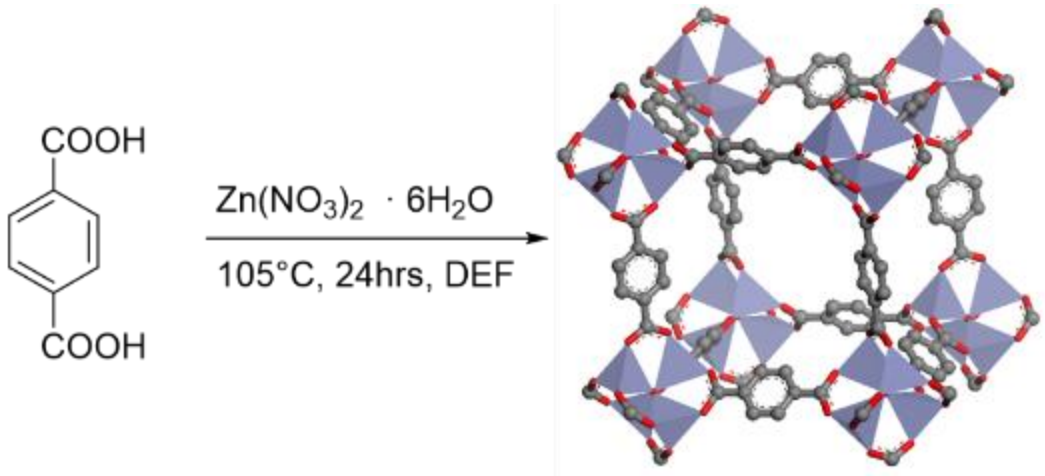

Figure 1.3 Hydrothermal synthesis of MOF-5. Red = oxygen, Grey = carbon, Blue = Zinc

Tunability is a primary advantage of MOFs compared to other porous materials. Alteration of activated carbon and zeolites is typically limited to surface modifications, including ion exchange and nanoparticle addition, due to their intrinsic structures and syntheses. In contrast, MOFs can be independently modified at the node metal, the node geometry, and the linker, allowing for a variety of frameworks to be developed for any specific application with only minor changes. For example, ditopic, tritopic, and tetratopic linkers can all been used in MOF synthesis.[37-40] Functional groups have also been incorporated directly into MOF linkers resulting in uniform distribution of amines, halogens or alcohols throughout the MOF.[41]

In 2002, Yaghi developed a series of MOFs all containing identical zinc nodes with various ditopic linkers. Commonly referred to as the IRMOF series,[41] this set of MOFs incorporates varying linker lengths and several functional groups. Several years later a similar approach was taken to generate the UiO series of MOFs. In this case the node was zirconium and the framework had both octahedral and trigonal pores.[42] The use of zirconium led to MOFs more resistant to thermal and hydrolytic decomposition. Other series of MOFs (e.g., HKUST-1) form identical framework geometry with a variety of node metals. Cr, Fe, Ni, Zn, Ni, Cu and Mo have all been shown to form isoreticular structures when combined with trimesic acids linkers.[43]

1.3 Post-synthetic modification of MOFs

MOFs are unique in their combination of both organic and inorganic components. This combination of moieties allows a degree of tunability and functionalization that would be difficult or impossible in entirely organic or inorganic porous materials. Leveraging the vast array of organic reactions, the organic moiety of MOFs can be functionalized with seemingly endless variety. Since a majority of MOFs are self-assembled hydrothermally, the modification to the organic linker must be tolerant of the synthesis conditions. In most cases, this requires re-optimization of synthesis conditions at the least and often times leads to low yield, mixed phases, and reduced crystallinity. Post-synthetic modification (PSM), as an alternative, encompasses any chemical changes to the material after the initial synthesis. PSM's major advantage is that the material need only be stable to modification conditions after self-assembly has occurred. The field of PSM is vast including modifications to metal node, ligand substitution, physisorption to MOF framework and reaction of organic linker. In this thesis, we will focus on describing PSM that involves chemical change at organic linkers, specifically the addition of sulfonic acids/sulfonate groups to MOFs and their ion exchange properties.

Sulfonic acid moieties have been used in several applications including catalysis, separations and ion-exchange. Combining sulfonic acids with highly porous materials can yield materials with improved properties. Sulfonic acids/sulfonates are an uncommon moiety in MOFs due to a tendency to interfere with self-assembly and harsh conditions for sulfonation post synthesis. A few MOFs, including MIL-101, referred to as MIL-101-SO_3X henceforth, have been synthesized containing free sulfonates. MIL-101-SO_3H has been shown by Zhou et al. to be a robust Bronsted acid catalyst for the alcoholysis of epoxides.[44] The active catalyst was generated

by treating the as-synthesized MIL-101-SO_3X, X = 40% Na and 60% H, with dilute HCl to yield a MIL-101-SO_3H containing no detectable Na. Several examples of ion exchange to yield catalyst bound MIL-101-SO_3X have also been reported in literature. Genna et al. reported loading of cationic catalyst (dppe)Rh(COD)BF_4 and $(MeCN)_2$Rh(COD)BF_4 (dppe = 1,2-bis(diphenylphosphino)ethane, COD = 1,5-cyclooctadiene, BF_4 = tetrafluoroborate) into MIL-101-SO_3X to generate catalysts that are directly impacted by the MOF framework leading to recyclability and size selectivity in the hydrogenation of alkenes.[45] Grigoropoulos et al. offer a follow up to this work by loading Crabtree's catalyst [Ir(COD)(PCy_3)(py)]PF_6 (PCy_3 = tricyclohexylphosphine, py = pyridine, PF_6 = hexafluorophosphate) into MIL-101-SO_3X and observing significantly higher conversion and improved selectivity in the hydrogenation of olefinic alcohols when compared to the homogeneous catalyst.[46] Chemistries by Sun et al. incorporate Ag at MIL-101-SO_3X for solvent free A^3 coupling reactions leading to a highly active and recyclable catalyst.[47] The scope of these works shows the exceptional value of cationically loaded catalysts in MOFs but leaves unanswered questions about the nature of the loading. All three examples report a single procedure leading to partial incorporation of catalyst and change catalyst equivalents by adding more or less of the catalyst loaded MOF to the reaction. The ability to fully exchange cations is essential for understanding the role sulfonate may play in these reactions as well as increasing applicability of cation exchanged materials in areas outside of catalysis.

1.4 MOF applications in Catalysis

The application of MOFs in catalysis is a fast-growing field. MOFs are highly tunable, which allows for specific design of catalysts for many transformations.[48, 49] MOFs can be utilized as traditional solid-state supports for a variety of catalysts,[50] but many MOFs act as a catalyst as well as a heterogeneous support.[51] Metrics for the classification of MOF catalysts are as widely

varied as MOFs themselves. Classification by active site location is common and will be used most in this thesis. Possible active catalytic sites in MOFs can be either at the metal node, in the pore, or at the linker **(Figure 1.4)**.

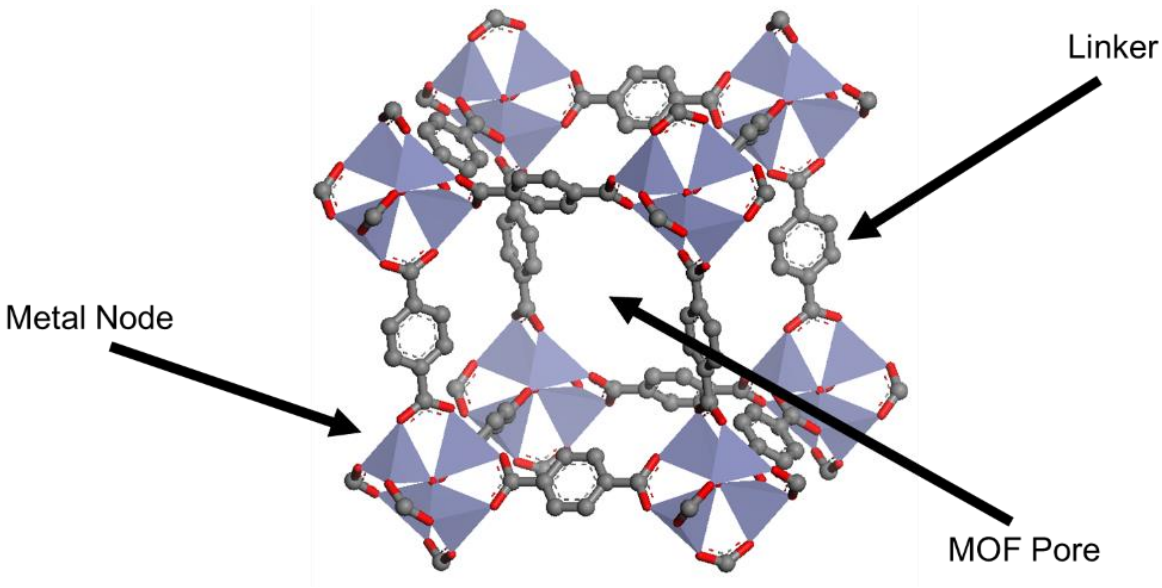

Figure 1.4 Possible sites of catalytic activity in MOFs (MOF-5 structure used for simplicity but does not display all these reactive sites without modification)

Catalysis at the metal node focuses on metal binding to activate organic substrates. Olefin hydrogenation and carbonation of epoxides are examples of reactions utilizing this approach **(Figure 1.5)**.[2, 4, 52-54] Examples of pore catalysis are widely varied from metal nanoparticles being deposited into the framework to "ship-in-a-bottle" type construction of porphyrins.[55] The uniform porosity of MOFs is an attractive feature for catalysis, and caution must be taken when modifiying MOF structures for catalysis purposes to maintain the porosity.[45, 56] The structure of MOFs allows for a third type of catalysis which most other porous materials cannot offer. Linkers can be modified to covalently insert catalyst ligands such as porphyrins, pyridines and phosphines[57-61]

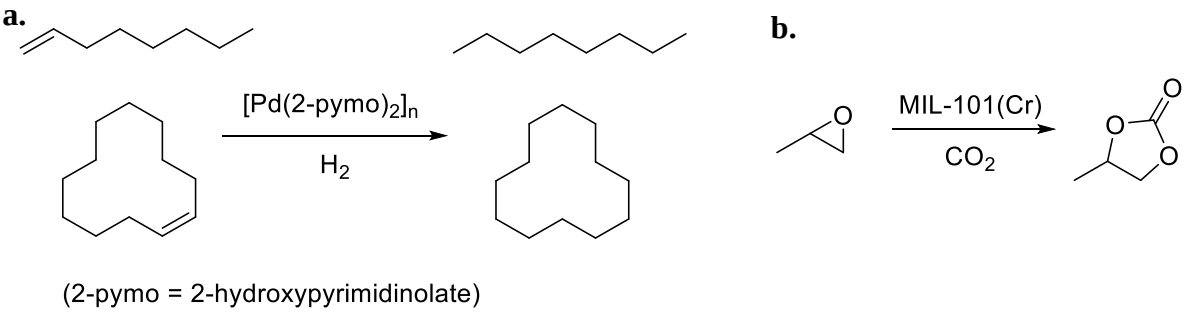

Figure 1.5 a. Olefin hydrogenation[2] **b.** Epoxide carbonation[4] in MOFs

into the network. All of these sites are then available to guests via entry into and out of the pores of the robust MOF frameworks.

We have focused on the last few years on the catalytic process to form cyclic carbonates, an important commodity chemical in Li-ion batteries, polymers, solvents.[62] The first commercial synthesis of these molecules was done with phosgene, which is toxic and has low atom economy. Later synthesis by Fukuoka et al. became greener with the combination of carbon dioxide and epoxides boasting 100% atom economy.[63] Many catalysts have been used for this transformation in literature, including zeolites and MOFs.[62] MOFs are of great interest in this area of research because of the large variety and tunability of materials. Designing dual functionalized MOFs has advanced the field by combining several catalytic sites that can work in tandem to give improved reactivity over either catalyst separately. However, these processes still suffer from the need for high temperatures, long reaction times, high reactor pressure, and catalyst separation post synthesis. Many of these challenges can be addressed by utilization of packed bed flow reactors, with research focused on optimizing the MOFs chosen for this transformation.

1.5 Organization of Thesis

The focus of this thesis is on novel applications for MOFs either through engineered solutions or post-synthetic modification (PSM). Chapter 2 focuses on utilizing a chromium-based MOF, namely MIL-101(Cr), as a catalyst for CO_2 capture and conversion into cyclic carbonates.

This reaction, while thoroughly investigated with MOFs in batch reactors, is relatively unexplored in the continuous flow literature. Structure activity relationships are established for a green method of propylene carbonate generation by utilization of a continuous flow reactor. Ultimately, a new catalyst is identified for the carbonation of propylene oxide. Chapter 3 will discuss the PSM of MIL-101(Cr)-SO_3X to generate MOFs with complete incorporation of a range of alkali metal cations. Preliminary results highlight the possible applications of these materials and how cation loading can be tuned to increase utility in a variety of applications. Concluding this work, we evaluate the PSM of a variety of MOFs in Chapter 4. Incorporation of sulfonate groups into MOFs is nontrivial in many cases. Our research expands the number of MOFs that can be functionalized to contain this moiety as well as proposes future applications for materials generated in this manner.

1.6 References

1. E. Robens, *Chemie Ingenieur Technik* **2010**, *82*, 763–768.
2. F. X. Llabrés i Xamena, A. Abad, A. Corma and H. Garcia, *Journal of Catalysis* **2007**, *250*, 294-298.
3. B. F. Hoskins and R. Robson, *Journal of the American Chemical Society* **1990**, *112*, 1546–1554.
4. B. R. James, J. A. Boissonnault, A. G. Wong-Foy, A. J. Matzger and M. S. Sanford, *RSC Advances* **2018**, *8*, 2132–2137.
5. F. Çeçen, Ö. Aktaş, I. ebrary and L. Wiley Online, *Activated carbon for water and wastewater treatment integration of adsorption and biological treatment*, Wiley-VCH, Weinheim, Germany **2012**.
6. P. Udomkun, B. Innawong, C. Siasakul and C. Okafor, *Food Chemistry* **2018**, *248*, 225–229.
7. J. T. Paprowicz, *Environmental Technology* **1990**, *11*, 71–82.
8. S. Wong, N. Ngadi, I. M. Inuwa and O. Hassan, *Journal of Cleaner Production* **2018**, *175*, 361–375.
9. C. T. Chiou and P. J. Reucroft, *Carbon* **1977**, *15*, 49–53.
10. H. Zhao, X. Luo, H. Zhang, N. Sun, W. Wei and Y. Sun, *Greenhouse Gases: Science and Technology* **2018**, *8*, 11–36.
11. H. Bamdad, K. Hawboldt and S. MacQuarrie, *Renewable and Sustainable Energy Reviews* **2018**, *81*, 1705–1720.

12. A. Zubiaur and N. Job, *Applied Catalysis B: Environmental* **2018**, *225*, 364–378.
13. K. C. O'Connell, J. R. Monnier and J. R. Regalbuto, *Applied Catalysis B: Environmental* **2018**, *225*, 264–272.
14. P. Li, X. Yin, Y. Yan, K. Zhan, J. Yang, B. Zhao and J. Li, *Journal of Materials Science* **2018**, *53*, 6124–6134.
15. H. Marsh, F. R. Reinoso and F. Rodriguez-Reinoso, *Activated Carbon*, Elsevier Science, Oxford **2006**.
16. W. Zhao, L. Luo, H. Wang and M. Fan, *2017* **2017**, *12*, 1246–1262.
17. J. Laine, A. Calafat and M. labady, *Carbon* **1989**, *27*, 191–195.
18. X. Yu, S. Wang and J. Zhang, *Journal of Materials Science* **2018**, *53*, 5458–5466.
19. M. Feldman and P. Desrochers, *Industry and Innovation* **2003**, *10*, 5–24.
20. A. J. P. Martin and R. L. M. Synge, *A theory of chromatography. 2. Application to the micro-determination of the higher monoamino-acids in proteins* **1941**, *35*, 1358–1368.
21. T. L. Chester, *Analytical Chemistry* **2013**, *85*, 579–589.
22. V. Pérez-Fernández, L. Mainero Rocca, P. Tomai, S. Fanali and A. Gentili, *Analytica Chimica Acta* **2017**, *983*, 9–41.
23. H. S. Taylor and A. J. Gould, *Journal of the American Chemical Society* **1934**, *56*, 1685–1687.
24. J. E. Myers, *Journal of the Society of Chemical Industry* **1925**, *44*, 1232–1232.
25. L. Falbo, M. Martinelli, C. G. Visconti, L. Lietti, C. Bassano and P. Deiana, *Applied Catalysis B: Environmental* **2018**, *225*, 354–363.
26. M. A. Semsarzadeh and A. Sabzevari, *Journal of Applied Polymer Science* **2018**, *135*, 46057.
27. S. T. Wilson, B. M. Lok, C. A. Messina, T. R. Cannan and E. M. Flanigen, *Journal of the American Chemical Society* **1982**, *104*, 1146–1147.
28. M. Hartmann and S. P. Elangovan, in *Advances in Nanoporous Materials*, ed. S. Ernst, Elsevier **2010**, vol. *1*, pp. 237–312.
29. M. E. Davis, C. Saldarriaga, C. Montes, J. Garces and C. Crowdert, *Nature* **1988**, *331*, 698.
30. A. F. Masters and T. Maschmeyer, *Microporous and Mesoporous Materials* **2011**, *142*, 423–438.
31. R. M. Barrer, *Journal of the Chemical Society (Resumed)* **1948**, 2158–2163.
32. R. M. Barrer, *Journal of the Chemical Society (Resumed)* **1948**, 127–132.
33. S. M. Csicsery, *Zeolites* **1984**, *4*, 202–213.
34. W. W. Kaeding, C. Chu, L. B. Young, B. Weinstein and S. A. Butter, *Journal of Catalysis* **1981**, *67*, 159–174.
35. Q.-N. Zhao, Q.-W. Song, P. Liu, Q.-X. Zhang, J.-H. Gao and K. Zhang, *Chinese Journal of Chemistry* **2018**, *36*, 187–193.
36. S. Seth and A. J. Matzger, *Crystal Growth & Design* **2017**, *17*, 4043–4048.
37. H. Li, M. Eddaoudi, M. O'Keeffe and O. M. Yaghi, *Nature* **1999**, *402*, 276–279.
38. S. S.-Y. Chui, S. M.-F. Lo, J. P. H. Charmant, A. G. Orpen and I. D. Williams, *Science* **1999**, *283*, 1148–1150.
39. O. K. Farha, K. L. Mulfort and J. T. Hupp, *Inorganic chemistry* **2008**, *47*, 10223–10225.
40. O. K. Farha and J. T. Hupp, *Accounts of Chemical Research* **2010**, *43*, 1166–1175.
41. M. Eddaoudi, J. Kim, N. Rosi, D. Vodak, J. Wachter, M. O'Keeffe and O. M. Yaghi, *Science* **2002**, *295*, 469–472.

42. J. H. Cavka, S. Jakobsen, U. Olsbye, N. Guillou, C. Lamberti, S. Bordiga and K. P. Lillerud, *Journal of the American Chemical Society* **2008**, *130*, 13850–13851.
43. C. R. Wade and M. Dinca, *Dalton transactions* **2012**, *41*, 7931–7938.
44. Y. X. Zhou, Y. Z. Chen, Y. Hu, G. Huang, S. H. Yu and H. L. Jiang, *Chemistry – A European Journal* **2014**, *20*, 14976-14980.
45. D. T. Genna, L. Y. Pfund, D. C. Samblanet, A. G. Wong-Foy, A. J. Matzger and M. S. Sanford, *ACS Catalysis* **2016**, *6*, 3569–3574.
46. A. Grigoropoulos, A. I. McKay, A. P. Katsoulidis, R. P. Davies, A. Haynes, L. Brammer, J. Xiao, A. S. Weller and M. J. Rosseinsky, *Angewandte Chemie* **2018**, *57*, 4532-4537.
47. W.-J. Sun, F.-G. Xi, W.-L. Pan and E.-Q. Gao, *Molecular Catalysis* **2017**, *430*, 36-42.
48. A. Zanon and F. Verpoort, *Coordination Chemistry Reviews* **2017**, *353*, 201–222.
49. J. Liang, Z. Liang, R. Zou and Y. Zhao, *Advanced Materials* **2017**, *29*, 1701139.
50. P. Falcaro, R. Ricco, A. Yazdi, I. Imaz, S. Furukawa, D. Maspoch, R. Ameloot, J. D. Evans and C. J. Doonan, *Coordination Chemistry Reviews* **2016**, *307, Part 2*, 237-254.
51. J. Lee, O. K. Farha, J. Roberts, K. A. Scheidt, S. T. Nguyen and J. T. Hupp, *Chemical Society reviews* **2009**, *38*, 1450-1459.
52. E. E. Macias, P. Ratnasamy and M. A. Carreon, *Catalysis Today* **2012**, *198*, 215–218.
53. C. M. Miralda, E. E. Macias, M. Zhu, P. Ratnasamy and M. A. Carreon, *ACS Catalysis* **2012**, *2*, 180–183.
54. M. Zhu, D. Srinivas, S. Bhogeswararao, P. Ratnasamy and M. A. Carreon, *Catalysis Communications* **2013**, *32*, 36–40.
55. T. Bogaerts, A. Van Yperen-De Deyne, Y. Y. Liu, F. Lynen, V. Van Speybroeck and P. Van Der Voort, *Chemical communications* **2013**, *49*, 8021–8023.
56. D. T. Genna, A. G. Wong-Foy, A. J. Matzger and M. S. Sanford, *Journal of the American Chemical Society* **2013**, *135*, 10586–10589.
57. S. A. Burgess, A. Kassie, S. A. Baranowski, K. J. Fritzsching, K. Schmidt-Rohr, C. M. Brown and C. R. Wade, *Journal of the American Chemical Society* **2016**, *138*, 1780–1783.
58. R. Van Zeeland, X. Li, W. Huang and L. M. Stanley, *RSC Adv.* **2016**, *6*, 56330–56334.
59. T. Van Vu, H. Kosslick, A. Schulz, J. Harloff, E. Paetzold, J. Radnik, U. Kragl, G. Fulda, C. Janiak and N. D. Tuyen, *Microporous and Mesoporous Materials* **2013**, *177*, 135–142.
60. M. Hartmann and M. Fischer, *Microporous and Mesoporous Materials* **2012**, *164*, 38-43.
61. K. Wang, D. Feng, T. F. Liu, J. Su, S. Yuan, Y. P. Chen, M. Bosch, X. Zou and H. C. Zhou, *Journal of the American Chemical Society* **2014**, *136*, 13983-13986.
62. M. Zhu and M. A. Carreon, *J Appl Polym Sci* **2014**, *131*, 1–13.
63. S. Fukuoka, M. Kawamura, K. Komiya, M. Tojo, H. Hachiya, K. Hasegawa, M. Aminaka, H. Okamoto, I. Fukawa and S. Konno, *Green Chemistry* **2003**, *5*, 497-507.

Chapter 2

Structure Activity Relationships in Metal-Organic Framework Catalysts for the Synthesis of Propylene Carbonate from CO_2 and Propylene Oxide

Published: James, B. R.; Boissonnault, J. A.; Wong-Foy, A. G.; Matzger, A. J.; Sanford, M. S., *RSC Advances* **2018**, 8, (4), 2132-2137

2.1 Introduction

Metal-organic frameworks (MOFs) have been widely studied as catalysts for a variety of transformations.[1] MOF-based catalysts combine well-defined, site-isolated metal active sites in structurally distinct and recyclable scaffolds. The secondary and tertiary structure of MOFs can be systematically varied via modification of the organic linker and metal nodes of these structures.[2, 3] Unlike most traditional heterogeneous catalysts, the active sites in MOFs can be tuned to generate catalysts that are optimized for a specific reaction.[4] The work described herein leverages the tunability of MOFs for the systematic study of catalysts for the reaction of carbon dioxide with propylene oxide (PO) to generate propylene carbonate (PC).

Cyclic carbonates are commodity chemicals that are widely used as solvents for Li-ion batteries as well as monomers for polycarbonate synthesis.[5] They have historically been prepared by the reaction of phosgene with the corresponding diol (**Figure 2.1a**).[6,7] An attractive alternative synthesis involves the reaction of epoxides with CO_2 to yield cyclic carbonate products (**Figure 2.1b**).[8] This transformation offers the advantages of high atom economy and the use of inexpensive and relatively non-toxic reagents.[9] As such, a wide variety of both homogeneous and

heterogeneous catalysts have been developed for epoxide carbonation, including single site metal complexes,[10-12] metalloporphyrins,[13] zeolites,[14,15] ionic liquids,[16,17] and MOFs.[18-23] Despite a number of reports of MOF-based catalysts for PO carbonation, there are few examples of systematic studies of the impact of MOF structure on catalytic performance for this transformation.[24]

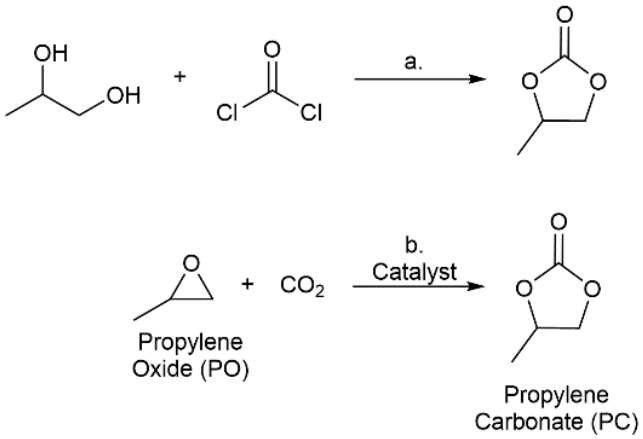

Figure 2.1. a. Phosgene/diol route to propylene carbonate; **b.** CO_2/epoxide route to propylene carbonate

The majority of previous studies on MOF-catalyzed PO carbonation have been performed in batch reactors.[23,25] We reasoned that a flow configuration would be better suited to systematic investigations, as it would enable continuous analysis of the reaction profile. This Chapter demonstrates the evaluation of different MOF catalysts for PO carbonation, using the known catalyst MIL-101(Cr) as a starting point. Systematic variation of the synthesis technique, activation conditions, metal node, and organic linker were conducted in order to determine the key features necessary for catalysis and to optimize catalyst performance. These studies ultimately led to the identification of co-catalyst-free conditions for MOF-catalyzed PO carbonation and identified MIL-100(Sc) as an improved catalyst for PO carbonation.

2.2 Results and Discussion

2.2.1 Development of Flow Reaction Conditions

MIL-101(Cr) was selected for initial study based on literature precedent that it catalyzes PO carbonation in batch reactors with tetrabutylammonium bromide (TBABr) as a co-catalyst.[26, 27] This MOF also offers the advantages that it is thermally robust, highly porous, and tunable at both the metal node and organic linker. We sought to translate this transformation to a flow reactor system in order to increase throughput as well as to facilitate continuous monitoring of catalyst performance.

Initial flow reaction conditions were selected to closely mimic published batch conditions.[25] The flow reactions were conducted at 100 °C and 5 bar of system pressure with a CO_2 flow rate of 4.0 sccm/min. The MOF catalyst was a fixed bed of 42 mg of MIL-101(Cr) dispersed in 42 mg of diatomaceous earth. A stock solution of 165 mM propylene oxide and 8.4

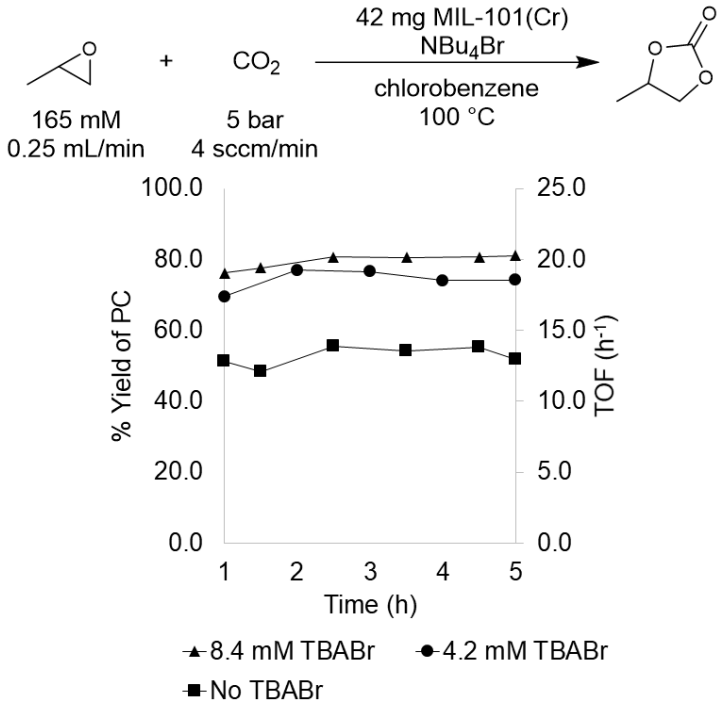

Figure 2.2. Effect of TBABr co-catalyst on PO carbonation catalyzed by MIL-101(Cr)

mM tetrabutylammonium bromide (TBABr) co-catalyst in chlorobenzene was used to deliver both substrate and co-catalyst at a rate of 0.25 mL/min. At steady state operation (established after approximately 1 h), these conditions afforded propylene carbonate with a TOF of 20 h^{-1} (**Figure 2.2**). This corresponds to 0.033 mmol/min of propylene oxide produced in a single pass, equivalent to an 80 ± 6% yield.

With flow conditions in hand, we first sought to eliminate the need for the TBABr co-catalyst in this system. This homogeneous co-catalyst is particularly disadvantageous in a flow configuration, because it must be added continuously along with the organic substrates. In addition, this additive could potentially obscure the inherent reactivity of the MOF catalysts.[25] As shown in **Figure 2.3**, the co-catalyst is believed to serve as a nucleophile to open the epoxide ring once it is activated by coordination to an electrophilic metal center, such as a metal in the node of the MOF.[28-30]

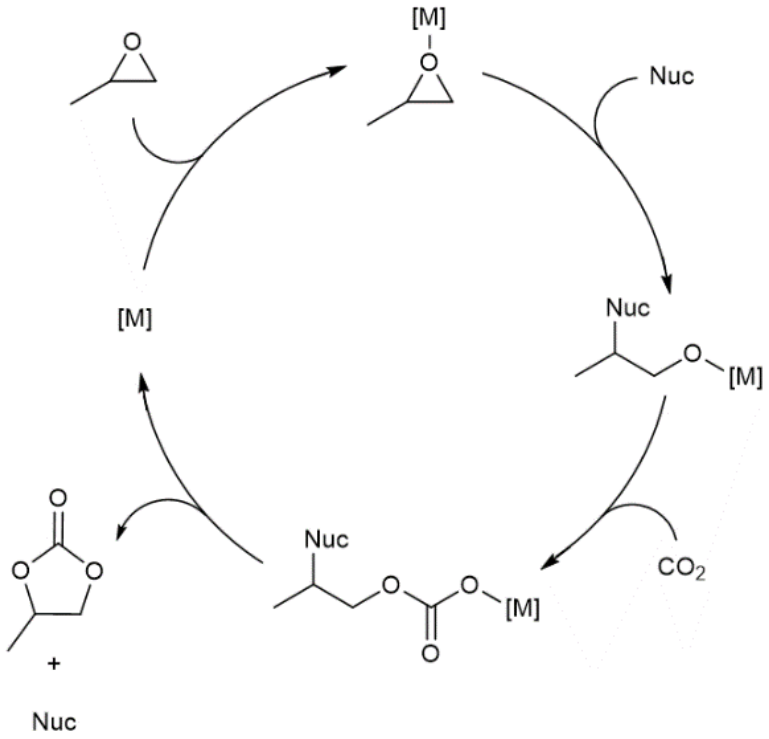

Figure 2.3 Proposed mechanism for conversion of PO to PC

Importantly, previous work has shown that in batch processes the yield of PC without co-catalyst is low.[31] However, we hypothesized that the high ratio of MOF catalyst to epoxide in a packed bed flow reactor relative to that in a batch reactor might result in increased reactivity, and that nucleophilic functional groups present at the MOF nodes (*e.g.* hydroxides, chlorides, fluorides, or carboxylates derived from the MOF synthesis) and/or in solution (*e.g.* residual water in the reaction solvent) could potentially serve as nucleophiles under these conditions. Indeed, when the reaction was conducted under our standard flow conditions without added TBABr, a 54 ± 2% yield was obtained (**Figure 2.2**) after a single pass over the catalyst bed. These co-catalyst free conditions were adopted moving forward for all subsequent studies.

2.2.2 Impact of Catalyst Synthesis Method and Catalyst Activation

We next evaluated the impact of the MOF synthetic method and activation procedure on the performance of MIL-101(Cr).[26,27,32] MIL-101(Cr) has several reported preparations in the literature that vary primarily based on the acid utilized. Hydrochloric, hydrofluoric, and acetic acid as well as an acid-free preparation have all been reported.[31,33-35] The role of the acid during synthesis is not completely understood, but it is known that halides/carboxylates derived from the acid as well as hydroxides derived from water are incorporated into the framework during synthesis.[34] As mentioned above, these halides, carboxylates, or hydroxides could potentially act as nucleophiles during catalysis, thereby providing an endogenous co-catalyst. To test the impact of synthesis conditions on catalytic performance, MIL-101(Cr) was prepared using hydrochloric acid, hydrofluoric acid, and acetic acid as well as under acid-free conditions. In all cases, the other synthesis parameters (reaction time, temperature, metal salt, solvent quantity) and catalyst activation procedure were the same. As summarized in **Figure 2.4a**, these four MIL-101(Cr) samples exhibited similar catalytic activity, with one-pass yields ranging from 33-41 ± 8%. These

results indicate that the synthesis method has relatively minimal impact on catalyst performance in this system and that catalysts containing different endogenous nucleophiles remain competent for PO carbonation.

We next probed the impact of MOF activation procedure on catalyst performance. MOFs are typically activated prior to catalysis by heating under vacuum in order to remove water and solvent that is in the MOF pores and bound to the metal nodes. We sought to assess whether this high temperature activation was beneficial or even necessary for PO carbonation catalysis. Initial experiments used MIL-101(Cr) that was activated according to the literature procedure (reduced pressure, overnight, 100 °C).[36] This process was reported to yield MIL-101(Cr) with 2.47 mmol/g of active sites,[35] which is close to our experimental value of 2.36 mmol/g. The advantage of low temperature activation is that it minimizes the possibility of thermally-induced MOF decomposition, which is problematic for some Sc MOFs that we sought to compare to MIL-101(Cr) (*vide infra*). Room temperature activation yielded MIL-101(Cr) with 1.15 mmol/g active

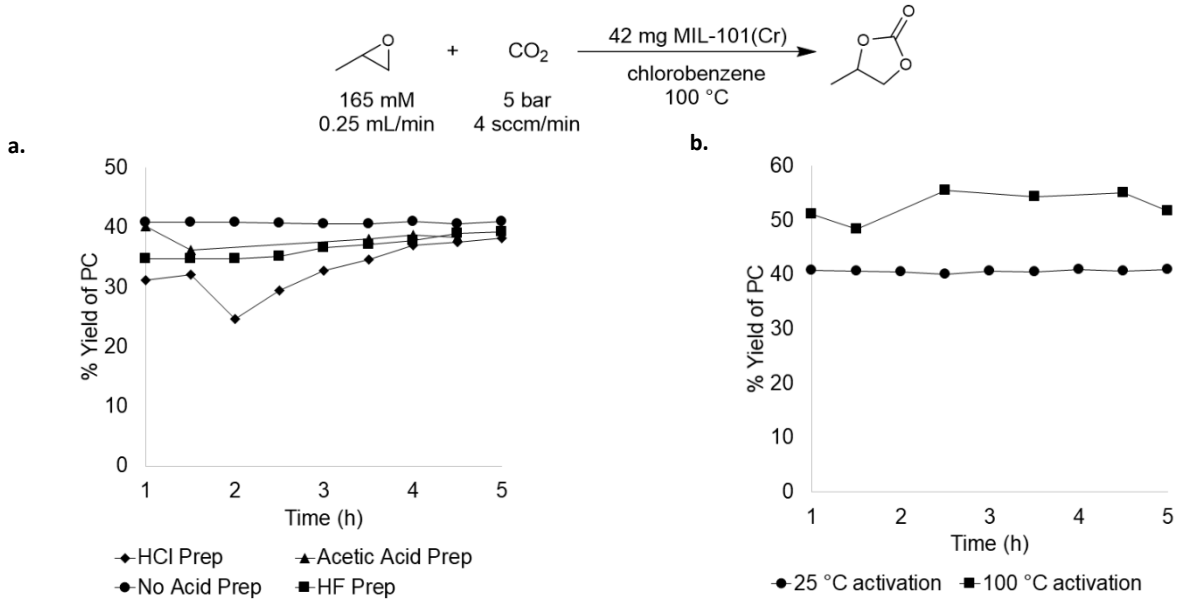

Figure 2.4a. Comparison of acids used for MOF synthesis; **b.** Comparison of 25 °C activation versus 100 °C activation of MIL-101(Cr)

sites as determined by temperature programmed desorption. This suggests that this activation procedure does not remove all of the water and solvent molecules from the pores and metal nodes. Nonetheless, the room temperature-activated material maintained similar activity, affording 37 ± 4% steady state yield and a TOF of 19 h^{-1} (**Figure 2.4b**). As such, the room temperature activation procedure was used for all of the studies below to enable direct comparison of the Cr-based MOFs with Sc-based materials that decompose at higher activation temperatures.

2.2.3 Comparison of Isostructural MOFs with Different Node Metals

A key feature of metal organic framework catalysts is that they are highly modular. As such, the metal(s) in the nodes, the overall structure of the nodes, and the organic linker(s) can be systematically varied to tune catalytic performance. We sought to exploit this tunability to develop second-generation catalysts for PO carbonation. As shown in **Figure 2.3**, epoxide carbonation involves Lewis acid activation of the epoxide,[35] and the literature suggests that the Cr centers at the nodes of MIL-101(Cr) are the active sites in this system.[35] Thus, we hypothesized that increasing the oxophilicity of these sites could enhance catalytic performance.

Initial investigations focused on a MIL-101 series of isostructural MOFs synthesized with different metals at the nodes. In addition to MIL-101(Cr), analogous Fe- and Sc-based MOFs have been reported in the literature and have been shown to participate in Lewis acid-catalyzed reactions.[37] Furthermore, a recent report by Kepp provided a quantitative scale of oxophilicity for these systems, with Sc = 0.8, Cr = 0.6, and Fe = 0.4 (higher numbers represent more oxophilic atoms).[38] The MIL-101(Cr), (Fe), and (Sc) series was synthesized according to literature procedures[31, 36, 39] and activated by several washes with ethanol followed by drying overnight under reduced pressure at 25 ºC. Under our standard catalysis conditions, MIL-101(Cr) afforded a yield

of 41 ± 1% at steady state operation and TOF of 21 h^{-1} for the material prepared under acid free conditions. In comparison, MIL-101(Fe) exhibited low activity, affording 1-2% yield under analogous conditions. This result is similar to the control reaction with no catalyst present and is consistent with the lower oxophilicity of Fe.[33] In contrast, the more oxophilic Sc-based catalyst, MIL-101(Sc), afforded higher activity than MIL-101(Cr) at initial time points. For instance, after 1 h the Sc and Cr MOFs afforded 53% and 41% yield of PC with TOFs of 87 h^{-1} and 21 h^{-1}, respectively. However, in the case of MIL-101(Sc), subsequent time points revealed rapidly declining yields, culminating in <10% at 3 h. This result suggests that the MIL-101(Sc) catalyst is unstable under the reaction conditions. Indeed, PXRD analysis of the spent catalyst confirmed that

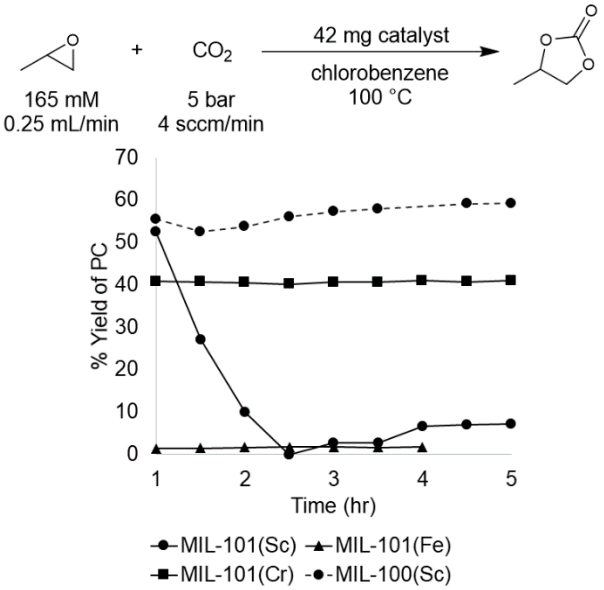

Figure 2.5. MOF node metal comparison for the conversion of PO to PC

MIL-101(Sc) loses crystallinity after 3 h under the reaction conditions. In contrast, minimal loss of crystallinity is observed for MIL-101(Cr) under analogous conditions. Overall, the high yield observed with MIL-101(Sc) at the start of the reaction provides promising initial evidence that Sc-based MOFs could offer improvements over the initial Cr-based catalyst.

A recent report showed that MIL-101(Sc) has low thermal stability, rapidly losing crystallinity at temperatures >100 ºC. In contrast, the related MOF MIL-100(Sc) was reported to be stable up to 270 ºC.[40] The primary structural difference between the MIL-100 and MIL-101 series is the size of the pores and the pore windows. This size difference results from the tritopic trimesic acid used as the linker for MIL-100 versus the ditopic terephthalic acid linker used for MIL-101. However, the node geometry and overall superstructure is otherwise identical in both series, suggesting that MIL-100(Sc) could potentially maintain the activity of MIL-101(Sc) while exhibiting enhanced stability. Gratifyingly, the data show that MIL-100(Sc) affords the highest yield among all the investigated catalysts, with a product yield of 57 ± 5% and a TOF of 28 h^{-1} at steady state operation under the standard conditions (**Figure 2.5**). Furthermore, this activity was maintained throughout the 5 h experiment.

2.2.4 Comparison of MOFs with the Same Node Metal

To further explore structure activity relationships in Sc-based MOFs, several analogues with different crystal structures and node geometries were explored (**Figure 2.6a**). MIL-100(Sc) and MIL-88D(Sc) both possess the same node coordination environment, with one coordination site at each Sc^{+3} center occupied by a labile water molecule. In contrast, MIL-68(Sc) has a node coordination environment consisting of chains of alternating Sc^{+3} and oxygen atoms, with the remaining coordination sites occupied by a poorly labile carboxylate ligand. As such, the Sc centers in MIL-68(Sc) are expected to be much less accessible for interaction with the epoxide. A comparison of catalytic performance in PO carbonation shows that MIL-100(Sc) and MIL-88D(Sc) afford 57 ± 5% and 11 ± 1% steady state yield and TOF of 28 h^{-1} and 12 h^{-1}, respectively. In contrast, MIL-68(Sc) affords <1% yield of PC (**Figure 2.6b**). These results are consistent with the hypothesis that the presence of accessible Lewis acidic sites on the metal nodes is a key

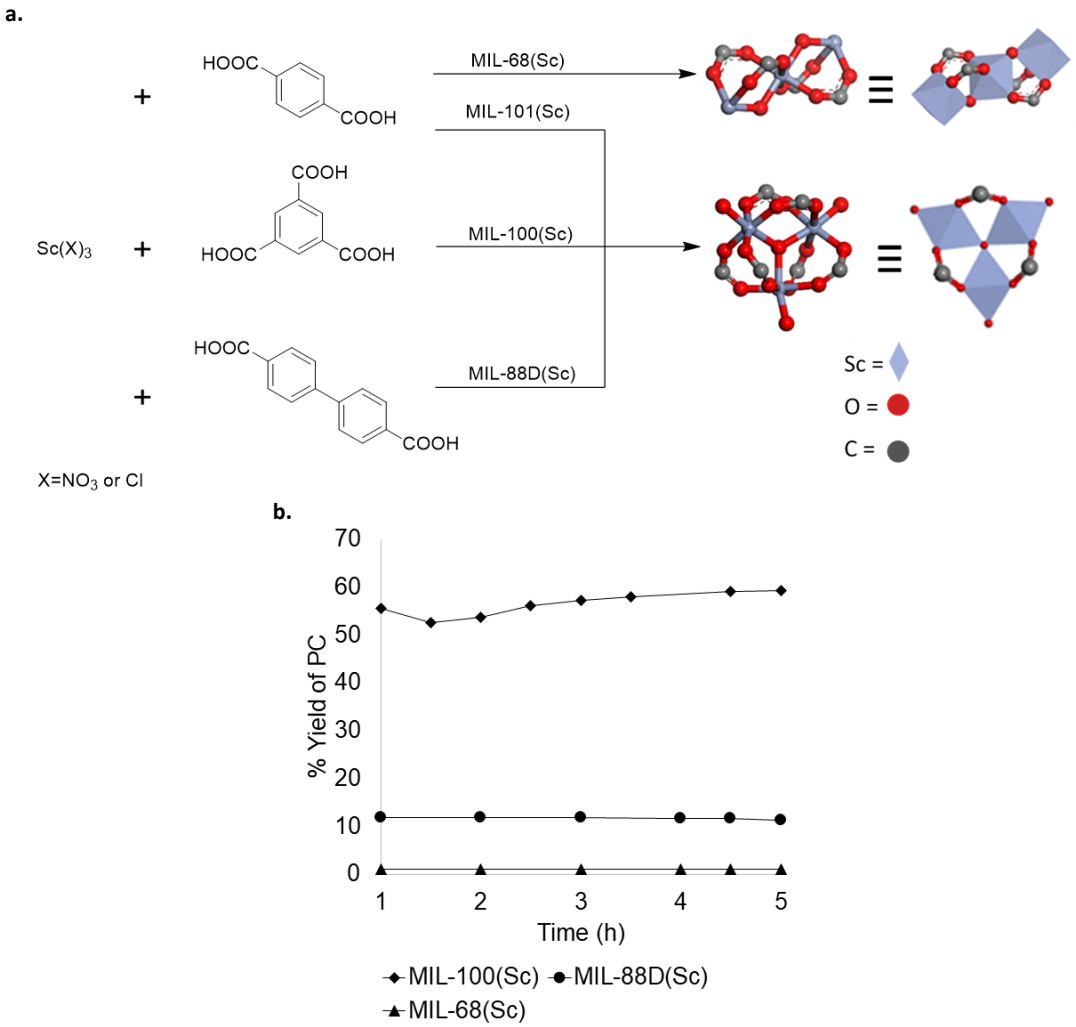

Figure 2.6a. Scandium-based materials derived from different metal node geometries; **b.** Comparison of Sc catalysts with different node geometries

requirement for activity in these MOF-based catalysts. Collectively, these data provide guidance for the design of future generations of catalysts.

2.2.5 Long Term Catalyst Stability

The robustness and reactivity of a MOF is often dictated by its metal-ligand interactions.[41] For example, some metal-containing clusters are susceptible to ligand substitution with water, leading to collapse of the frameworks upon exposure to moist environments. [42] Other frameworks can collapse upon heating or even at room temperature. [39] The stability of a MOF is a critical

property that determines its practicality and potential in catalysis applications. Flow conditions provide an excellent platform for studying catalyst stability over long periods of time. The best catalyst, MIL-100(Sc), was subjected to 24 h of continuous operation at 100 °C in chlorobenzene. As shown in Figure **2.7**, MIL-100(Sc) exhibits minimal loss in reactivity over the time examined.

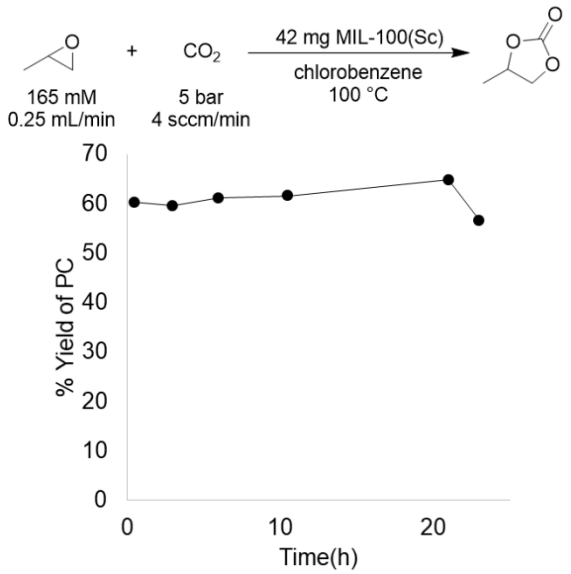

F**igure 2.7**. Long term stability of MIL-100(Sc) for the conversion of PO to PC

2.3 Conclusions

In conclusion, a detailed evaluation of catalyst performance as a function of different variables for the carbonation of propylene oxide catalyzed by a variety of Cr, Sc, and Fe-based MOFs was performed. The MOF synthesis method had minimal impact on MOF activity. High temperature post-synthetic activation of MOF catalyst was shown to be beneficial, but not necessary, for significant reactivity. A systematic optimization study yielded reaction conditions with significant advantages over previous protocols for this transformation. First, the requirement for TBABr as a co-catalyst has been eliminated. Second, MOF tunability has been leveraged to identify a Sc-based catalyst that outperforms the previously reported Cr material. Overall, these

results provide important information on the parameters that impact MOF catalysis for the carbonation of propylene oxide.

2.4 Experimental Methods

2.4.1 Synthesis and Characterization of Catalysts

MIL-101(Cr),[36] MIL-101(Fe),[31] MIL-101(Sc),[39] MIL-100(Sc),[39] MIL-88D(Sc),[39] and MIL-66(Sc) [39] were all prepared according to reported procedures. All reagents were obtained from Fisher or Sigma-Aldrich and used without further purification, with the exception of N,N'-dimethylformamide (DMF) (which was dried over 4Å molecular sieves) and N,N'-diethylformamide (DEF) (which was purified by stirring over activated charcoal followed by filtration through silica gel).

Powder X-ray Diffraction (PXRD) data were recorded at room temperature on a Bruker AXS D8 Advance powder diffractometer at 40 kV, 40 mA with a CuKα source (λ = 1.5406 Å) between 3 and 30° 2θ with a scan speed of 0.1 s/ step and a step size of 0.04. Samples were measured on a glass microscope slide in an aluminum holder. All powder patterns were taken in a mixture (1:3 or 1:1) of MOF to diatomaceous earth. The diatomaceous earth is visible as a sharp peak at 22° 2Θ

Temperature Programmed Desorption (TPD) data were collected on a Micromeritics ASAP 2920, using a quartz reactor with a quartz wool bed according to the following procedure. The line was purged with He for 15 min (20 mL/min). NH_3 was passed through the sample for 180 min (20 mL/min) at 40 °C in order to saturate all Lewis acidic sites with NH_3. The gas was switched to He and He was passed over the sample for 30 min at 40 °C (30 mL/min) in order to remove physisorbed NH_3. The temperature was then ramped to 350 °C (5 °C/min) to desorb the chemisorbed NH_3 and the desorbed NH_3 was detected via mass spectrometry.

MIL-101(Cr) $Cr(NO_3)_3 \cdot 9H_2O$ (400 mg, 1.10 mmol, 1 equiv), hydrofluoric acid (48-51% in H_2O, 1.10 mmol, 1 equiv), and terephthalic acid (76 mg, 0.46 mmol, 0.42 equiv) were combined in a Teflon-lined autoclave containing H_2O (4.8 mL). The resulting solution was placed in a room temperature oven and the temperature was ramped over 1 h to 220 ºC. The solution was heated at 220 °C for 8 h. The temperature ramp was found to be essential for the reproducible formation of active catalyst. The mixture was then cooled to room temperature, the solids were collected by centrifugation, and the product was washed with DMF (4 x 10 mL), water (3 x 10 mL), and ethanol (2 x 10 mL). The solids were dried under reduced pressure at either room temperature or 100 ºC for 16 h. Modifications to the synthesis of MIL-101(Cr) were performed by the substitution of HF with 1 equiv of HCl or acetic acid, as well as the omission of acid in the synthesis. The PXRD pattern for all samples matched that reported in the literature.[30, 36, 43, 44] TPD analysis of the material that was activated at room temperature yielded 1.2 mmol/g. TPD analysis of the material that was activated at 100 ºC yielded 2.4 mmol/g.

MIL-101(Fe) $FeCl_3$ (405 mg, 2.49 mmol, 1 equiv) and terephthalic acid (206 mg, 1.25 mmol, 0.5 equiv) were combined in a Teflon-lined autoclave containing DMF (15 mL) and H_2O (0.27 mL, 15 mmol, 6 equiv). This mixture was heated at 135 °C for 8 h. The mixture was cooled to room temperature, the solids were collected by centrifugation, and the product washed with DMF (3 x 10 mL) and ethanol (3 x 10 mL). The solids were dried under reduced pressure at room temperature for 16 h. The PXRD pattern for all samples matched that reported in the literature,[31] and TPD analysis yielded 1.3 mmol/g

MIL-101(Sc). Solutions of $ScCl_3$ (0.580 mmol, 1.45 M in H_2O, 1 equiv) and terephthalic acid (106 mg, 0.638 mmol, 1.1 equiv) were combined in a Teflon-lined autoclave containing DMF (4 mL) and ethanol (200 proof, 5 mL). The autoclave was heated at 80 °C for 1 d. The mixture was cooled

to room temperature and the solids were collected by centrifugation before being washed with DMF (3 x 10 mL) and ethanol (3 x 10 mL). The solids were dried under reduced pressure at room temperature for 16 h. The PXRD pattern for all samples matched that reported in the literature,[39] and TPD analysis yielded 0.4 mmol/g.

MIL-100(Sc). Benzene-1,3,5-tricarboxylic acid (90 mg, 0.428 mmol, 1 equiv) and scandium nitrate (246 mg, 1.07 mmol, 2.49 equiv) were combined in a Teflon-lined autoclave containing DMF (20 mL). The autoclave was heated at 150 ºC for 48 h. The mixture was cooled to room temperature and the solids were collected by centrifugation before being washed with water (3 x 10 mL) and ethanol (3 x 10 mL). The solids were then dried under reduced pressure at room temperature for 16 h. The PXRD pattern for all samples matched that reported in the literature,[39] and TPD analysis yielded 1.2 mmol/g.

MIL-88D(Sc). Biphenyl-4,4'-dicarboxylic acid (121 mg, 0.500 mmol, 1 equiv) and scandium nitrate (143 mg, 0.535 mmol, 1 equiv) were combined in a Teflon-lined autoclave containing DEF (6 mL). This solution was heated at 110 °C for 72 h. The mixture was cooled to room temperature and the solids were collected by centrifugation before being washed with water (3 × 10 mL) and ethanol (3 × 10 mL) and dried in air at 60 °C for 16 h. The PXRD pattern for all samples matched that reported in the literature[39] and TPD analysis yielded 0.5 mmol/g.

MIL-68(Sc). Solutions of $ScCl_3$ (0.460 mmol, 1.45 M in H_2O, 1 equiv) and terephthalic acid (76 mg, 0.457 mmol, 1 equiv) were combined in a Teflon-lined autoclave containing DMF (3.0 mL), water (5.0 mL), and ethanol (200 proof, 5 mL). This mixture was heated at 90 ºC for 12 h. The resulting solids were collected by centrifugation, washed with ethanol (3 × 10 mL), and dried in air at 60 °C for 16 h. The PXRD pattern for all samples matched that reported in the literature[39] and TPD analysis yielded 0.6 mmol/g.

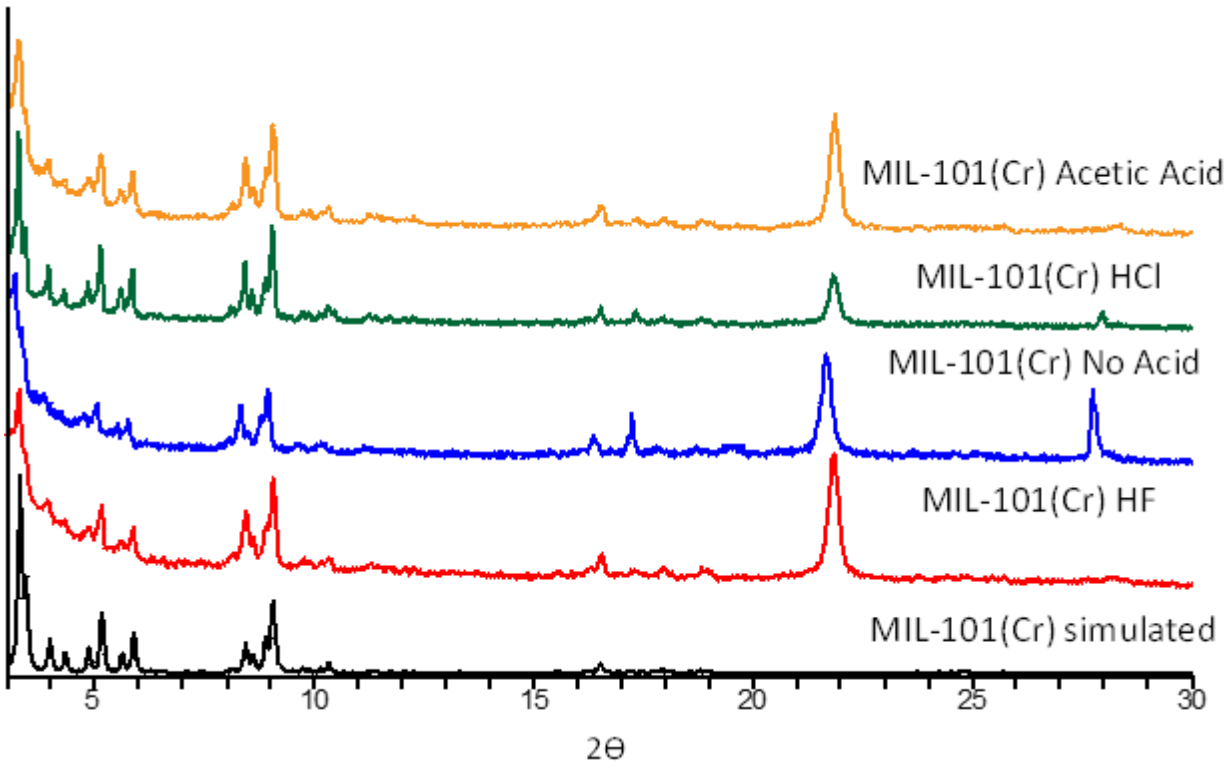

Figure 2.8. PXRD of MIL-101(Cr) (black: simulated, red: HF prep, blue: no acid prep, green: HCl prep, yellow: acetic acid prep)

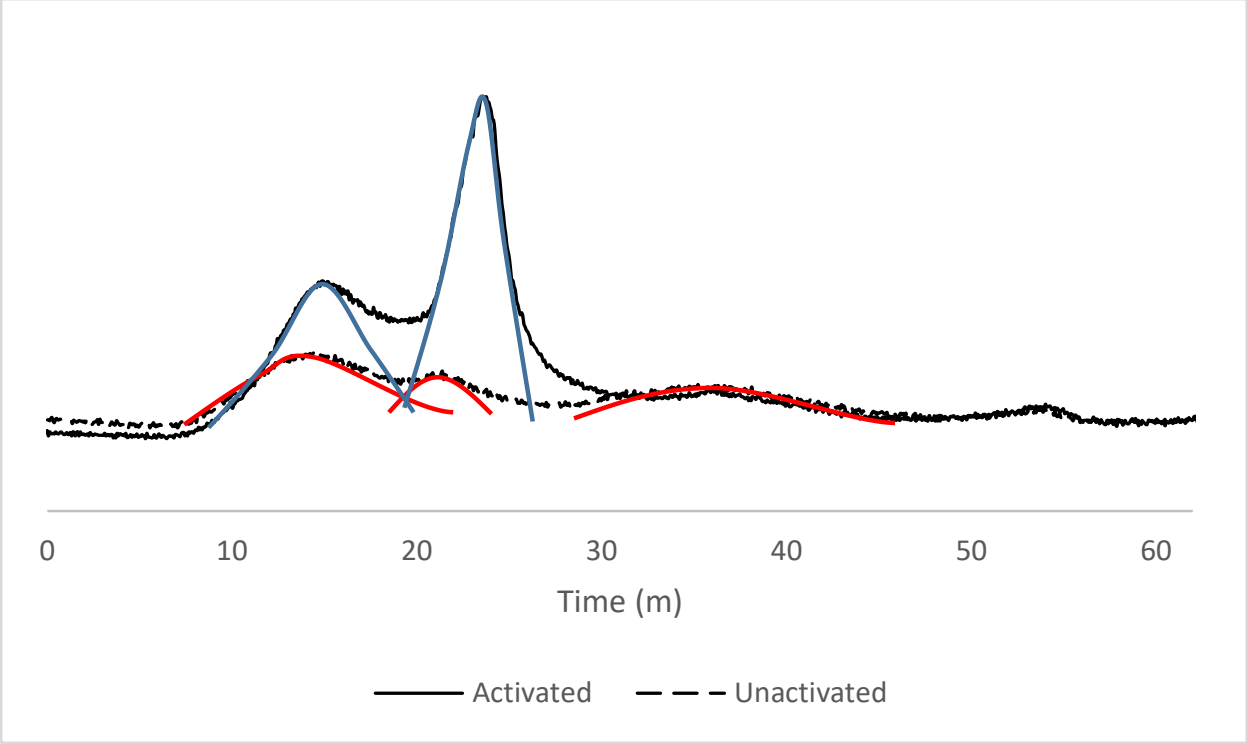

Figure 2.9. NH_3 TPD of MIL-101(Cr) no acid with activation at 125 ºC (activated) and activated at 25 ºC (unactivated)

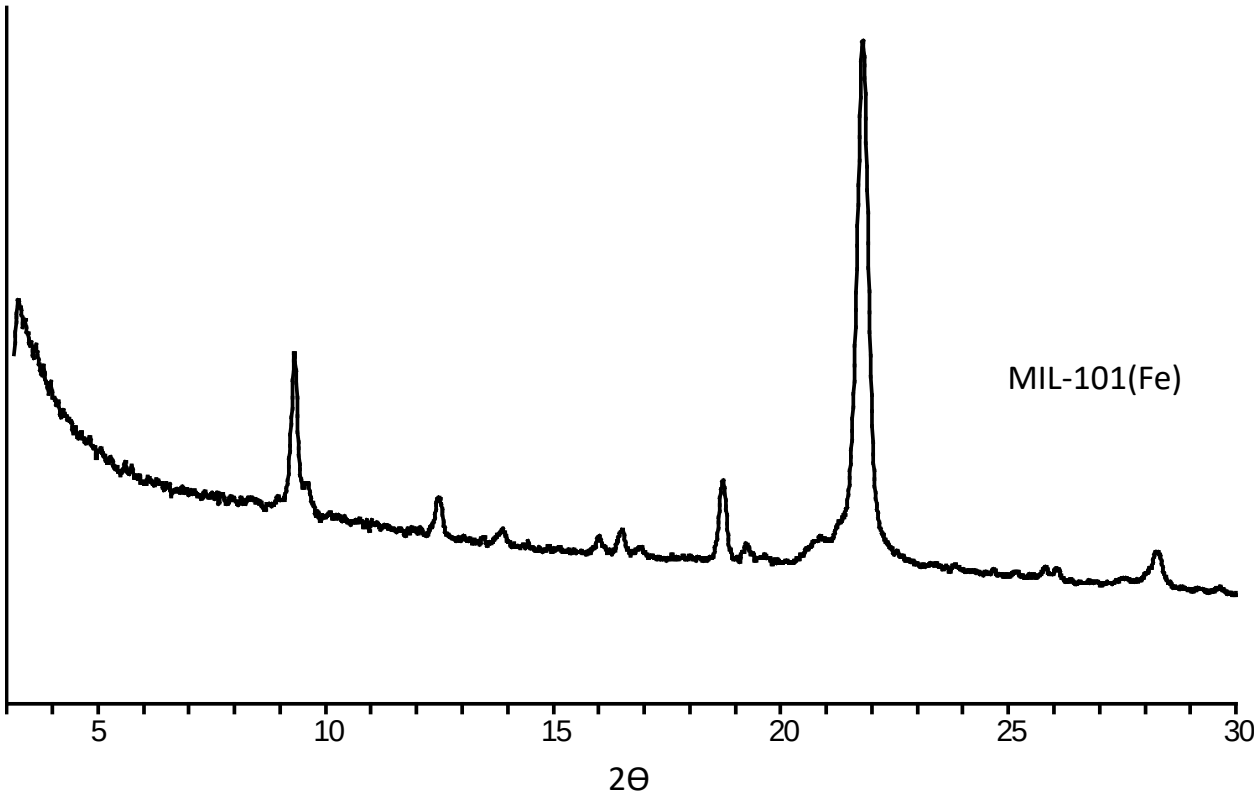

Figure 2.10. PXRD of MIL-101(Fe)

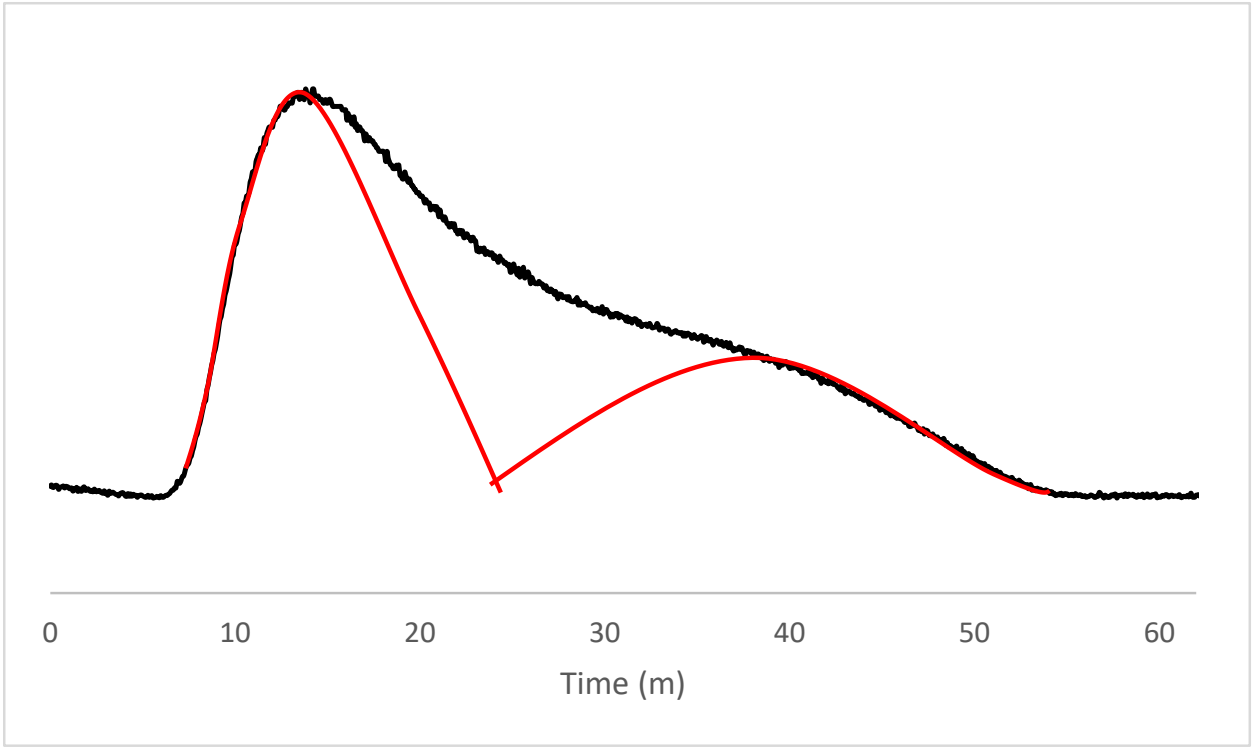

Figure 2.11. NH_3 TPD of MIL-101(Fe)

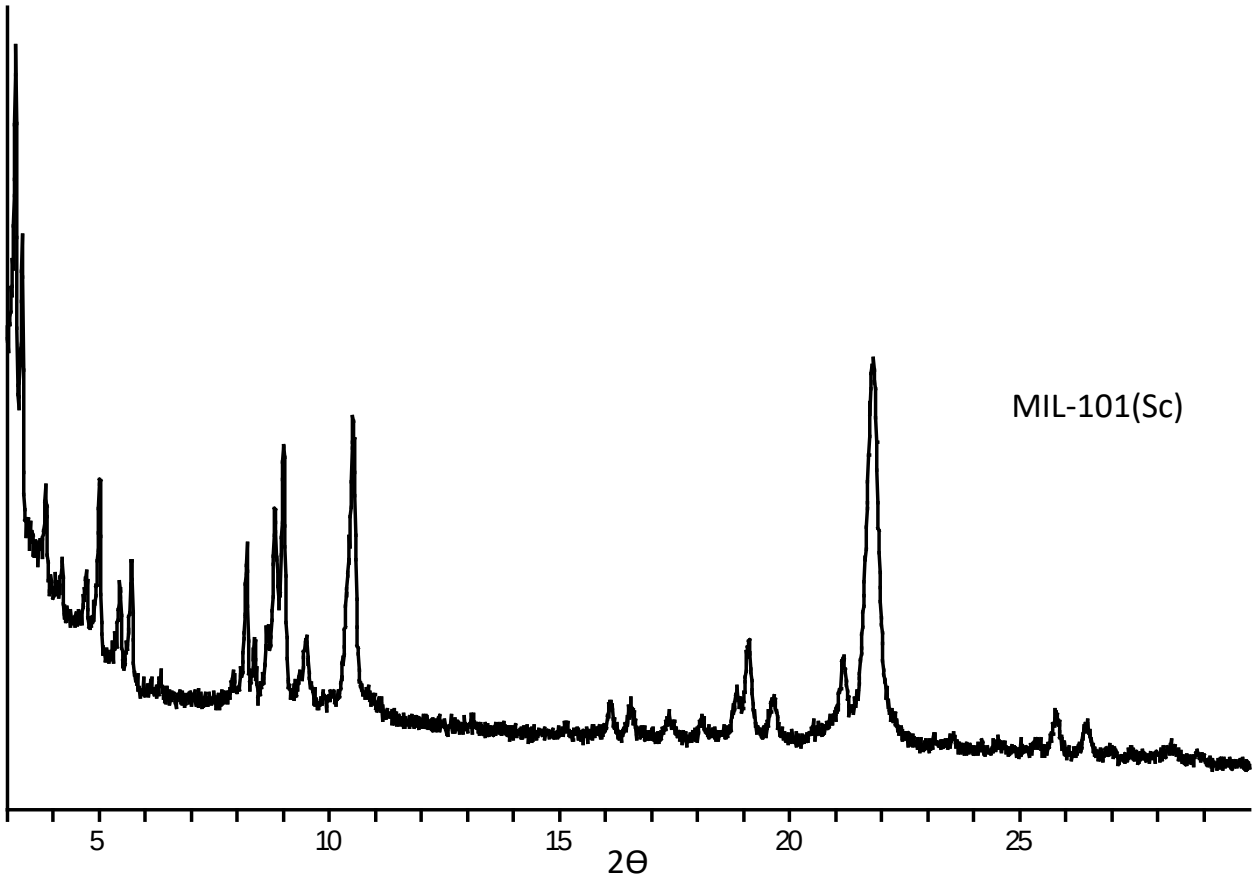

Figure 2.12. PXRD of MIL-101(Sc)

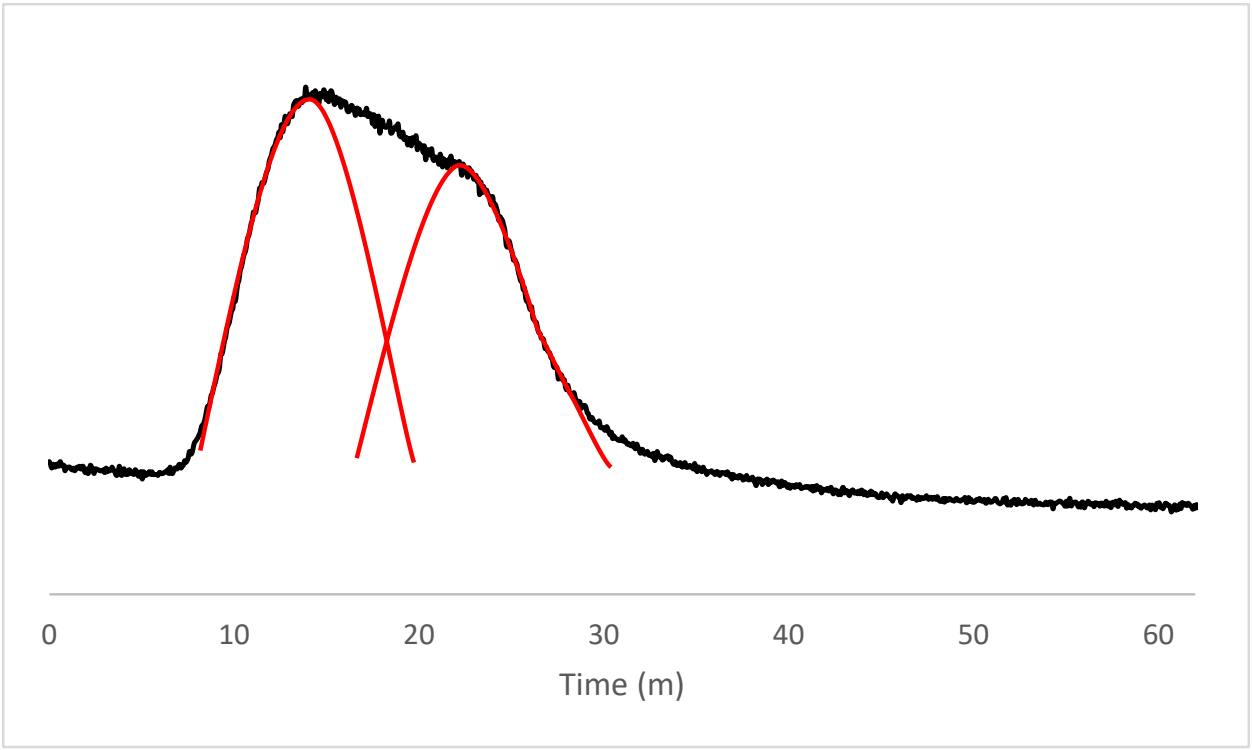

Figure 2.13. NH_3 TPD of MIL-101(Sc)

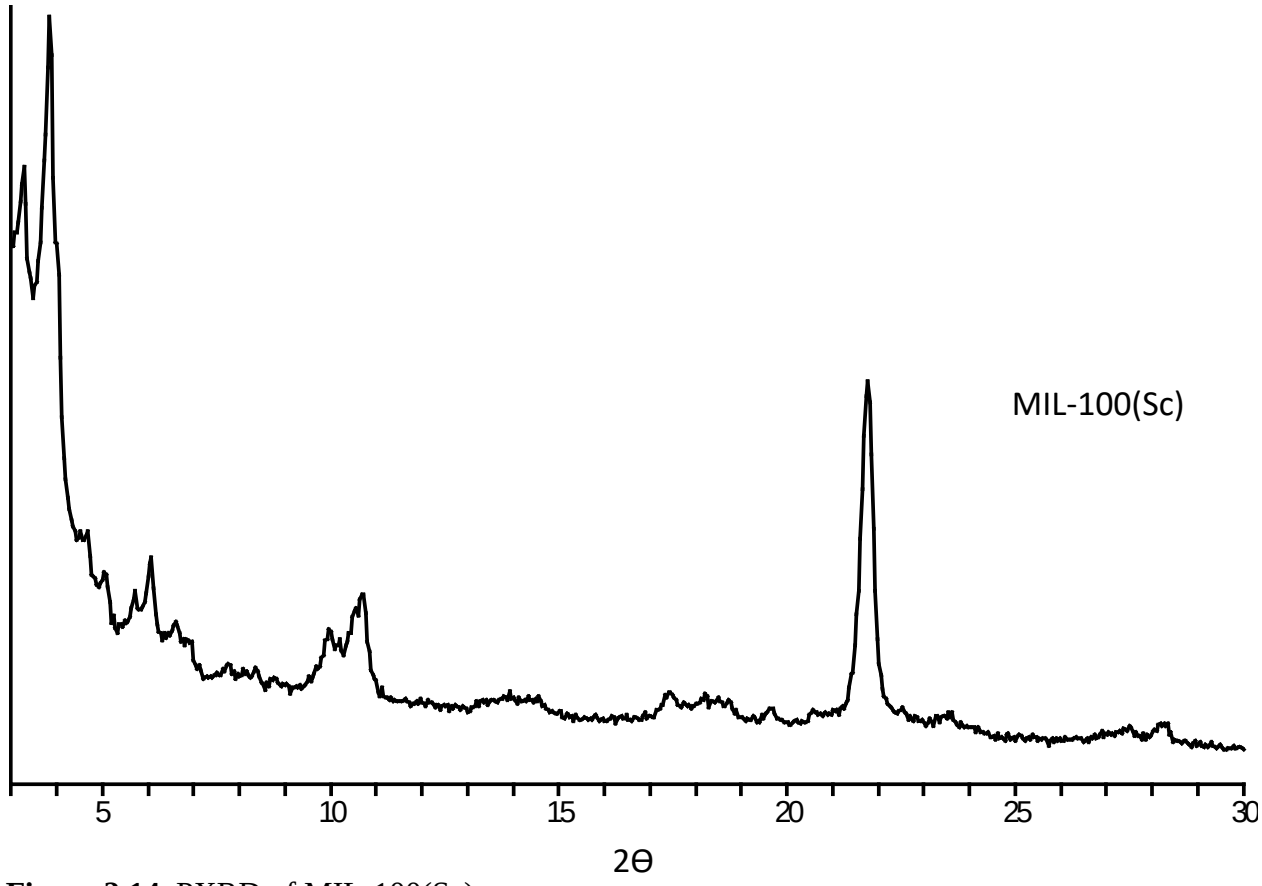

Figure 2.14. PXRD of MIL-100(Sc)

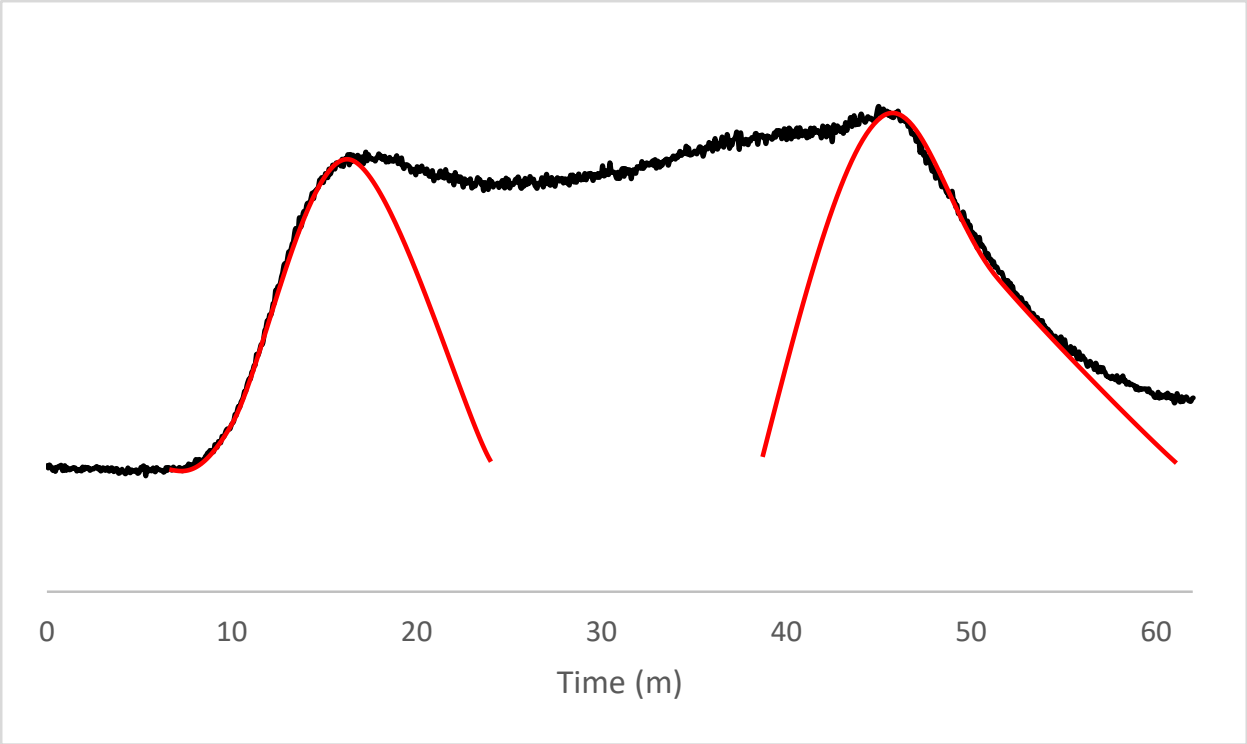

Figure 2.15. NH_3 TPD of MIL-100(Sc)

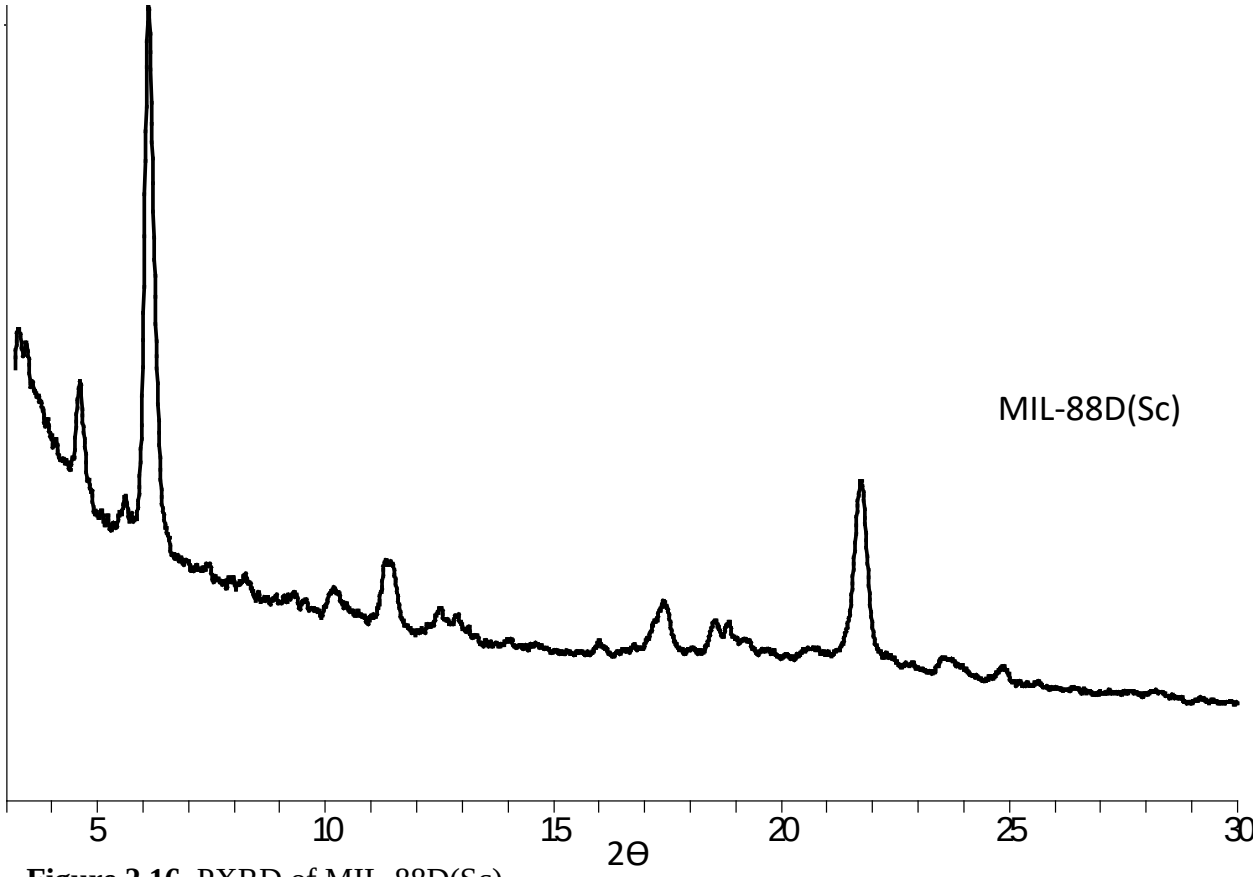

Figure 2.16. PXRD of MIL-88D(Sc)

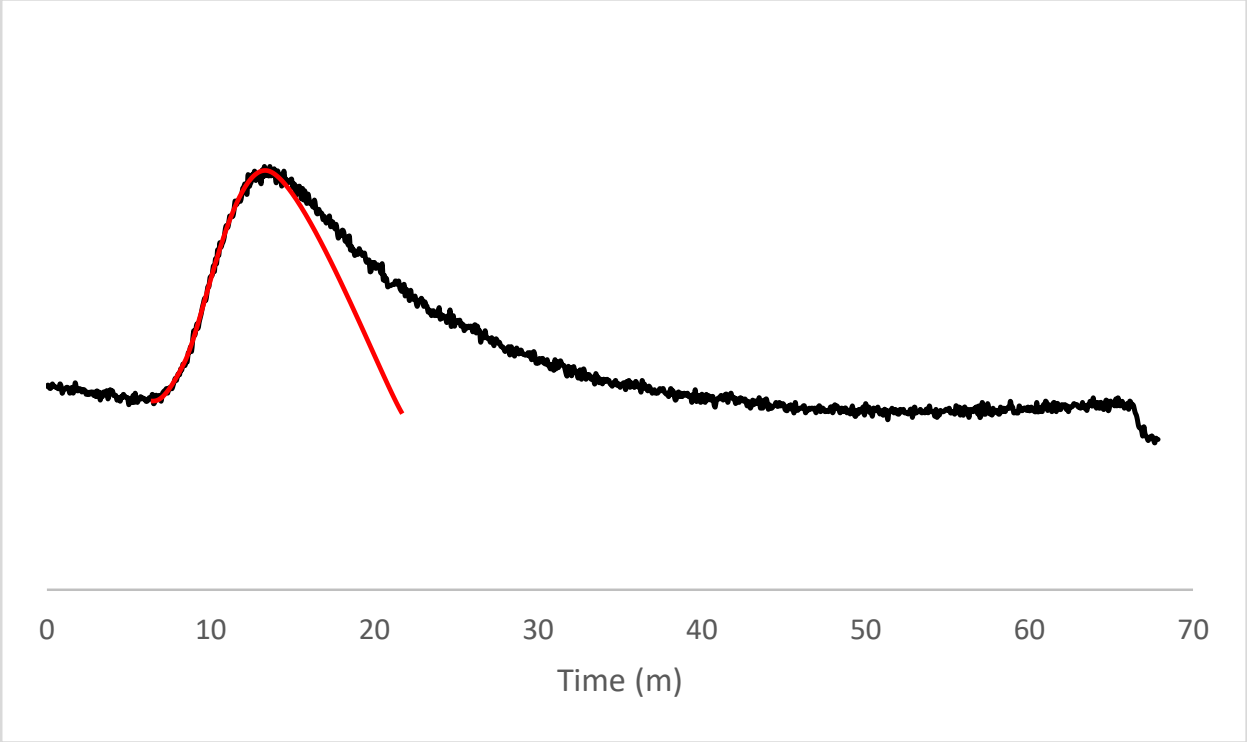

Figure 2.17. NH_3 TPD of MIL-88D(Sc)

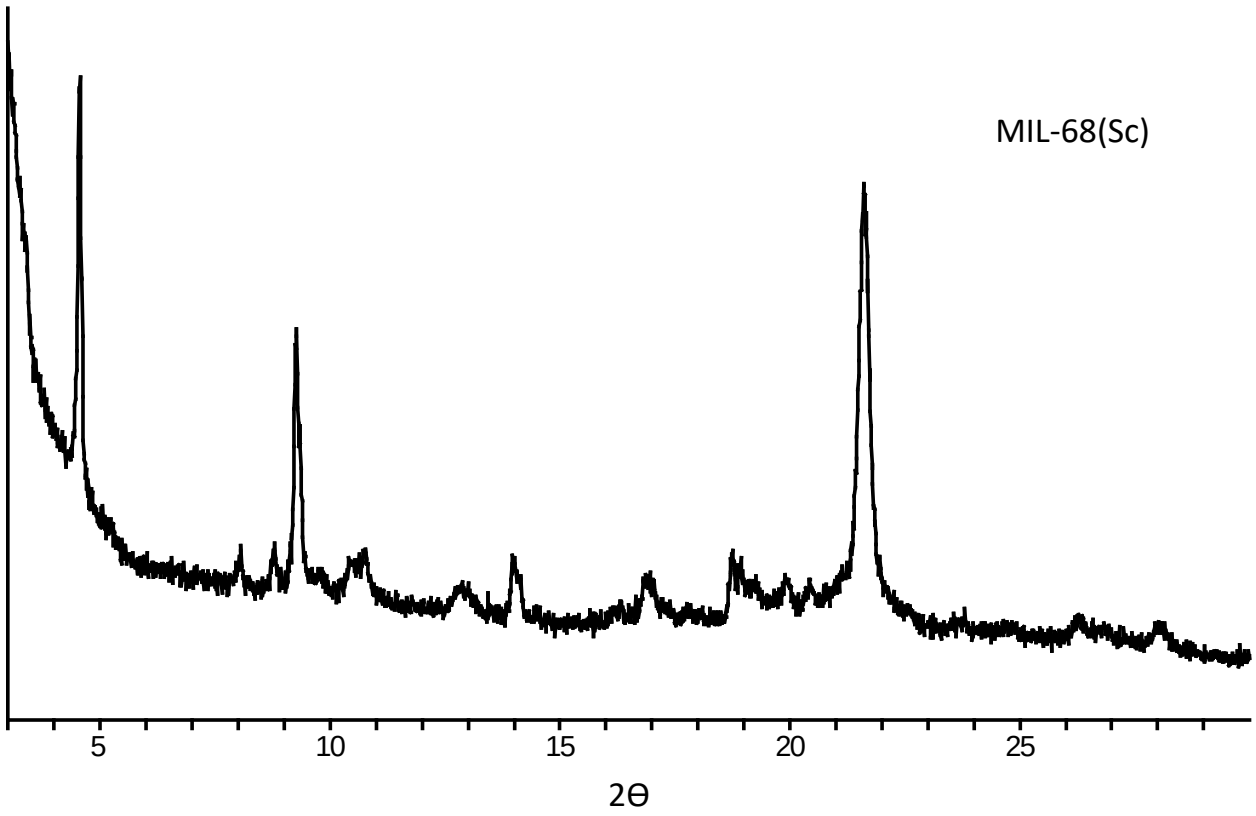

Figure 2.18. PXRD of MIL-68(Sc)

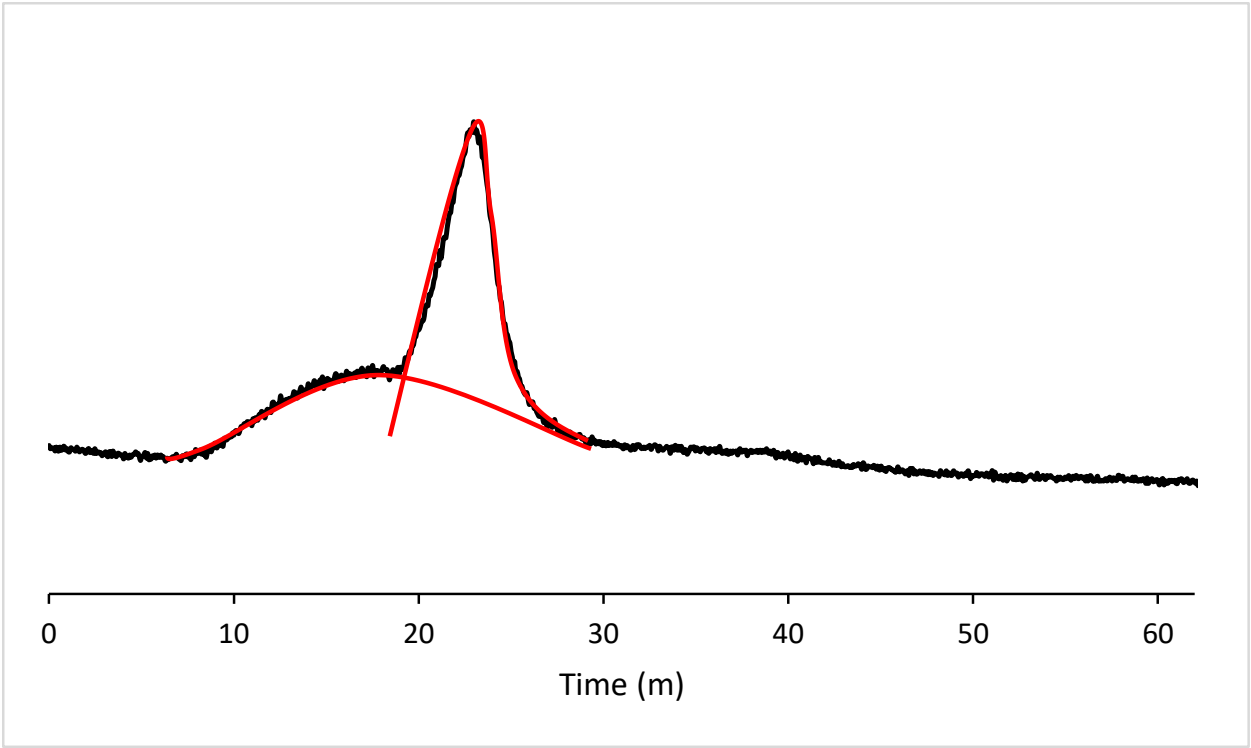

Figure 2.19. NH_3 TPD of MIL-68(Sc)

2.4.2 Design and construction of a packed bed reactor

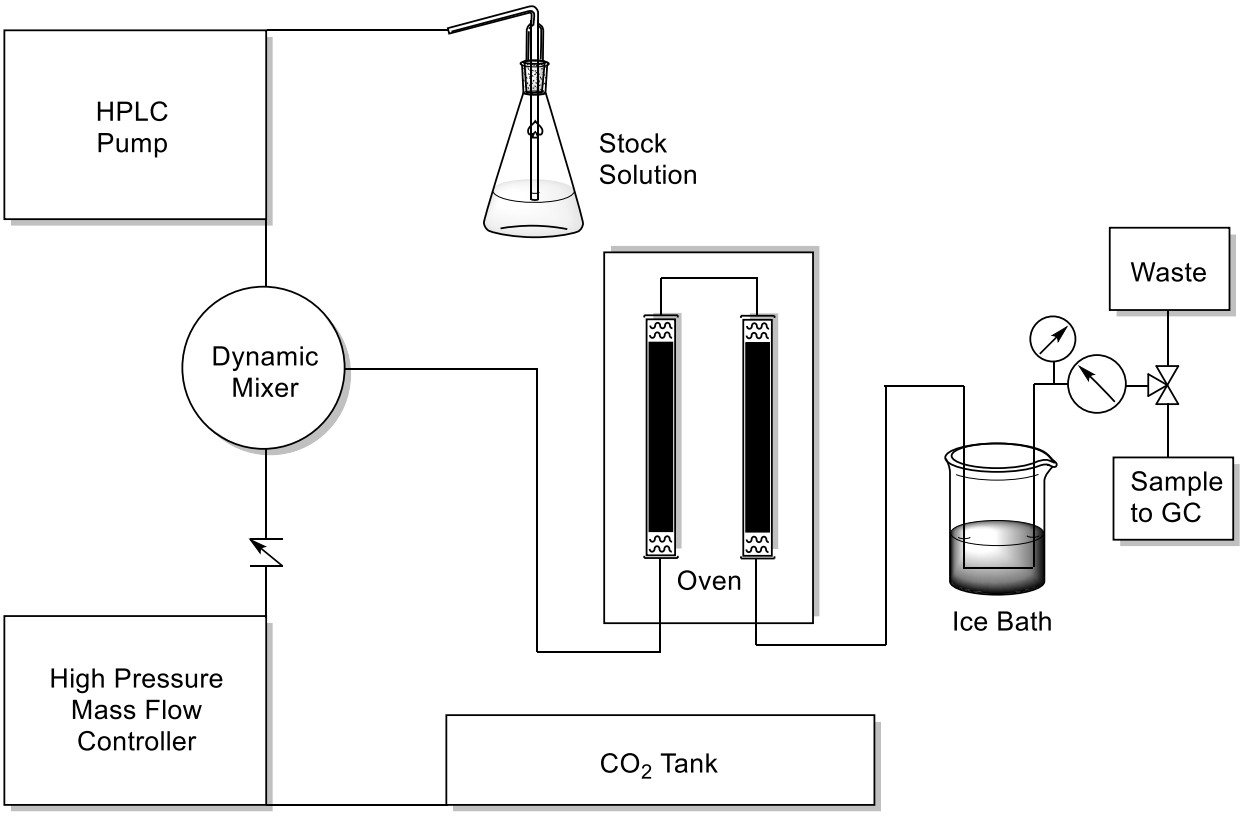

Figure 2.20. Box diagram of continuous flow system

An HPLC pump was used to deliver liquid stock solutions and a gas tank and high-pressure mass flow controller were used to deliver high-pressure carbon dioxide. A four-way dynamic mixer was used to allow for thorough mixing and expansion if more stock feeds were needed. The oven was constructed from copper pipe covered in silicone-wrapped heating tape connected to a temperature controller. The catalyst bed was a glass tube fitted with Vespel/graphite ferrules and packed with a mixture of catalyst and diatomaceous earth. A thermocouple was placed in direct contact with the outside surface of the bed for temperature regulation. An ice bath was used to minimize evaporation as the solution exits the reactor. The system pressure was controlled using a back-pressure regulator, and the outlet consisted of a three-way ball valve to facilitate sampling.

2.4.3 Typical Procedure for Catalytic Testing

The catalyst and Fisher lab-grade diatomaceous earth were combined in either a 1:1 w/w ratio or a 1:3 w/w ratio. The mixture was transferred to a mortar and pestle and ground until visibly homogeneous. The mixture was packed between two glass wool plugs in a ¼ inch OD, 1/20-inch wall thickness glass tube. The column was installed into the flow system, and both gas and stock solution streams were started simultaneously. CO_2 flow rates were varied from 1–4 sccm/min, and stock flow rates were varied from 0.25–0.5 mL/min. A second column in series was designed into the system for larger quantities of catalyst. The second column was packed with glass wool when smaller quantities of catalyst were used. The system was allowed to run until reaching the desired system pressure (between 1 and 10 bar) before heating was started. Aliquots were collected every 30 to 60 min and analyzed by GC-FID on a Shimadzu GC-17A. Mesitylene was included in the feed as internal standard.

2.4.4 Typical GC chromatogram

Peaks correspond to propylene oxide (1.2 min), Mesitylene (6.9 min) and propylene carbonate (7.2-7.7 min). Longer GC experiments, up to 30 min, show no additional peaks.

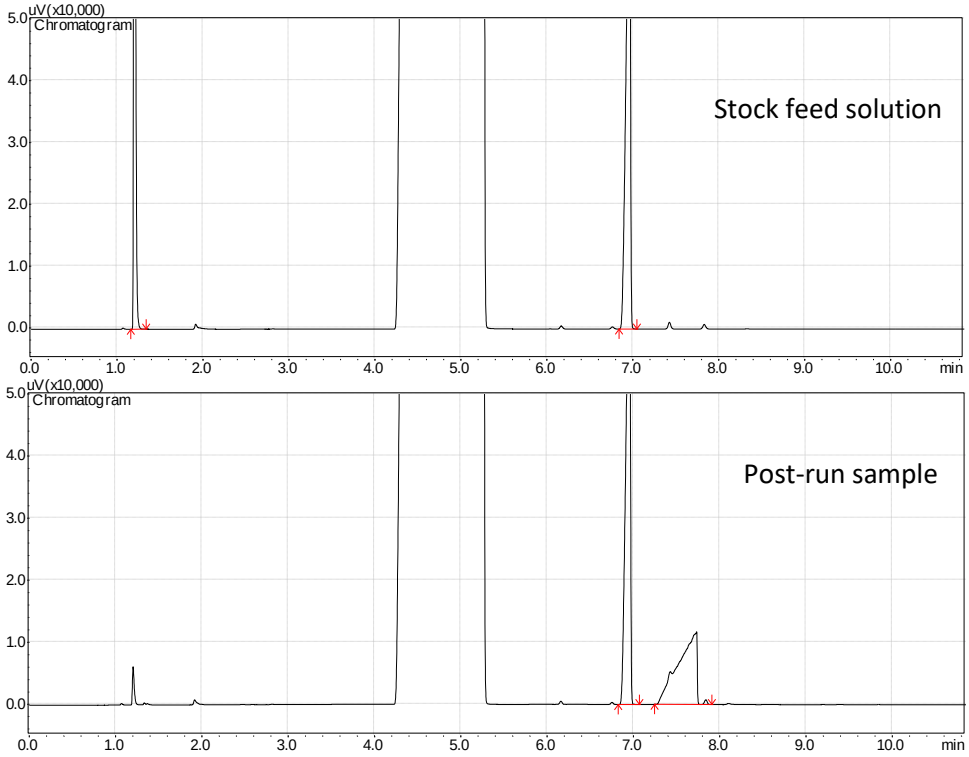

Figure 2.21 Sample GC traces of stock feed solution and post catalytic run sample

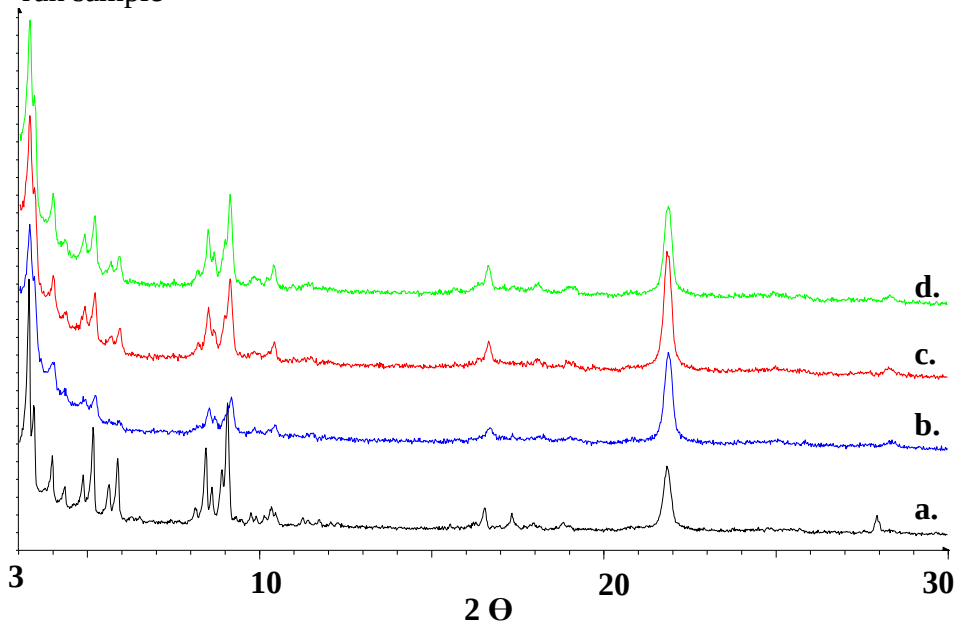

Figure 2.22 a. XRD of MIL-101(Cr) before reaction and from the **b.** inlet, **c.** middle and **d.** outlet of the packed bed post-reaction

2.5 References

1. J. Liu, L. Chen, H. Cui, J. Zhang, L. Zhang and C. Y. Su, *Chemical Society reviews* **2014**, *43*, 6011–6061.
2. S. M. Cohen, *Journal of the American Chemical Society* **2017**, *139*, 2855–2863.
3. P. Deria, J. E. Mondloch, O. Karagiaridi, W. Bury, J. T. Hupp and O. K. Farha, *Chemical Society reviews* **2014**, *43*, 5896–5912.
4. P. García-García, M. Müller and A. Corma, *Chemical Science* **2014**, *5*, 2979.
5. T. Sakakura and K. Kohno, *Chemical communications* **2009**, 1312–1330.
6. G. Rokicki, *Progress in Polymer Science* **2000**, *25*, 259–342.
7. A.-A. G. Shaikh and S. Sivaram, *Chemical reviews* **1996**, *96*, 951–976.
8. M. North, R. Pasquale and C. Young, *Green Chemistry* **2010**, *12*, 1514.
9. K. Kasuga, T. Kato, N. Kabata and M. Handa, *Bulletin of the Chemical Society of Japan* **1996**, *69*, 2885–2888.
10. W. M. Ren, Y. Liu and X. B. Lu, *J Org Chem* **2014**, *79*, 9771–9777.
11. A. Behr, *Angewandte Chemie International Edition in English* **1988**, *27*, 661–678.
12. V. D'Elia, J. D. A. Pelletier and J. M. Basset, *ChemCatChem* **2015**, *7*, 1906–1917.
13. R. L. Paddock, Y. Hiyama, J. M. McKay and S. T. Nguyen, *Tetrahedron Letters* **2004**, *45*, 2023–2026.
14. R. Srivastava, D. Srinivas and P. Ratnasamy, *Applied Catalysis A: General* **2005**, *289*, 128–134.
15. R. Srivastava, D. Srinivas and P. Ratnasamy, *Tetrahedron Letters* **2006**, *47*, 4213–4217.
16. J. Peng and Y. Deng, *New Journal of Chemistry* **2001**, *25*, 639–641.
17. L.-F. Xiao, F.-W. Li, J.-J. Peng and C.-G. Xia, *Journal of Molecular Catalysis A: Chemical* **2006**, *253*, 265–269.
18. X. Zhou, Y. Zhang, X. Yang, L. Zhao and G. Wang, *Journal of Molecular Catalysis A: Chemical* **2012**, *361–362*, 12–16.
19. H. S. Kim, J. J. Kim, H. Kim and H. G. Jang, *Journal of Catalysis* **2003**, *220*, 44–46.
20. J. Kim, S.-N. Kim, H.-G. Jang, G. Seo and W.-S. Ahn, *Applied Catalysis A: General* **2013**, *453*, 175–180.
21. D.-A. Yang, H.-Y. Cho, J. Kim, S.-T. Yang and W.-S. Ahn, *Energy Environ. Sci.* **2012**, *5*, 6465–6473.
22. J. Tharun, G. Mathai, A. C. Kathalikkattil, R. Roshan, Y.-S. Won, S. J. Cho, J.-S. Chang and D.-W. Park, *ChemPlusChem* **2015**, *80*, 715–721.
23. R. Babu, A. C. Kathalikkattil, R. Roshan, J. Tharun, D.-W. Kim and D.-W. Park, *Green Chem.* **2016**, *18*, 232–242.
24. W. Kleist, F. Jutz, M. Maciejewski and A. Baiker, *European Journal of Inorganic Chemistry* **2009**, *2009*, 3552–3561.
25. M. Zhu and M. A. Carreon, *J Appl Polym Sci* **2014**, *131*, 1–13.
26. O. V. Zalomaeva, A. M. Chibiryaev, K. A. Kovalenko, O. A. Kholdeeva, B. S. Balzhinimaev and V. P. Fedin, *Journal of Catalysis* **2013**, *298*, 179–185.
27. N. V. Maksimchuk, O. V. Zalomaeva, I. Y. Skobelev, K. A. Kovalenko, V. P. Fedin and O. A. Kholdeeva, *Proceedings of the Royal Society A: Mathematical, Physical and Engineering Sciences* **2012**, *468*, 2017–2034.
28. Z. Zhang, X. Sun, X. Zhang and X. Fang, *Catal Lett* **2016**, *146*, 2098–2104.

29. P. P. Pescarmona and M. Taherimehr, *Catalysis Science & Technology* **2012**, *2*, 2169–2187.
30. P. B. S. Rallapalli, M. C. Raj, S. Senthilkumar, R. S. Somani and H. C. Bajaj, *Environmental Progress & Sustainable Energy* **2015**, 1–8.
31. A. Santiago-Portillo, S. Navalón, F. G. Cirujano, F. X. L. i. Xamena, M. Alvaro and H. Garcia, *ACS Catalysis* **2015**, *5*, 3216–3224.
32. O. V. Zalomaeva, N. V. Maksimchuk, A. M. Chibiryaev, K. A. Kovalenko, V. P. Fedin and B. S. Balzhinimaev, *Journal of Energy Chemistry* **2013**, *22*, 130–135.
33. L. Bromberg, Y. Diao, H. Wu, S. A. Speakman and T. A. Hatton, *Chemistry of Materials* **2012**, *24*, 1664–1675.
34. C. Y. Huang, M. Song, Z. Y. Gu, H. F. Wang and X. P. Yan, *Environ Sci Technol* **2011**, *45*, 4490–4496.
35. E. A. Berdonosova, K. A. Kovalenko, E. V. Polyakova, S. N. Klyamkin and V. P. Fedin, *The Journal of Physical Chemistry C* **2015**, *119*, 13098–13104.
36. G. Ferey, C. Mellot-Draznieks, C. Serre, F. Millange, J. Dutour, S. Surble and I. Margiolaki, *Science* **2005**, *309*, 2040–2042.
37. T. Cheng, Q. Zhao, D. Zhang and G. Liu, *Green Chem.* **2015**.
38. K. P. Kepp, *Inorganic chemistry* **2016**, *55*, 9461–9470.
39. L. Mitchell, B. Gonzalez-Santiago, J. P. S. Mowat, M. E. Gunn, P. Williamson, N. Acerbi, M. L. Clarke and P. A. Wright, *Catal. Sci. Technol.* **2013**, *3*, 606–617.
40. Y.-T. Li, K.-H. Cui, J. LI, J.-Q. Zhu, X. Wang and Y.-Q. Tian, *Chinese Journal of Inorganic Chemistry* **2011**, *27*, 951–956.
41. A. J. Howarth, Y. Liu, P. Li, Z. Li, T. C. Wang, J. T. Hupp and O. K. Farha, *Nature Reviews Materials* **2016**, *1*, 1–15.
42. S. Hausdorf, J. Wagler, R. Moβig and F. O. R. L. Mertens, *The Journal of Physical Chemistry A* **2008**, *112*, 7567–7576.
43. L. Bromberg, Y. Diao, H. Wu, S. A. Speakman and T. A. Hatton, *Chem. Mater.* **2012**, *24*, 1664-1675.
44. D.-Y. Hong, Y. K. Hwang, C. Serre, G. Férey and J.-S. Chang, *Advanced Functional Materials* **2009**, *19*, 1537-1552.

Chapter 3

Post-Synthetic Modification of MIL-101-SO_3X to Generate Cation Loaded Adsorbents

3.1 Introduction

Metal-organic frameworks (MOFs) are coordination polymers comprised of organic linkers and metals nodes that form crystalline 2D or 3D networks.[1] MOFs are commonly highly porous, and this porosity is an attractive feature for a myriad of applications.[2-9] MOFs have other attractive features as well, including high thermal stability and tunability. However, synthesis of MOFs is primarily performed through hydrothermal self-assembly, which can be sensitive to many factors. Temperature, pressure, solvent and pH all must be delicately balanced during MOF synthesis to generate the desired structure.

Post-synthetic modification (PSM) is a way to circumvent sensitive synthesis conditions by reacting an already assembled MOF under a new, milder set of conditions, in order to modify a node, linker, or pore structure. The idea to post-synthetically modify MOFs was proposed concurrently with the earliest examples of MOFs in 1990. An early report by Robson sttaed, "Relatively unimpeded migration of species throughout the lattice may allow chemical functionalization of the rods subsequent to construction of the framework."[10] However, while this idea was first proposed in 1990, it was not until almost 5 years later that the first successful reports of PSM began to appear.[11] Since this time, PSM has proven a valuable tool in the

synthesis of novel MOF materials that contain functional groups that are incompatible with hydrothermal synthesis such as alcohols, nitriles and phosphines.[11] PSM of MOFs is of increasing value as it allows for rapid diversification of known materials.

The sulfonate moiety is currently rare in MOFs, as this functional group can interfere with self-assembly. MIL-101-SO_3X is one of a small number of sulfonated MOFs and is the most well studied. This functionality is desirable for inclusion in MOFs as it can be useful for acid-base reactions that can benefit from the presence of both an acidic linker and basic node. Alternatively, the sulfonic acid can deprotonated and used to ionically bind cations.[12] This type of PSM can theoretically yield a variety of cation bound materials, and several cations have already been exchanged into MIL-101-SO_3X (**Figure 3.1**).[12-15] The ability to load cations into MOFs, while reported, [12, 16-18] has not been well investigated for this system. Genna and coworkers initially reported loading of hydrogenation catalysts into ZJU-28 over a 3 day period but only achieve partial cation exchange over this time period. The authors proceed with the

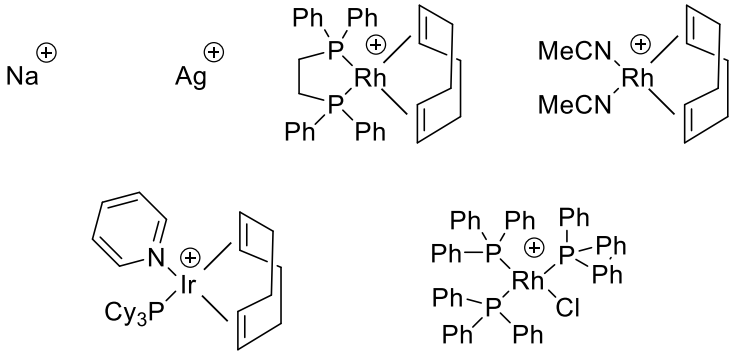

Figure 3.1 Cations previously loaded into MIL-101-SO_3X

partially loaded material most likely due to the lower activity that is afforded by higher loading.[16] Higher loadings of cation, in most catalytic cases, give lower catalyst activity ascribed to increased pore clogging.[20] While lower loading may be desirable for catalytic applications, other applications such as separations or water sorption may benefit from higher loadings and more uniform sites throughout. Grigoropoulos and coworkers were able to expand on this approach by

incorporation of Crabtree's catalyst [Ir(cod)(PCy3)] for gas phase hydrogenation. The cation exchanged MOFs provide increased selectivity and conversion for olefinic alcohols. The cation exchange in this MOF approaches the upper limit calculated by accounting for guest accessible space and the size of the cationic guest molecule. Previous reports have utilized exchange times from 20–72 hours and/or elevated temperatures to yield loading of cationic metal complexes but multiple conditions for different cation loadings are rarely reported.[13, 14, 19] Utilizing monoatomic cations enabled us to thoroughly investigate the exchange process without risk of pore obstruction. Herein, we evaluate ion-exchange in MIL-101-SO_3X and propose applications for these cation loaded materials.

3.2 Results and Discussion

3.2.1 Post-Synthetic Modification of MIL-101-SO_3X

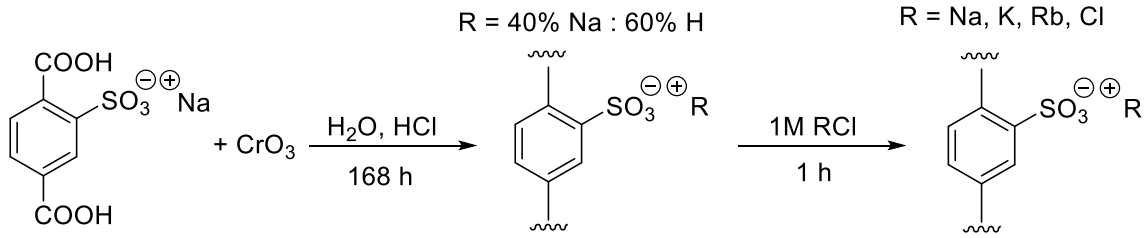

Figure 3.2 Synthesis and post-synthetic modification of MIL-101-SO_3X

The typical synthesis of MIL-101-SO_3X uses monosodium sulfonate terephthalic acid as the linker (**Figure 3.2**). The linker is combined with water and concentrated HCl and reacted at 180 °C for 7 days, during which time the sulfonate is partially protonated and the MOF self assembles. This protonation can be confirmed by elemental analysis, which shows less sodium with respect to sulfur than expected based on linker stoichiometry. There are two theories as to the state of the sulfonate/sulfonic acid as synthesized. Either the sulfonate is protonated and exists as the sulfonic acid, which is supported by titration experiments,[20] or the sulfonate exists as a zwitterion with a cation on the metal node of the MOF balancing the overall charge of the material. Whichever theory may be correct, the ability to generate materials containing complete

	exchange salt (5 equiv)	K:S (±0.05)	Na:S (±0.06)	pKa
As Synthesized MIL-101-SO_3X	KCl	0.64	—	-6.3
As Synthesized MIL-101-SO_3X	KBF_4	0.38	—	0.5
As Synthesized MIL-101-SO_3X	KH_2PO_4	0.84	—	2.16
As Synthesized MIL-101-SO_3X	KOAc	1.02	—	4.756
As Synthesized MIL-101-SO_3X	$KHCO_2$	1.16	0.07	6.35

Table 3.1 Potassium loading with various anions

incorporation of the acid or a cation is necessary in order to evaluate acid or cation interactions in pure form. To this end, the material was initially treated with a variety of potassium salts to generate the potassium bound sulfonate anion throughout the structure. The as synthesized material contains approximately 40% sodium with the remainder of the sites believed to be sulfonic acid. Therefore, any loading above 40% would require not only the complete exchange of sodium for potassium but also the deprotonation of the sulfonic acid moieties. When treated with potassium salts in water, all salts show the complete exchange of sodium cation with potassium. The more basic salts, potassium acetate and potassium bicarbonate, show high

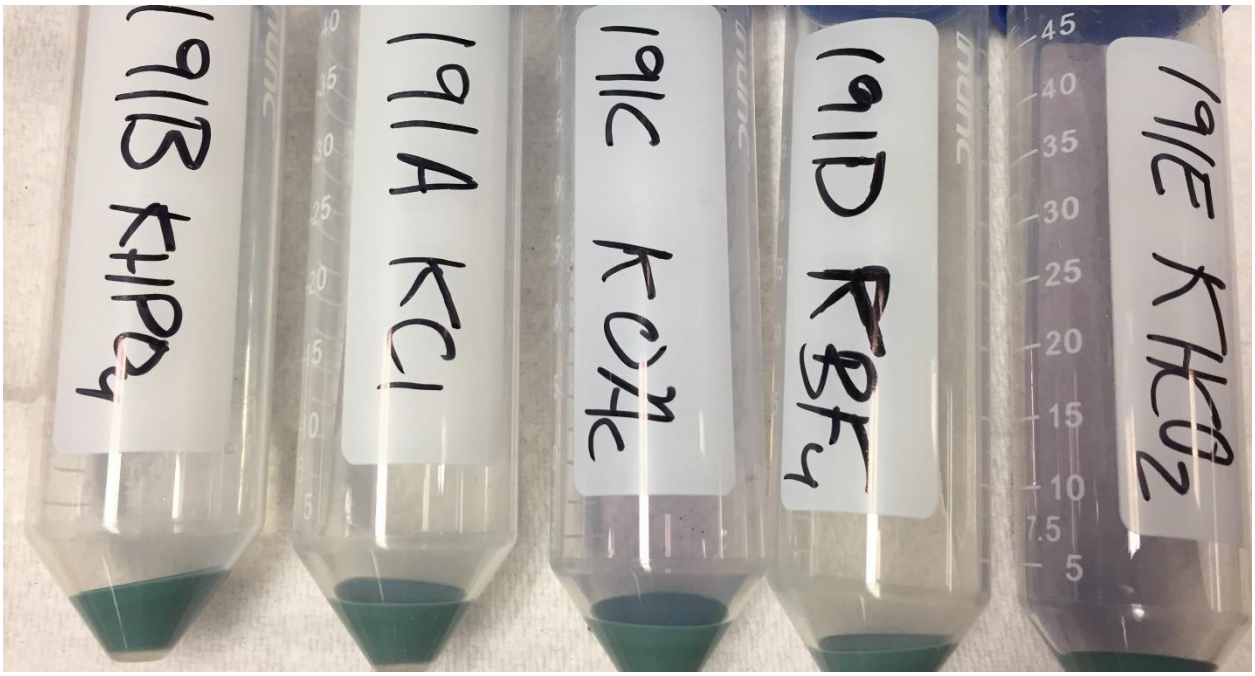

Figure 3.3 MIL-101-SO_3X samples post treatment with potassium salts. Sample 191C and 191E are colored (purple) indicative of dissolved chromium

loadings, but signs of degradation are also apparent. While the PXRD of the materials remains unchanged, the supernatant is purple indicative of chromium in solution (**Figure 3.3**). Potassium phosphate monobasic and potassium chloride both show loadings above the 40% threshold, indicating exchange of sulfonic acids as well as sodium ions. Finally, potassium tetrafluoroborate shows low loading, most likely due to its decreased solubility in water (**Table 3.1**).

In order to establish conditions to completely deprotonate the sulfonic acids in MIL-101-SO_3X, a variety of conditions were explored. The main challenge with deprotonation is that MIL-101-SO_3X is known to be unstable to strong base in that it undergoes rapid loss of crystallinity and surface area.[21] Therefore, investigation of base and exchange time was undertaken to determine optimal conditions for full exchange without reducing crystallinity.

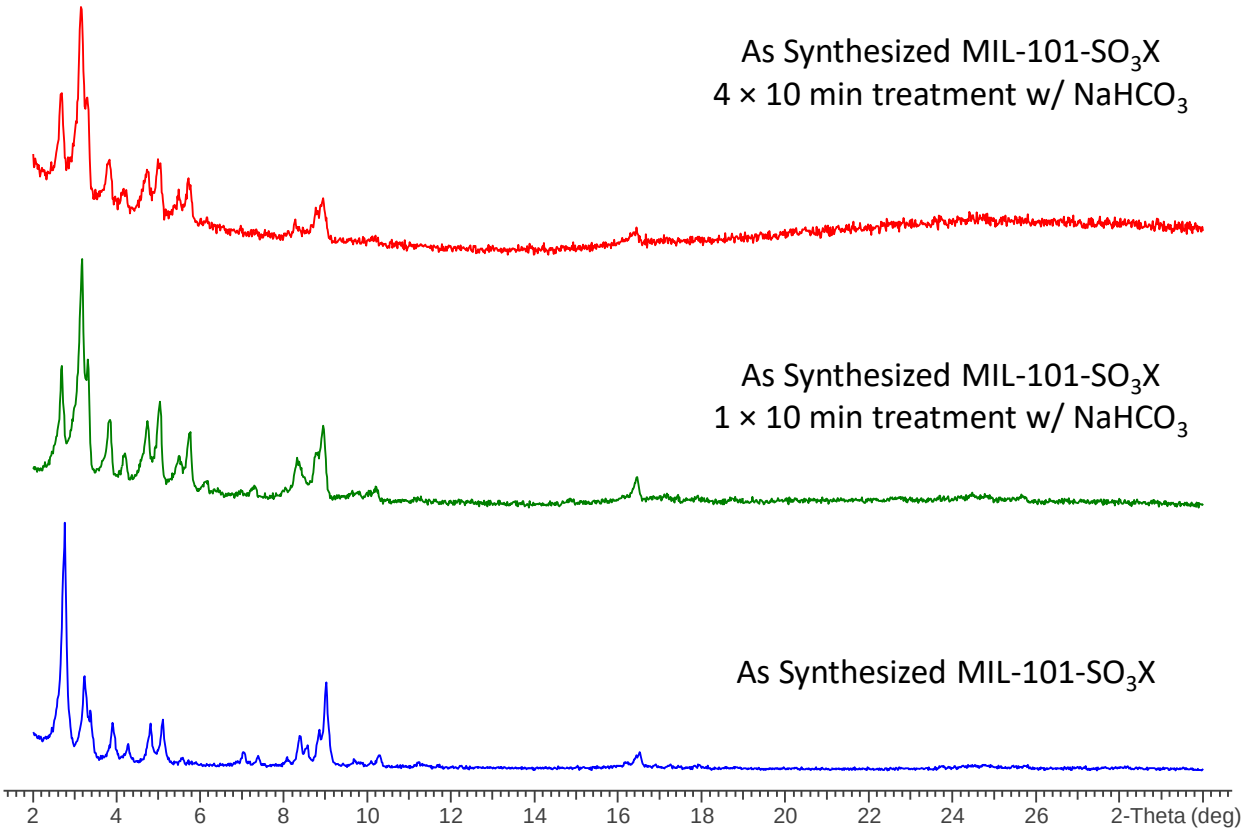

Figure 3.4 MIL-101-SO_3X samples post treatment with 0.1 M NaOH. Degradation of crystallinity can start to be seen after several treatments.

Trials with dimethylamine, carbonate salts, and hydroxide salts all lead to rapid decomposition. Triethylamine in water (1 equivalent relative to incorporated sulfonate) was ultimately identified as a suitable base that did not impact crystallinity or surface area after 48 hours of soaking. While exchange with triethylamine yielded the desired deprotonation results, we hypothesize that removal of triethylammonium from the structure could be challenging during cation exchange based on previous studies with ZJU-28, containing dimethylammonium cation, only obtained partial exchange after 3 days of treatment.[16] As an alternative, brief 10 min washings with dilute sodium bicarbonate solution were attempted to remove the acid and generate the sodium sulfonate without degrading crystallinity (**Figure 3.4**). This not only maintained crystallinity but replaced the protons with more the easily exchangeable sodium cation, producing fully deprotonated sites (**Figure 3.5a**). The fully protonated MIL-101-SO_3H structure has previously been accessed in the literature through washing the as-synthesized material with dilute hydrochloric acid.[22] The incorporation of protons was evidenced by loss of sodium, determined by inductively coupled plasma optical emission spectrometry, and subsequent base titration as well. Following a similar procedure on larger scale, we are also able to obtain full incorporation of acid sites (**Figure 3.5b**).

The effect of molar equivalents of salt on exchange was investigated using potassium chloride. Potassium chloride was chosen due to its simplicity, availability, and favorable detection limit of chloride by X-ray fluorescence (XRF). As synthesized MIL-101-SO_3X, 40% Na/60% H, and base treated MIL-101-SO_3X were exchanged with 20, 10, 5 and 1 molar equivalents of potassium chloride based on SO_3^- (**Table 3.2**). The resulting trends show that high molar equivalents are necessary to deprotonate the sulfonate but all sodium cations are removed even at 1 equivalent. The base-treated material, containing only sodium cations, was completely

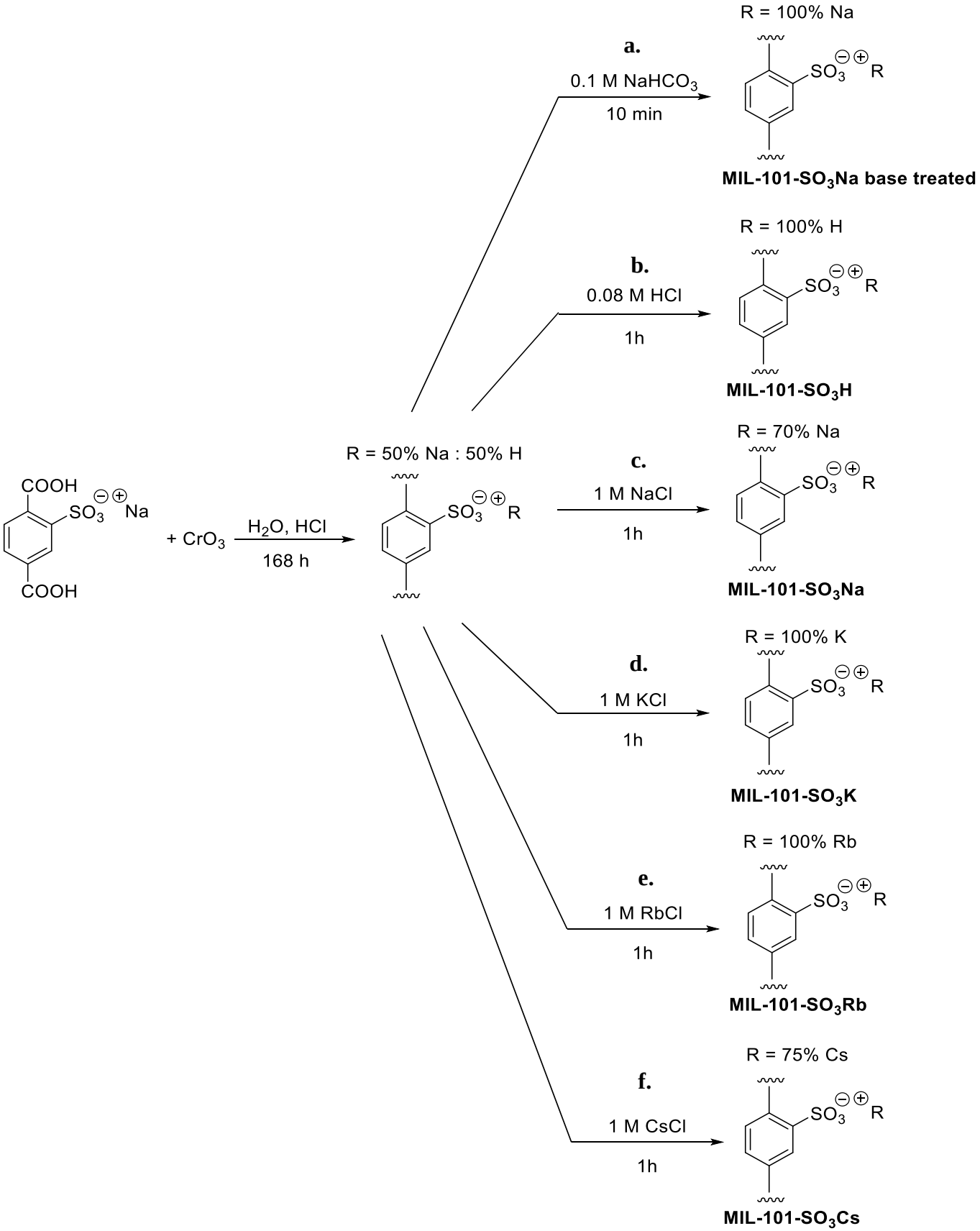

Figure 3.5 Synthesis of MIL-101-SO_3X and PSM for incorporation of **a.** sodium **b.** acid **c,d,e,f.** alkali metals

exchanged with as little as 5 equivalents of potassium chloride. Based on these studies leveraging Le Chatelier's principle, the exchange of as-synthesized MIL-101-SO_3X to materials with full incorporation of sodium, potassium, and rubidium was possible with slightly lower loadings for cesium (**Figure 3.5c,d,e,f**). Notably, these substituted materials contain no excess chloride and maintain crystallinity in all samples (**Figure 3.10**). FTIR spectra of the PSM MOFs show strong bands at approximately 1180, 1080, and 1025 cm^{-1}, all characteristic of the sulfonate group. Interactions between the sulfonate group and bound cation are not readily detectable by IR in this series of structures, and analogous results have previously been reported in similar systems (**Figure 3.11**).[15] One important feature is that while each cation can fully be incorporated starting from the as-synthesized material, the incorporation steps can also be performed sequentially, allowing for rapid and full conversion of a single material to several

	Equiv KCl	K:S (±0.05)	Na:S (±0.06)	Cl:S (±0.04)
As Synthesized MIL-101-SO_3X	20	0.95	0.00	0.00
As Synthesized MIL-101-SO_3X	10	0.80	0.06	0.00
As Synthesized MIL-101-SO_3X	5	0.62	0.00	0.00
As Synthesized MIL-101-SO_3X	1	0.41	0.00	0.00
Base Treated* MIL-101-SO_3X	20	1.10	0.00	0.08
Base Treated* MIL-101-SO_3X	10	1.05	0.00	0.04
Base Treated* MIL-101-SO_3X	5	1.03	0.00	0.00
Base Treated* MIL-101-SO_3X	1	0.77	0.06	0.05

Table 3.2 Potassium loading with potassium chloride at various molar equivalents of as synthesized and pretreated MIL-101-SO_3X. *Base treated material was treated for 10 min in 5ml 0.1M $NaHCO_3$ followed by 3 X 40ml washes with H_2O

different materials (**Figure 3.6**). This is, to our knowledge, the first example of incorporation of potassium, rubidium and cesium cations into MIL-101-SO_3X.

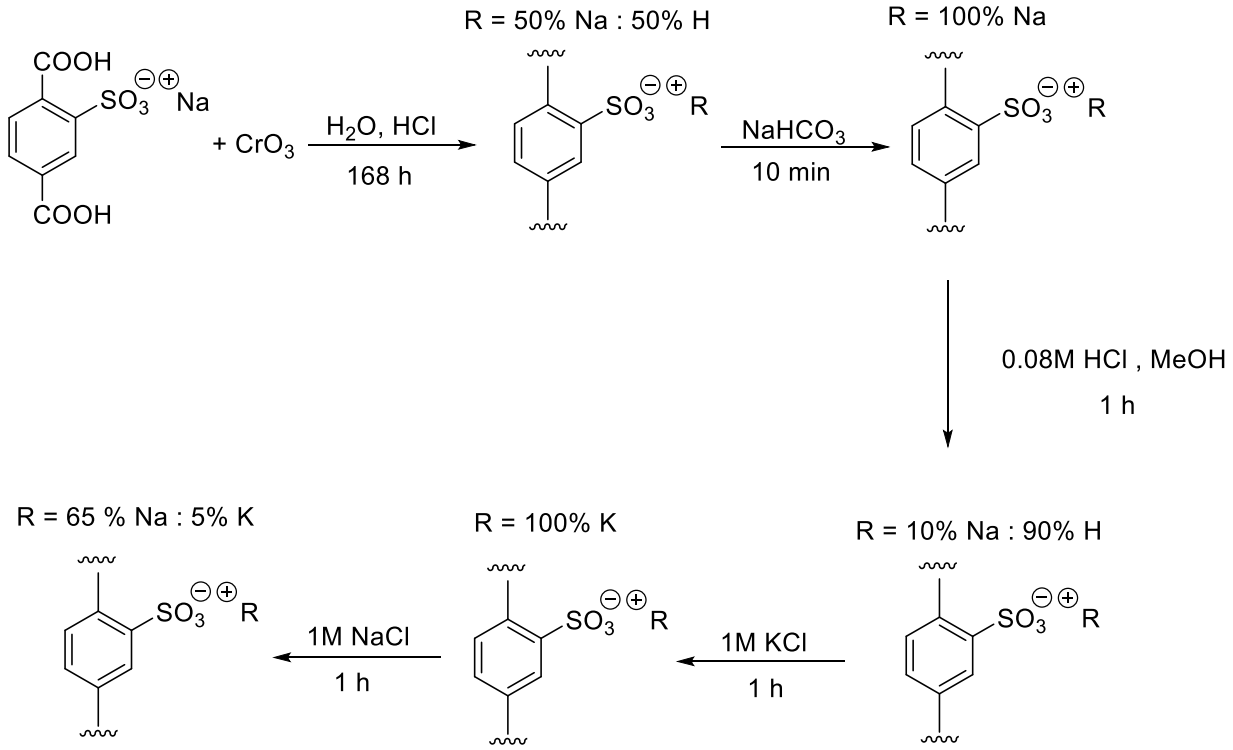

Figure 3.6 Synthesis and continuous treatment of MIL-101-SO_3X for facile generation of cation loaded materials

3.2.2 Applications of Cation Loaded MIL-101-SO_3X

Based on the previous observation that water plays a role in both separations and catalytic applications in MIL-101-SO_3X we sought to investigate the water sorption of our prepared materials. Reports by Guo et al. evaluate MIL-101 and MIL-101-SO_3H, referred to in this manuscript as "as-synthesized MIL-101-SO_3X", as sorbents for air dehumidification.[23] They conclude that the addition of sulfonate lowers the total water capacity of MIL-101 by partial pore volume displacement, but also changes the two-step breakthrough of MIL-101 to a one-step curve.[23] MIL-101-SO_3Cs appears to uptake 30% more water by wt than MIL-101-SO_3H. The cesium loaded material also shows two rapid adsorption steps, one at 25% and another at 35% relative humidity, alternative to the protonated MOF which shows only one rapid adsorption step at 35% relative humidity. This difference in adsorption can be attributed to various pore sizes adsorbing favorably at different relative humidity or an initial hydration of the cation followed by sorption at the MOF pores.

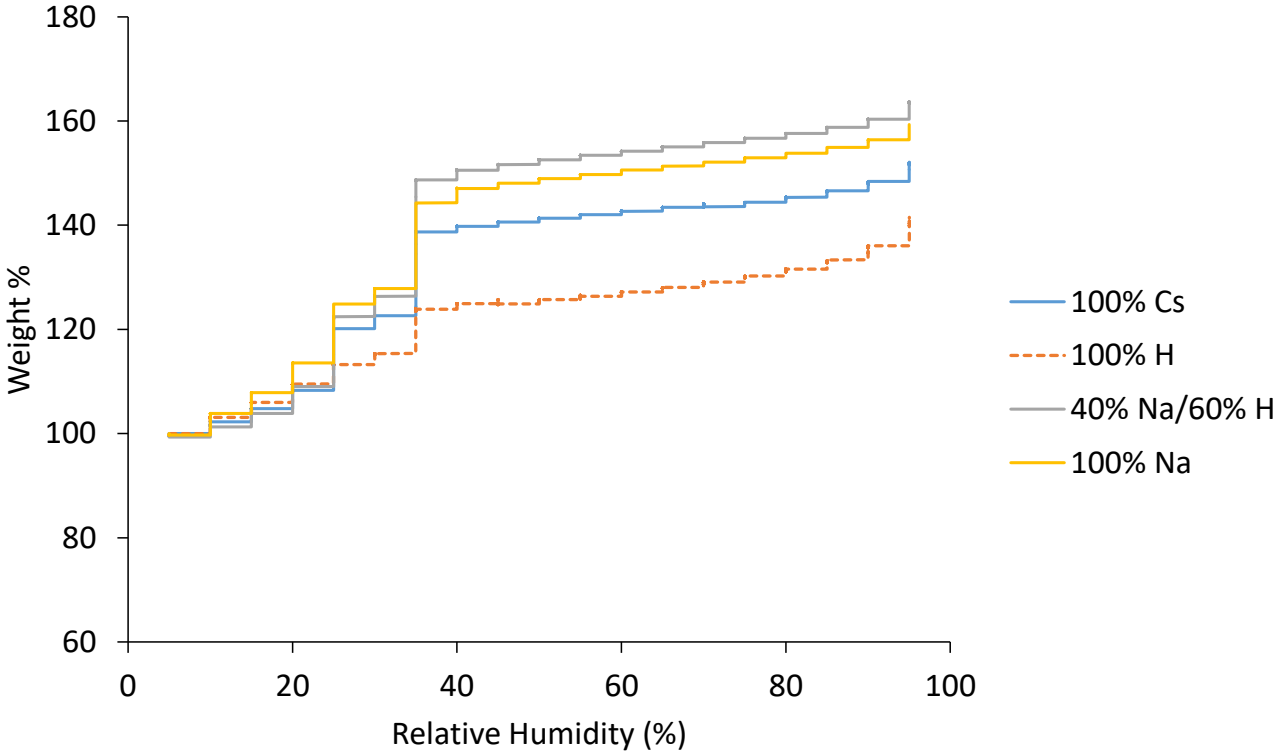

Figure 3.7 Dynamic vapor sorption of fully protonated, as synthesized, sodium loaded and cesium loaded MIL-101-SO_3X

Separations with MOFs are based on a combination of size exclusion and electrostatic interactions. The sheer scope of available MOFs makes it possible to find a sorbent with uniform pore size ranging from microporous to mesoporous for a variety of applications. Separations of molecules with similar kinetic radii, however, requires tuning of pore electronics to differentiate the sorption properties of the molecules. When considering exclusively electronic properties, most MOFs can be divided into two categories: those that contain coordinatively unsaturated sites (CUS) and those that do not. Examples of materials without CUS are MOF-5 or UiO-66; these materials tend to show lower molecular retention times due to weaker π-π interactions in aromatic substrates and weaker dispersion forces in substrates without π systems (**Figure 3.8a**).[24-26] Materials that contain CUS, such as MIL-101 or HKUST-1, display strong π-metal interactions and have shown success in separations of sterically similar substrates (for example styrene and ethylbenzene).[24, 27] By addition of further interactions, through PSM of MOFs, we posit that it should be possible to increase retention for targeted substrates and allow for improved separations (**Figure 3.8b**). A previous report has shown MIL-101 to be a competent sorbent for separation of substituted aromatic compounds of industrial relevance.[27]

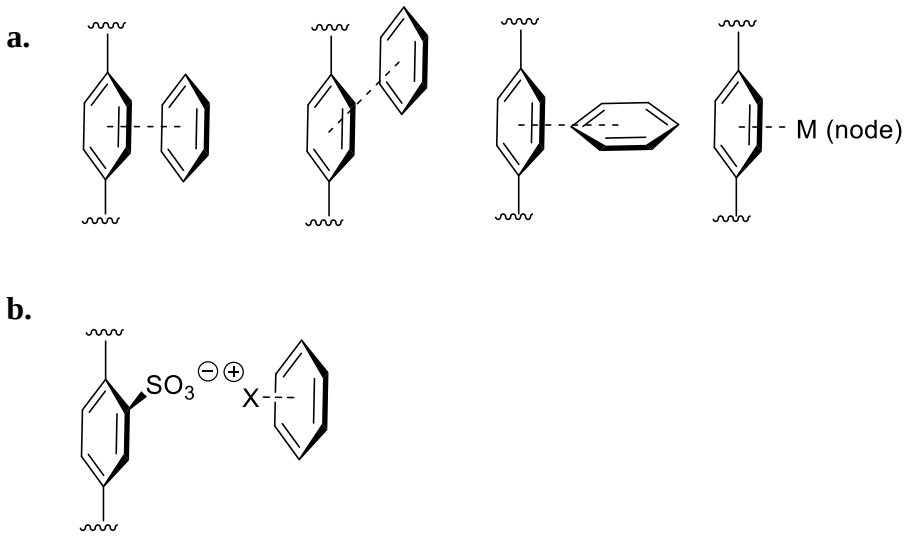

Figure 3.8 a. commonly cited intermolecular interactions between frameworks and substrates **b.** Proposed interaction (this work)

Initial investigations into MIL-101-SO_3X as sorbent resulted in broad peaks and high pressure drops across the column when run at flow rates of 1 ml/min or higher. However, trends can be seen in retention at flow rates as low as 0.5 ml/min. Incorporation of cesium shows an increase in retention for all substrates tested. Both proton and cesium loaded MOFs show the same order of elution: hexafluorobenzene, benzene, toluene, mesitylene. Cation-π interactions are strongest between electron rich aromatic rings and monoatomic cations with smaller radii such as sodium. The trend observed is opposite of the expected interaction strength, suggesting that the sorbent is not interacting directly with the cation but instead with the solvent shell formed upon exposure to water. Uniformity of particle size needs to be increased to improve column efficiency and improve peak shape.[28] Peak broadening could also be caused by column packing issues leading to substrate channeling.

Applications of cation substituted materials are extensive including catalysis, where the role of cation-π interactions has been extensively investigated.[29] MOFs can provide cation-π interactions in a confined geometry leading to high reactivity and selectivity. Ramamurthy et. al. were able to show that incorporation of alkali metals into zeolites increased cis/trans selectivity in the photoisomerization of diphenylcyclopropane. The strong cation-π binding of small cations, sodium and lithium, leads to 90% conversion to the desired product.[30] Similar reactions could be performed in cation loaded MOFs leading to catalysts with higher surface area and more defined catalytic sites than zeolites. Furthermore, Doughtery was able to show computationally that in the presence of water, sodium binds water selectively over benzene. This interaction is reversed for potassium, which binds benzene selectively even in the presence of water.[31] This suggest that selectivity of catalysts could be tuned using a specifically loaded cation and to enable selectivity switching based on incorporated water.

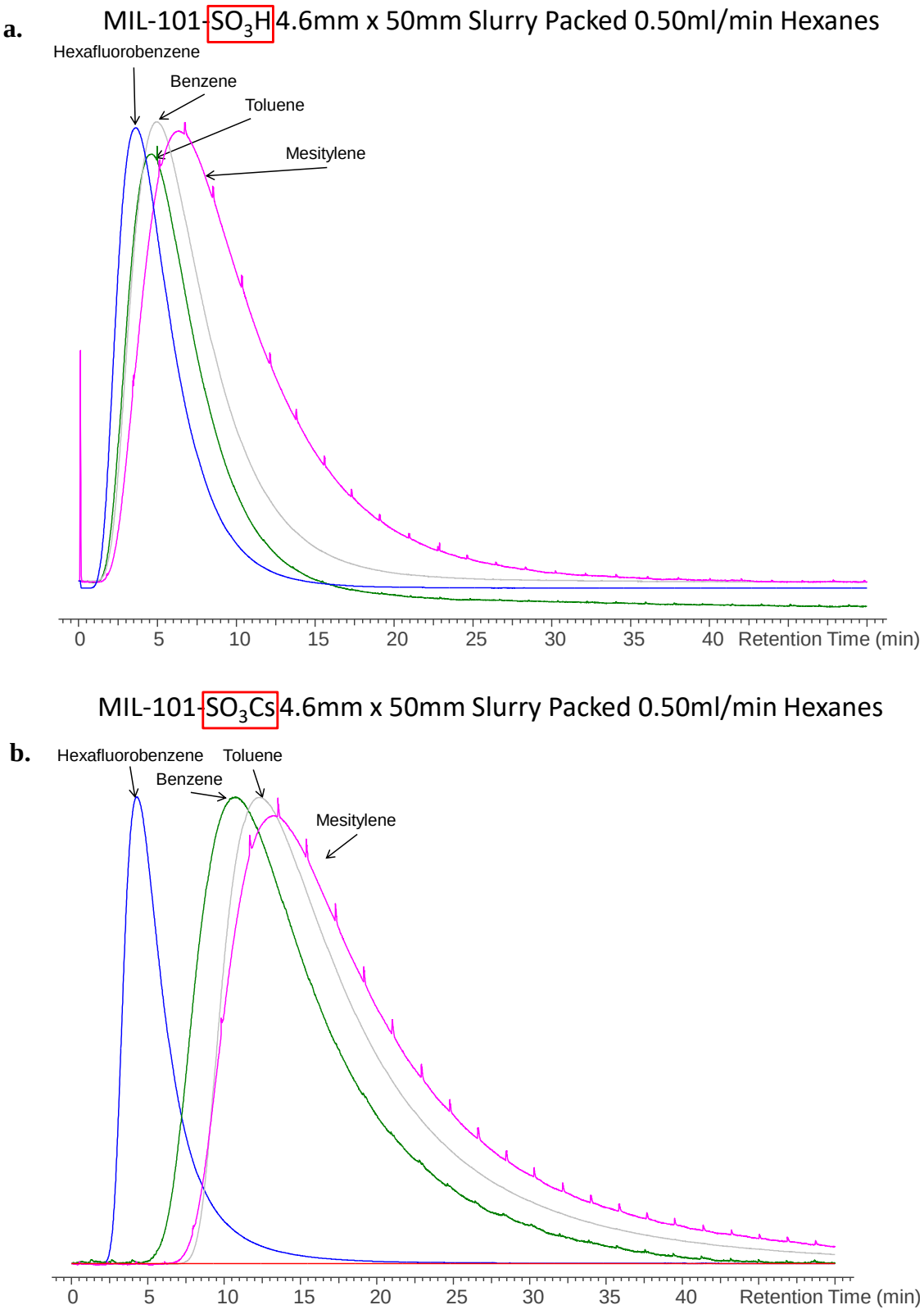

Figure 3.9 a. HPLC trace for fully protonated MIL-101-SO_3X **b.** HPLC trace for fully cesium exchanged MIL-101-SO_3X

3.3 Conclusions

Post synthetic cation loading in MIL-101-SO_3X was thoroughly investigated using various alkali metal cations as a model system. MIL-101-SO_3X could be generated with 100% incorporation of sulfonic acid or a range of alkali metal cations. The exchange of cations is facile, allowing complete conversion between cations in an hour. Deprotonation of sulfonic acids within the material is possible by two strategies, either high equivalents of desired cation or a brief treatment with base followed by cation exchange. The effect of anions on loading can be directly related to the sensitivity of the material to degradation by base and the ability of base to deprotonate sulfonic acids. Some applications for these materials have been preliminarily investigated, including separations, catalysis and water sorption. Future work will be focused on further investigating applications of cation loaded MOFs.

3.4 Experimental Methods

3.4.1 Synthesis of MIL-101(Cr)-SO_3X

MIL-101-SO_3 was synthesized according to a modified procedure.[32] Monosodium 2-sulfoterephthalic acid (6.7 g, 25 mmol) and chromium trioxide (2.5 g, 25 mmol) were added to a 250 ml jar charged with 100 ml deionized water. Concentrated hydrochloric acid (1.5 ml, 17.5 mmol) was added. The mixture was sealed and sonicated until clear and the solution displayed a dark brown-red color. The solution was divided evenly into 10 × 20 ml Teflon pressure vessels. The vessels were sealed and placed in a 180 °C oven for 7 days. The solids were collected by centrifugation and combined into 2 × 50 ml centrifuge tubes. The solids were washed with water followed by vigorous agitation and placed on a shaker for 2 hours. This washing procedure was

repeated 3 times. Fresh water was added and the mixture placed on an orbital shaker at 120 rpm, overnight. The solids were again collected and washed with ethanol as above before being soaked in ethanol overnight. The solids were then collected and dried at room temperature under vacuum overnight.

3.4.2 Cation-exchange in MIL-101-SO_3X

A 2 ml aliquot of 0.1M $NaHCO_3$ was added to a vial containing 50 mg MIL-101-SO_3. The mixture was placed on a shaker for 10 min before being centrifuged @ 5000 rpm for 10 min. The supernatant was decanted and the solids washed with 4 ml DI H_2O × 3. This procedure was scaled 10 times to generate sufficient quantities for column packing with no noticeable change in material powder X-ray diffraction pattern (PXRD) or cation loading. This material is referred to as MIL-101-SO_3Na.

A 1.0 M solution of XCl (X = Na, K, Rb or Cs) in water was placed into a 20 ml vial charged with 500 mg of MIL-101-SO_3. The mixture was placed on an orbital shaker at 120 rpm for 1 hour. The supernatant liquid was removed by centrifugation and the solids were washed with water followed by vigorous agitation and placed on a shaker for 1 hours. This washing procedure was repeated 3 times. The solids were then collected and activated by drying at ambient temperature under vacuum overnight.

3.4.3 Analysis of MIL-101-SO_3X (X = H, Na, K, Rb, Cs)

Powder X-ray Diffraction (PXRD) data were recorded at room temperature PANalytical Empyrean diffractometer using Cu-Kα radiation (λ = 1.54187 Å) and operating at 45 kV and 40 mA between 2 and 30° 2θ with a scan speed of 0.03 °/s and a step size of 0.017. Samples were measured on a glass microscope slide in an aluminum holder.

X-ray Fluorescence (XRF) was collected on AR QUANT'X EDXRF Spectrometer. Data was processed using Uniquant ED 6.27. Custom Kappa values were generated from iterative refinement of a parent Kappa list to give calibrations within 1% of known weight % ratios in alkali metal chloride salts. Kappa is defined as follows:

$$Kappa\left[\frac{cps}{0.1mg}\right] = \frac{Net\ intensity\ [cps] * Matrix\ Mu}{Area\ [mm^2] * concentration\ [wt\%]}$$

A template accounting for carbon, hydrogen and oxygen mass in the MOF linker was used to obtain more accurate ratios.

Dynamic Vapor Sorption isotherms were generated at 25 °C using a TA Instruments Q5000 SA. The Q5000 is equipped with a thermobalance and an autosampler. The instrument was calibrated using sodium bromide deliquescence. All experiments were conducted using metal-coated quartz pans. MOF was dried at ambient temperature overnight before the experiments. The procedure involved equilibration at 5% relative humidity (RH), followed by 5% steps of RH between 5-95% RH. Equilibrium was assumed to be established when there was a weight change of no more than 0.01% over a period of 5 min., with a maximum dwell time of 180 min. Isotherms were analyzed using TA Universal Analysis 2000, V 4.5A.

3.4.4 Typical Procedure for HPLC Separation

A slurry of 5 ml dichloromethane (DCM) and 500 mg MIL-101-SO_3X (X = Li, Na, K, Rb or Cs) was packed into a 4.6 × 50 mm stainless steel HPLC column. The column was treated with DCM for 30 min at a flow rate of 0.5ml/min. The column was treated with hexanes at a flow rate of 0.5ml/min until DCM was no longer detected by UV/Vis. A 5 µl aliquot of sample

was injected into 0.5 ml/min flow of hexanes. Full UV/Vis spectra were obtained for each sample.

3.5 Supplemental Figures

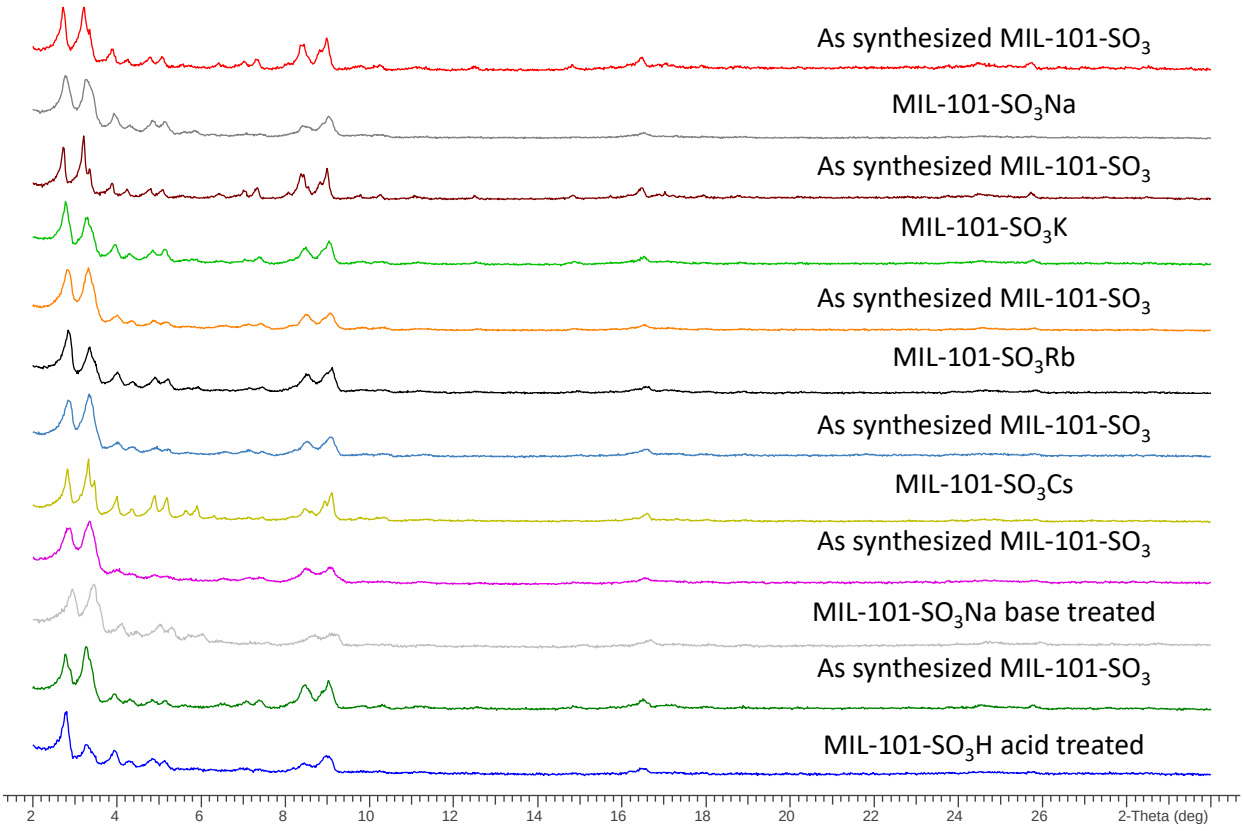

Figure 3.10 PXRD patterns of pre- and post- treated MIL-101-SO_3X

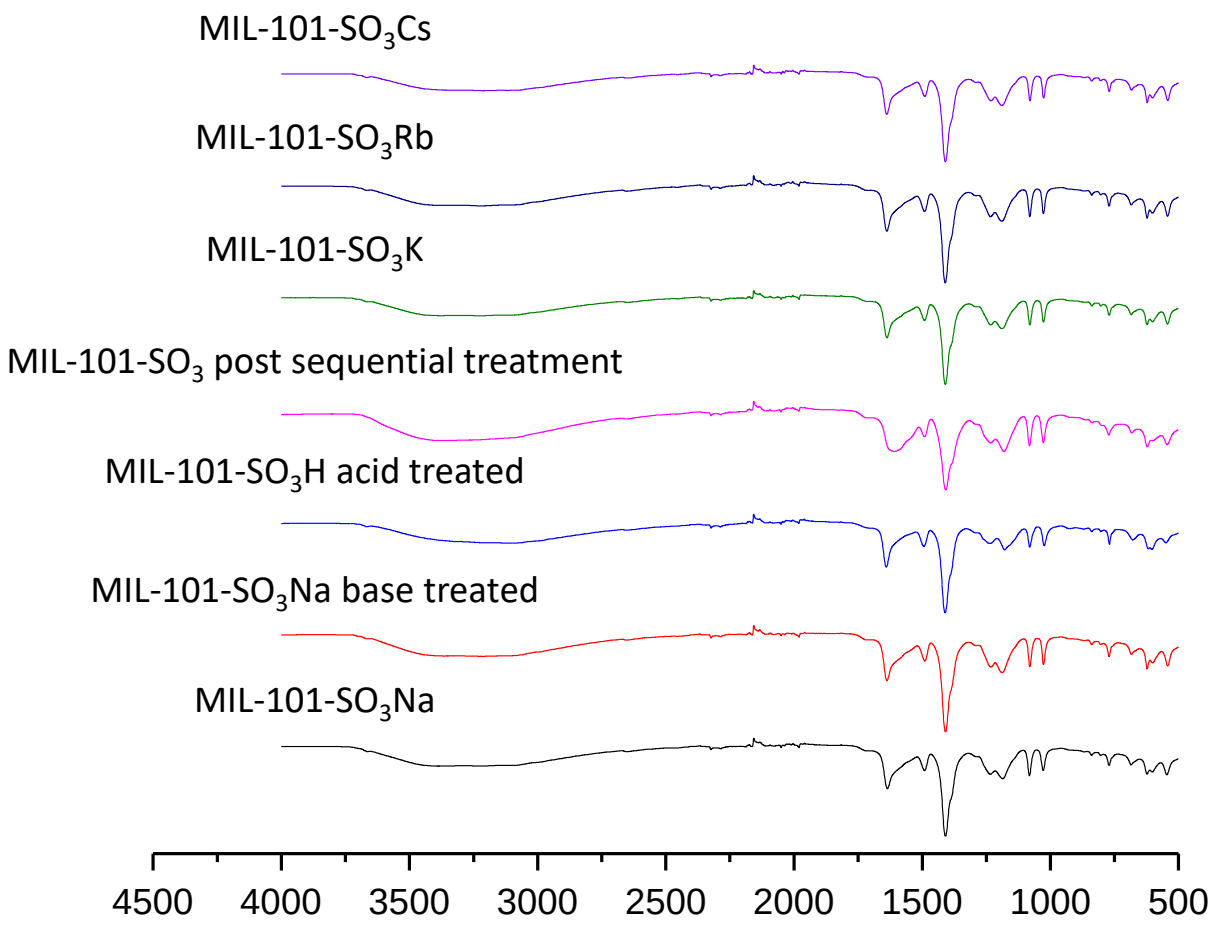

Figure 3.11 FTIR of treated MIL-101-SO_3X

3.6 References

1. B. R. James, J. A. Boissonnault, A. G. Wong-Foy, A. J. Matzger and M. S. Sanford, *RSC Advances* **2018**, *8*, 2132–2137.
2. Z. Y. Gu and X. P. Yan, *Angewandte Chemie* **2010**, *49*, 1477-1480.
3. J. R. Li, J. Sculley and H. C. Zhou, *Chemical reviews* **2012**, *112*, 869-932.
4. Z. R. Herm, E. D. Bloch and J. R. Long, *Chemistry of Materials* **2013**, *26*, 323-338.
5. W. W. Zhao, C. Y. Zhang, Z. G. Yan, L. P. Bai, X. Wang, H. Huang, Y. Y. Zhou, Y. Xie, F. S. Li and J. R. Li, *J Chromatogr A* **2014**, *1370*, 121-128.
6. W. Qin, M. E. Silvestre, Y. Li and M. Franzreb, *J Chromatogr A* **2016**, *1432*, 84-91.
7. J. Liu, L. Chen, H. Cui, J. Zhang, L. Zhang and C. Y. Su, *Chemical Society reviews* **2014**, *43*, 6011–6061.
8. H.-Y. Cho, D.-A. Yang, J. Kim, S.-Y. Jeong and W.-S. Ahn, *Catalysis Today* **2012**, *185*, 35-40.
9. J. Lee, O. K. Farha, J. Roberts, K. A. Scheidt, S. T. Nguyen and J. T. Hupp, *Chemical Society reviews* **2009**, *38*, 1450-1459.
10. B. F. Hoskins and R. Robson, *Journal of the American Chemical Society* **1990**, *112*, 1546–1554.
11. S. M. Cohen, *Chemical reviews* **2012**, *112*, 970-1000.
12. D. T. Genna, L. Y. Pfund, D. C. Samblanet, A. G. Wong-Foy, A. J. Matzger and M. S. Sanford, *ACS Catalysis* **2016**, *6*, 3569–3574.
13. A. Grigoropoulos, A. I. McKay, A. P. Katsoulidis, R. P. Davies, A. Haynes, L. Brammer, J. Xiao, A. S. Weller and M. J. Rosseinsky, *Angewandte Chemie* **2018**, *57*, 4532-4537.
14. Y. Takashima, Y. Fukuhara, Y. Sato, T. Tsuruoka and K. Akamatsu, *European Journal of Inorganic Chemistry* **2017**, *2017*, 5344-5349.
15. W.-J. Sun, F.-G. Xi, W.-L. Pan and E.-Q. Gao, *Molecular Catalysis* **2017**, *430*, 36-42.
16. D. T. Genna, A. G. Wong-Foy, A. J. Matzger and M. S. Sanford, *Journal of the American Chemical Society* **2013**, *135*, 10586–10589.
17. S. Yang, G. S. B. Martin, J. J. Titman, A. J. Blake, D. R. Allan, N. R. Champness and M. Schröder, *Inorganic chemistry* **2011**, *50*, 9374-9384.
18. S. Yang, X. Lin, A. J. Blake, G. S. Walker, P. Hubberstey, N. R. Champness and M. Schröder, *Nature chemistry* **2009**, *1*, 487.
19. Y. Zhang, B. Li, R. Krishna, Z. Wu, D. Ma, Z. Shi, T. Pham, K. Forrest, B. Space and S. Ma, *Chemical communications* **2015**, *51*, 2714-2717.
20. P. Ramaswamy, R. Matsuda, W. Kosaka, G. Akiyama, H. J. Jeon and S. Kitagawa, *Chemical communications* **2014**, *50*, 1144-1146.
21. A. J. Howarth, Y. Liu, P. Li, Z. Li, T. C. Wang, J. T. Hupp and O. K. Farha, *Nature Reviews Materials* **2016**, *1*, 1–15.
22. Y. X. Zhou, Y. Z. Chen, Y. Hu, G. Huang, S. H. Yu and H. L. Jiang, *Chemistry – A European Journal* **2014**, *20*, 14976-14980.
23. P. Guo, A. G. Wong-Foy and A. J. Matzger, *Langmuir* **2014**, *30*, 1921-1925.
24. R. Ahmad, A. G. Wong-Foy and A. J. Matzger, *Langmuir* **2009**, *25*, 11977–11979.
25. H.-Y. Kim, S.-N. Kim, J. Kim and W.-S. Ahn, *Materials Research Bulletin* **2013**, *48*, 4499-4505.

26. M. A. Moreira, J. C. Santos, A. F. P. Ferreira, J. M. Loureiro, F. Ragon, P. Horcajada, K.-E. Shim, Y.-K. Hwang, U. H. Lee, J.-S. Chang, C. Serre and A. E. Rodrigues, *Langmuir* **2012**, *28*, 5715-5723.
27. C. X. Yang and X. P. Yan, *Anal Chem* **2011**, *83*, 7144–7150.
28. S. Chen, X. X. Li, L. Shu, P. Somsundaran and J. R. Li, *J Chromatogr A* **2017**, *1510*, 25-32.
29. C. R. Kennedy, S. Lin and E. N. Jacobsen, *Angewandte Chemie International Edition* **2016**, *55*, 12596-12624.
30. P. Lakshminarasimhan, R. B. Sunoj, J. Chandrasekhar and V. Ramamurthy, *Journal of the American Chemical Society* **2000**, *122*, 4815-4816.
31. R. Kumpf and D. Dougherty, *Science* **1993**, *261*, 1708-1710.
32. G. Akiyama, R. Matsuda, H. Sato, M. Takata and S. Kitagawa, *Adv Mater* **2011**, *23*, 3294-3297.

Chapter 4

Post-Synthetic Sulfonation of Metal-Organic Frameworks

4.1 Introduction

Metal-organic frameworks are a subset of coordination polymers that are distinguished by their crystalline 2D or 3D structure.[1] The crystalline network seen in MOF structures produces many empty spaces, or pores, which can be utilized in a variety of ways. In fact, MOFs have exhibited the highest experimental Brunauer–Emmett–Teller (BET) surface areas of any porous materials reported to date, leading to intense interest in their sorbent properties.[3] While traditional porous materials such as activated carbon can have surface areas as high as 3200 m^2/g,[4] NU-110, one of the highest surface area materials ever reported, has an average BET surface area upwards of 7000 m^2/g.[3] This high surface area drives the study of MOFs for use in applications such as gas storage[5, 6] and separations.[7, 8]

Thousands of MOF structures have been reported in literature;[9, 10] however, the rational design of specific materials can pose challenges.[11] While many combinations of linker and node are known, the typical conditions needed for MOF synthesis and crystal self-assembly can be high temperature and chemically harsh.[12-14] Conditions for these MOF syntheses can also be specific and highly sensitive to changes in temperature and pH.[11] Ideally, syntheses would be easy to adapt for the incorporation of new functional groups in the MOF, but in reality, the addition of certain groups often requires a complete re-optimization of the reaction conditions, a

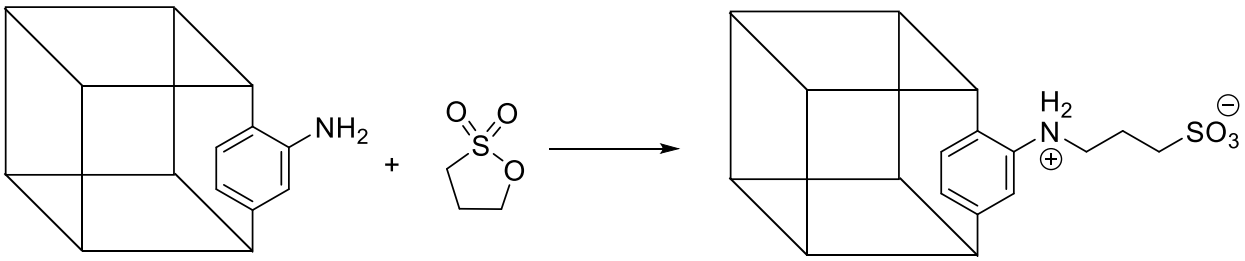

Figure 4.1 Post-synthetic ring opening reaction of IRMOF-3 (adapted from [2])

costly and time consuming process. Therefore, the incorporation of functional groups can be challenging with conventional synthetic approaches.

Post-synthetic modification (PSM) can serve to install desired functional groups after initial synthesis to avoid challenges with self-assembly that occur with some MOFs.[15-19] With PSM, a MOF framework can be crystallized, and subsequent reactions can replace or install novel functional groups to the system.[15] This approach also has some limitations, as the functionalization must be mild enough to maintain the crystallinity of the MOF. However, PSM reactions can be easier to tune than re-engineering the synthetic pathway to the desired MOF. In this Chapter, we describe the use of this approach to install sulfonates within the frameworks of several known MOFs and perform cation exchange to ultimately synthesize an ionically bound, single-site catalyst within a series of porous, crystalline scaffolds.

The incorporation of acidic functional groups into MOFs enables the catalysis of several reactions. For example, Luan et. al. demonstrated the acetalization of a range of substrates with low loading of UiO-66- SO_3 as catalyst.[20] Additionally, the modified MOF catalysts show high selectivity for the synthesis of benzimidazole and benzothiazoles.[20] Other reported catalytic reactions include the tandem deacetalization–Knoevenagel of (dimethoxymethyl)benzene to 2-benzylidenemalononitrile and a similar strategy to convert (dimethoxymethyl)benzene to (2-

nitrovinyl)benzene. These reactions can serve as a starting point for further catalytic applications with bifunctionalized MOFs.

Sulfonate containing MOFs have also shown promise for applications in separations. Substitution of the cation associated with the sulfonate or ammonium functionality can lead to enhanced separations through cation-π interactions. For instance, Huang et al. demonstrated that the inclusion of silver into a MIL-101-SO_3 framework led to effective desulfurization of liquid fuels.[21] Sulfonates have long been used for separations in a variety of materials including silica[22, 23] and polymers.[24-26] Similar methods could be adapted to sulfonated MOF materials yielding novel ion exchange materials.

4.2 Results and Discussion

4.2.1 Post-Synthetic Modification of MOFs

Sulfonate groups have been shown in the literature to be capable of generating solid state acids upon incorporation in heterogeneous materials.[27-29] Acid-catalysed reactions of many substrates can occur with these functionalities; however, selectivity and control of the reactions can be difficult to achieve. Previously in the literature, sulfonate groups have been tethered to zeolites in order to utilize the mesoporous structures for improved control in these types of reactions. [30] Progress in the synthesis of MOFs has expanded in the past few decades, allowing for the production of a wide variety of porous frameworks. Additionally, MOFs allow for more tunability of active sites toward increasing catalyst activity and selectivity.[31] These MOF structures can be designed specifically for reaction selectivity based on the linker choice and pore size options more easily than zeolites.

Addition of sulfonate functionality to MOFs is rare because of the sensitivity of synthesis conditions to varying pH. Traditional aromatic sulfonation involves strong acid and high

temperatures, both which can cause degradation of MOF crystallinity, making this type of PSM only viable in highly stable MOFs. Alternatively, this functionality has been incorporated into MOFs through sultone opening, reported in amine functionalized MOF-5,[2] UiO-66,[20] and MIL-101(Cr).[32] MOF-5 and UiO-66 both suffer from poor stability toward water and acid, limiting their applications. MIL-101(Cr), while stable to acid and water, cannot be synthesized directly using the amine functionalized linker and must instead be nitrated and reduced to generate the amine moiety.[33] Furthermore, MIL-101(Cr) contains coordinatively unsaturated sites (CUS) that can lead to undesired substrate binding and catalytic reactions.[34, 35] We aim to expand on this area and show that this method can be adapted to a larger range of materials including different node metals and mixed linker systems. Additionally, by combining this sultone functionalization with previous reports by Genna et. al., [36, 37] we hope to generate ionically bound single-site catalysts in porous, high surface area materials.

The chosen systems of IRMOF-3,[38] UiO-66-NH_2,[39] MIL-53-NH_2,[40] and UMCM-1-NH_2[19] were synthesized according to literature procedures. MOFs with an amine group incorporated at the linker were targeted, as this would provide a functional handle for PSM. Next, the MOFs were reacted with 1,3-propanesultone at 45 °C for 16 h (**Figure 4.1**). Subsequent washings with dimethylformamide (DMF) and methylene chloride (CH_2Cl_2) and drying under vacuum, yield functionalized MOF crystals. Previously reported materials that are re-explored here (IRMOF-3-SO_3 and UiO-66-NH_2-SO_3) display some disadvantages but are valuable for evaluating ionic loading of single site catalysts. To our knowledge, this is the first example of post synthetic sultone opening in MIL-53-NH_2 and UMCM-1-NH_2.

4.2.2 Characterization of MOFs

Powder X-ray diffraction (PXRD) patterns of sulfonated materials match closely with materials synthesized with terephthalic acid and 2-aminoterephthalic acid as linker. (**Figures 4.4, 4.6, 4.8, 4.10**) This suggest the functionalization conditions are sufficiently mild to maintain MOF structure. MOFs were digested in sodium deuteroxide/D_2 and nuclear magnetic resonance (NMR) spectra provided diagnostic peaks for determination of functionalization. (**Figure 4.2**) ^{1}H NMR shows approximately 30% of aryl amines have been functionalized in UiO-66-NH_2, UMCM-1-NH_2, and MIL-53-NH_2 (**Figures 4.7, 4.9, 4.11**). Increased amounts of functionalization were seen in IRMOF-3 under identical functionalization conditions, up to 60%.

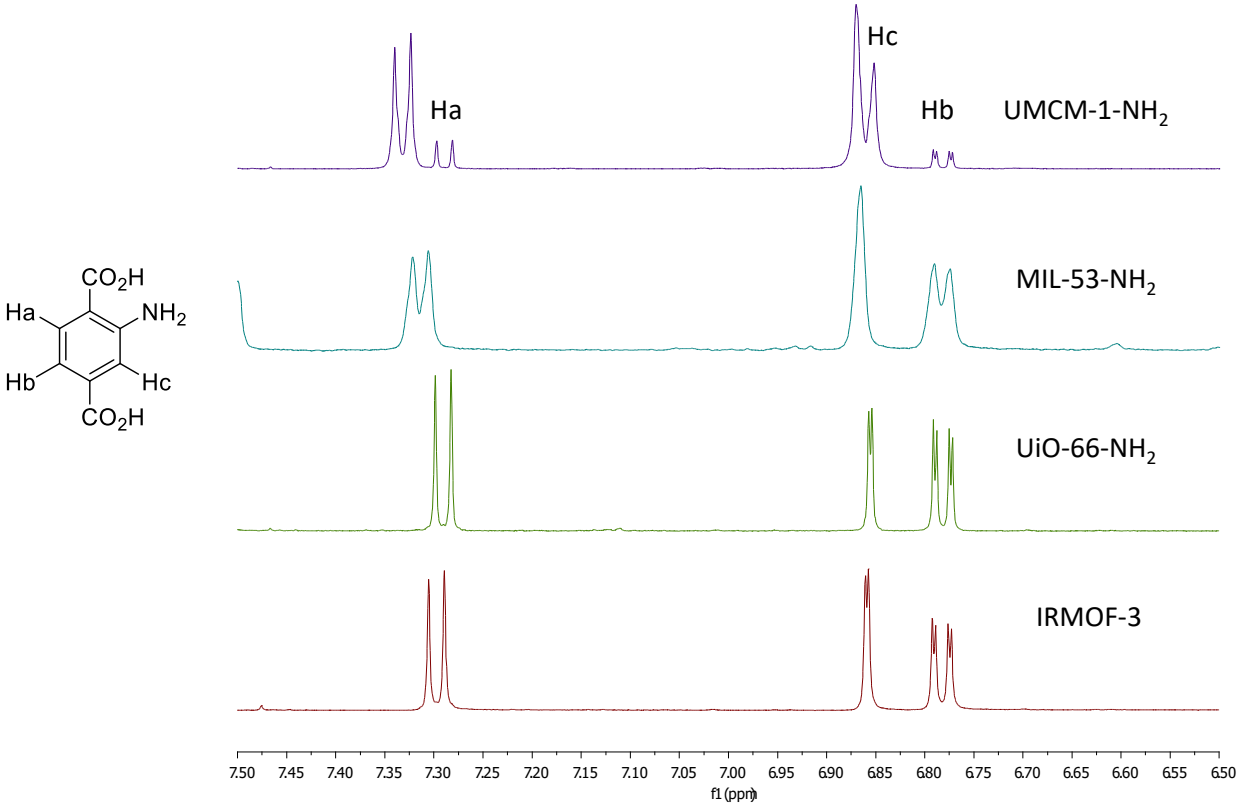

Figure 4.2 ^{1}H NMR of chemically digested MOFs highlighting the diagnostic aromatic peaks in the amino linkers.

Sulfonate groups have been shown to allow the installation of ionically bound single site catalysts.[36] Along these lines, Crabtree's catalyst, $[Pd(CH_3CN)_2COD]BF_4$ and $[Rh(CH_3CN)_2COD]BF_4$, COD = 1,5-cyclooctadiene, were loaded into the functionalized MOFs.

	%wt loading Crabtree's catalyst	%wt loading $[Pd(CH_3CN)_4]$ $(BF_4)_2$	%wt loading $[Rh(CH_3CN)_2(COD)]$ BF_4
UiO-66	1.0	<0.5	—
UiO-66-NH_2	1.3	<0.5	<0.5
UiO-66-SO_3	2.3 (13.4)	1.2 (7.5)	<0.5 (7.3)
MIL-53	<0.5	<0.5	—
MIL-53-NH_2	0.9	<0.5	—
MIL-53-SO_3	1.8 (16.4)	0.6 (9.8)	—
MOF-5	<0.5	<0.5	—
IRMOF-3	<0.5	1.0	<0.5
IRMOF-3-SO_3	1 (49.2)	1.3 (27.8)	<0.5 (26.9)
UMCM-1	<0.5	1.8	—
UMCM-1-NH_2	0.7	5.8	<0.5
UMCM-1-SO_3	0.9 (5.3)	7.8 (2.9)	2.4 (2.8)

Table 4.1 Catalyst loadings in PSM MOFs. Theoretical maximum loading if all sulfonates bind one metal ion listed in parenthesis

Typical loading involved suspending the MOF in a solution of catalyst in DMF for 3 days before thurough washing with DMF. Materials with incorporated sulfonate groups show increased weight percent loadings of catalyst metal. A wide range of catalysts were incorporated into the tested materials (**Table 4.1**). Pore clogging has previously been cited as a possible issue in sulfonated MOFs.[32] Even materials such as MIL-101-NH_2-SO_3, with pore windows of 30-34 Å[41], can show slow substrate diffusion.[32] MIL-53 is a channel MOF, displaying porosity in only a single dimension (**Figure 4.3a**) and UMCM-1 has a large central channel surrounded by smaller pores (**Figure 4.3b**). These unique structural features were expected to minimize pore obstruction. Nonetheless, experimental loading data show that high catalyst loading is still not possible with these materials. While this shows loading of catalyst is possible and improved by sulfonates, the exact nature of catalyst loaded is unknown. Due to steric restraints, presumably ligand shedding or at least counter ion shedding must take place before the metal can be incorporated. Higher Pd catalyst loading may be due to the weakly coordinated ligand

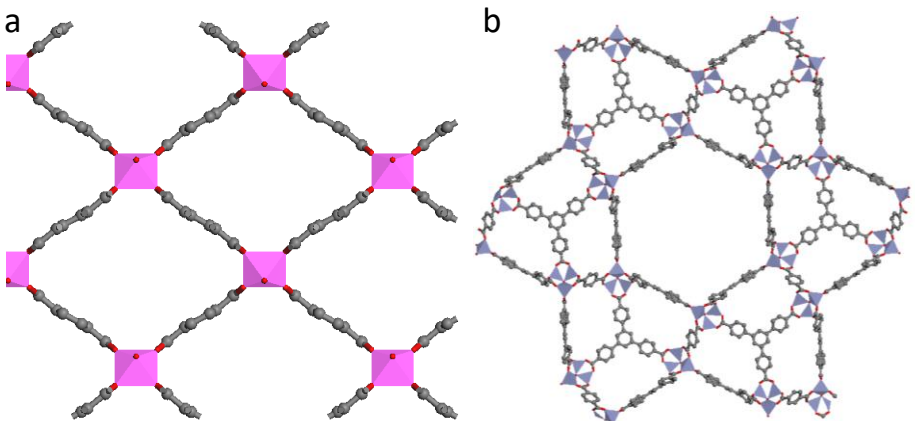

Figure 4.3a Structure of MIL-53 displaying MOF channels **b** Structure of UMCM-1 displaying large central channel surrounded by smaller pores

environment or decreased steric bulk of BF_4 relative to PF_6. UMCM-1 has the largest pore of all the MOFs tested allowing for more facile mass transport of the catalyst. The loading of UMCM-1 exceeds the theoretical maximum in some cases, suggesting the metal is not being bound exclusively at the sulfonate but may be deposited on the surface of the MOF or incorporated at the node.

Catalyst loadings in most cases was significantly lower than maximum possible based on incorporated sulfonate but future studies can be guided by our previous work in cation exchange. Loading of alkali metal cations in sulfonated MOFs is facile even over short time periods (1 h) and the same will be applicable in this PSM MOF as well. Excess equivalents of desired catalyst can result in increased loading for MIL-101(Cr)-SO_3X; while all the MOFs evaluated for PSM with propanesultone have smaller pore volume, they may exhibit the same behavior for catalyst with kinetic radii below the MOF pore window size. Additionally, it we have shown the treatment with base prior to cation loading can be beneficial for increasing loading amounts. This approach is applicable for MOFs that are stable to basic conditions such as MIL-101(Cr) but will rapidly degrade crystallinity of Zr and Zn based MOF making this approach non-viable.

Attempts at catalytic hydrogenation of 2,3-dimethyl-2-butene and styrene with loaded materials at 65 bar H_2 and 100 °C were unsuccessful in sealed batch reactions. We have several hypotheses for the lack of activity. Catalytically it has been shown that high sulfonate functionalization can lead to decreased.[32] This reduction in catalyst activity could originate from two sources. First, the pores could become occupied during functionalization, thus limiting substrate access to active sites. While the materials have large surface area, the arrangement of the functionalized groups is not fully known, and protrusion into the pore windows could block substrate diffusion. The second, less relevant in our case, arises from the zwitterionic nature of the loaded group containing both a positive ammonium and negative sulfonate. Another possible explanation is the catalyst loaded does not have the same ligand environment as the homogeneous catalyst leading to a species that is inactive for hydrogenation. Gas phase hydrogenation of propene was also attempted but an irreversible change in the catalyst took place during heating, most likely the reduction of the catalyst in the highly reducing H_2 atmosphere.

4.3 Conclusions

PSM of MOFs is a valuable strategy for the generation of a diverse set of materials. The incorporation of sulfonate group, previously rare in MOFs, was achieved across several materials with various metal nodes, pore sizes, and surface areas. Advancements in MOF design are continually increasing the stability of MOFs, making them an increasingly attractive target for industrial applications. Further study could yield applications in separations, catalysis, gas sorption, or batteries.

4.4 Experimental Methods

4.4.1 MOF synthesis

IRMOF-3 $Zn(NO_3)_2 \bullet 4H_2O$ (695 mg, 2.66 mmol) and 2-aminoterephthalic acid (96 mg, 0.53 mmol) were dissolved in 30 ml diethylformamide (DEF). The solution was sparged with N_2 for 10 minutes before being placed in an 85 °C oven for 4 days. The cubic crystals were collected by centrifugation, washed with dimethylformamide (DMF) (3 × 10 ml), followed by exchange with dichloromethane (3 × 10 ml) over a 3 day period. The crystals were dried at ambient temperature under vacuum overnight.

UiO-66-NH_2 $ZrCl_4$ (125 mg, 0.54mmol) was added to a 20 ml vial charged with 5 ml DMF and 1 ml conc. HCl, the mixture was sonicated until all solids were dissolved. 2-Aminoterephthalic acid (134 mg, 0.75 mmol) and 10 ml DMF were added to the solution and sonicated again until completely dissolved. The vial was placed in an 80 °C oven for 16 hours. The resulting solids were collected by centrifugation, washed with DMF (3 × 10 ml), followed by exchange with ethanol (3 × 10 ml) over a 3-day period. The crystals were dried at 90 °C under vacuum pressure overnight.

UMCM-1-NH_2 $Zn(NO_3)_2 \bullet 4H2O$ (2.83 g, 10.8mmol), 2-aminoterephthalic acid (0.49 g, 2.7 mmol), and Benzene-1,3,5-tribenzoic acid (BTB, 0.42 g, 0.97 mmol) were dissolved in 100 ml of DMF. The solution was divided evenly into 10 × 20 ml scintillation vials. The vials were placed in an aluminium heating block, and the block was heated at 85 °C for 2 days. The resulting solids were collected by centrifugation, washed with DMF (3 × 10 ml), followed by exchange with $CHCl_3$ (3 × 10 ml) over a 3-day period. The crystals were dried at 75 °C under vacuum pressure overnight.

MIL-53(Al)-NH_2 $Al(NO_3)_3$ •9H2O (787mg, 2.10mmol) was dissolved in 15 ml DMF. 2-aminoterephthalic acid (565 mg, 3.12 mmol) was dissolved in 15 ml DMF. The solutions were combined in a 50 ml jar then split evenly into two teflon lined reaction vessels. The vessels were placed in a 130 °C oven for 3 days. The resulting solids were collected by centrifugation, washed with acetone (3 × 10 ml). The acetone was removed under vacuum pressure at ambient temperature before being washed with methanol (3 × 10 ml) over a 3-day period. The crystals were dried at 110 °C under vacuum pressure overnight.

Sultone opening procedure was adapted from [20]. 50 mg of MOF was added to a vial charged with a 2 ml of neat 1,3-propanesultone or 0.085 mmol 1,3-propanesultone solution in $CHCl_3$. The vial was placed in a 45 °C oven for 16 hours. The resulting solids were collected by centrifugation, washed with DMF (3 × 2 ml), followed by exchange with $CHCl_3$ (3 × 2 ml) over a 3-day period. The crystals were dried using the above conditions for each specific material.

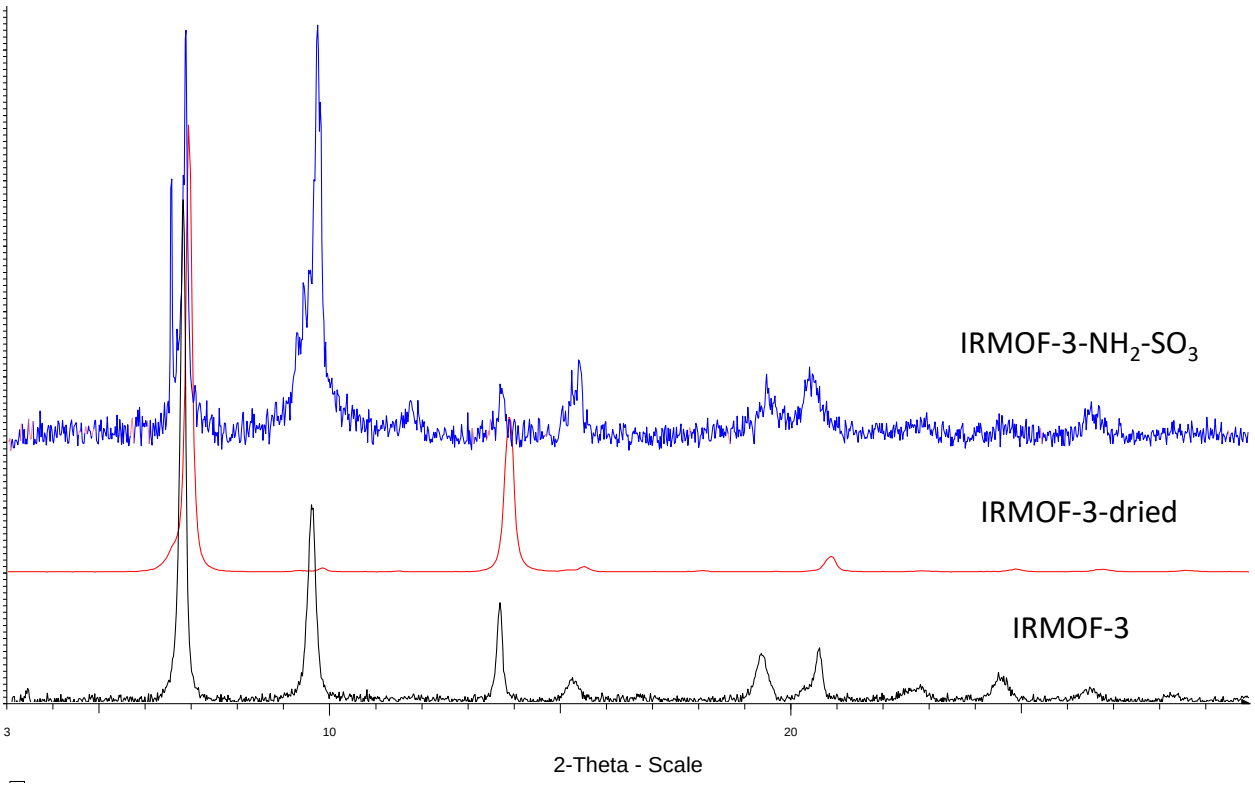

Figure 4.4 PXRD of IRMOF-3, IRMOF-3 that has been evacuated under vacuum (IRMOF-3-dried) and sulfonate functionalized IRMOF-3 (IRMOF-3-SO_3)

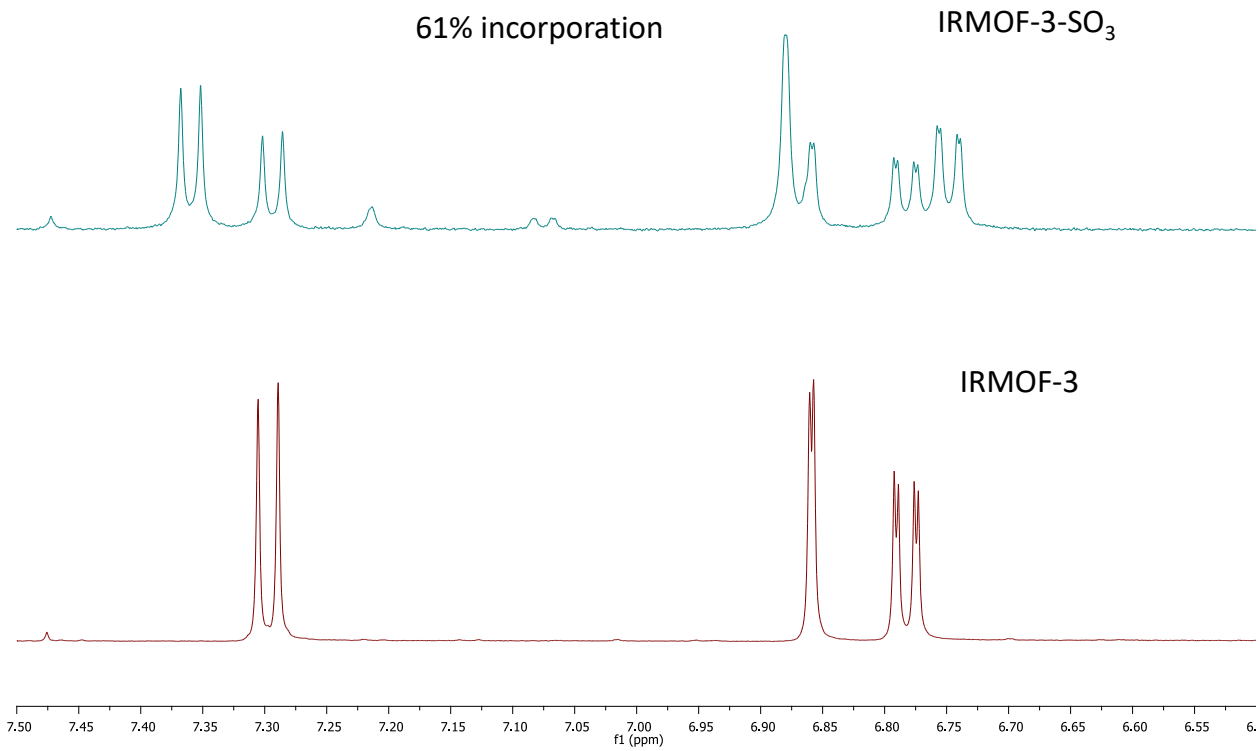

Figure 4.5 ^{1}H NMR of chemically digested IRMOF-3 and sulfonated functionalized IRMOF-3-SO_3 highlighting the diagnostic signals in the amino and sulfonate functionalized linker

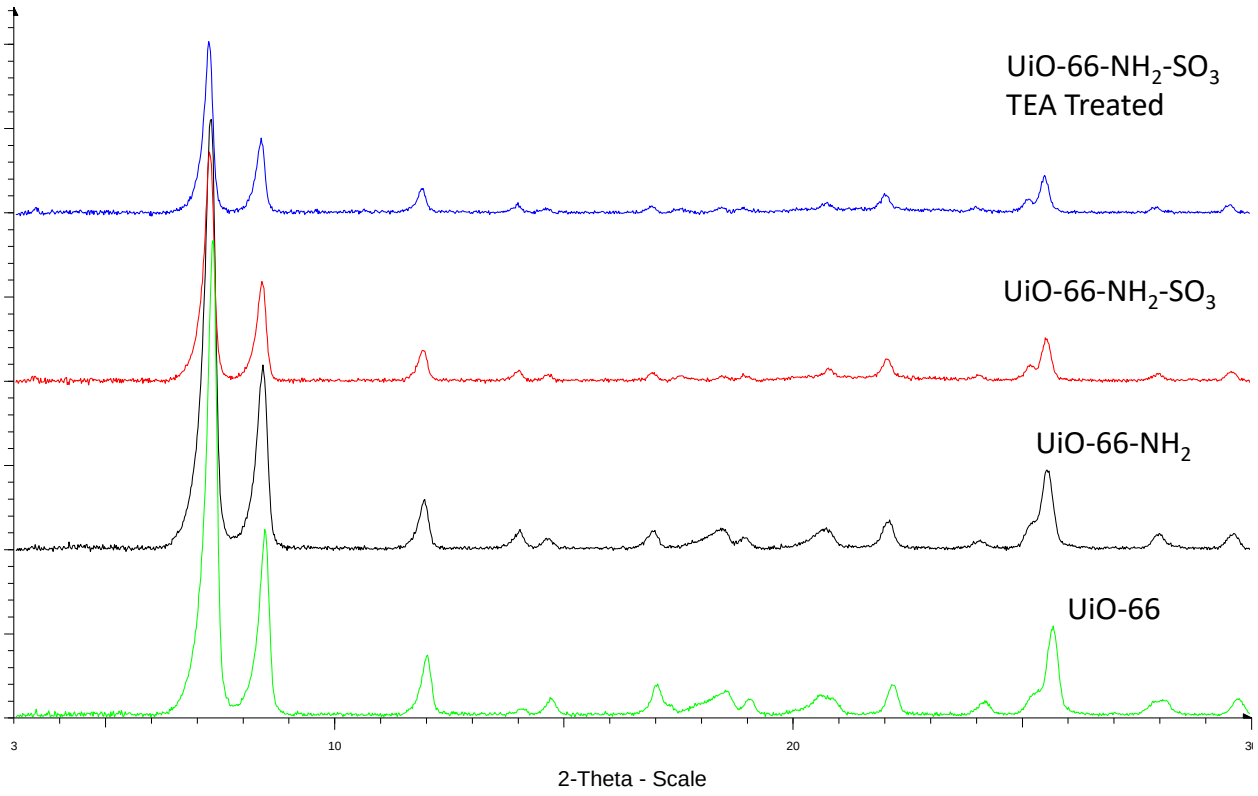

Figure 4.6 PXRD of UiO-66, UiO-66-NH_2, sulfonate functionalized UiO-66 (UiO-66-NH_2-SO_3) and UiO-66- NH_2-SO_3 treated with triethylamine (TEA)

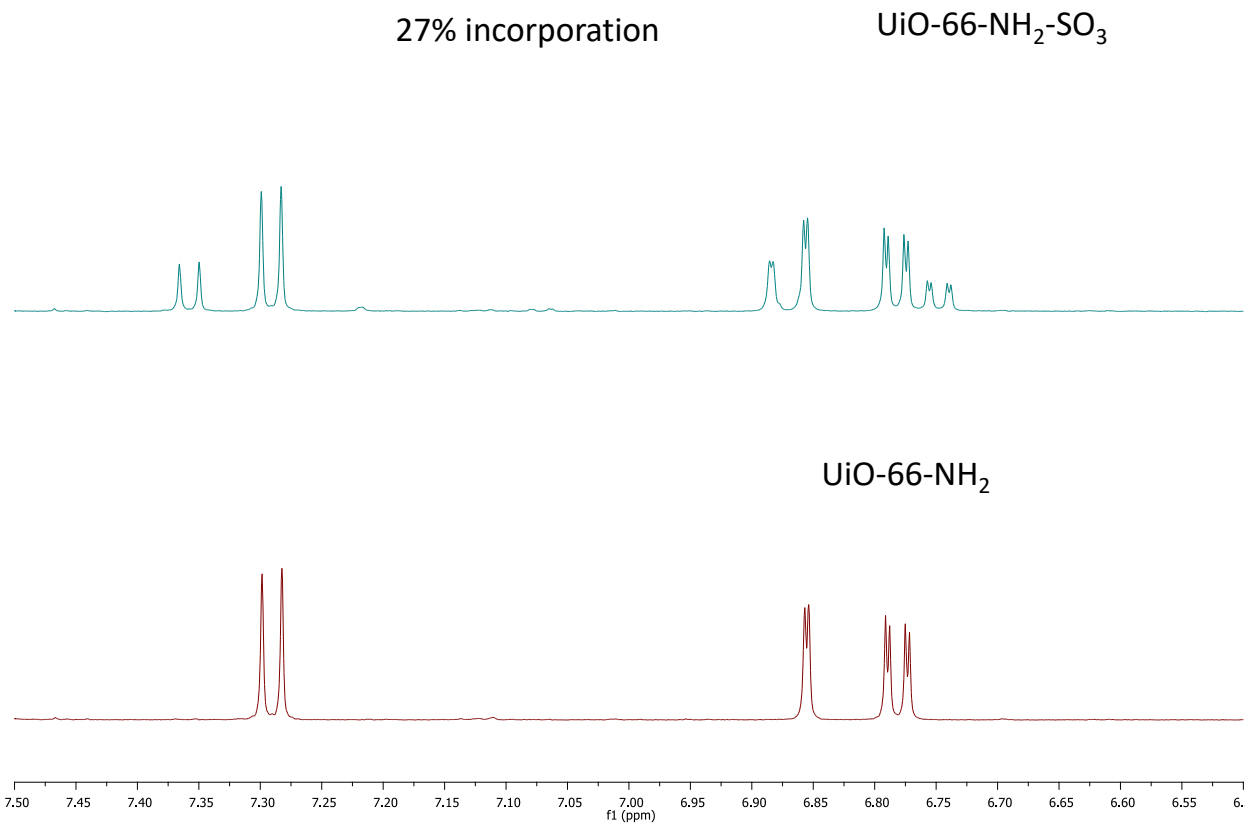

Figure 4.7 ^1H NMR of chemically digested UiO-66-NH_2 and UiO-66-NH_2-SO_3 highlighting the diagnostic signals in the amino and sulfonate functionalized linker

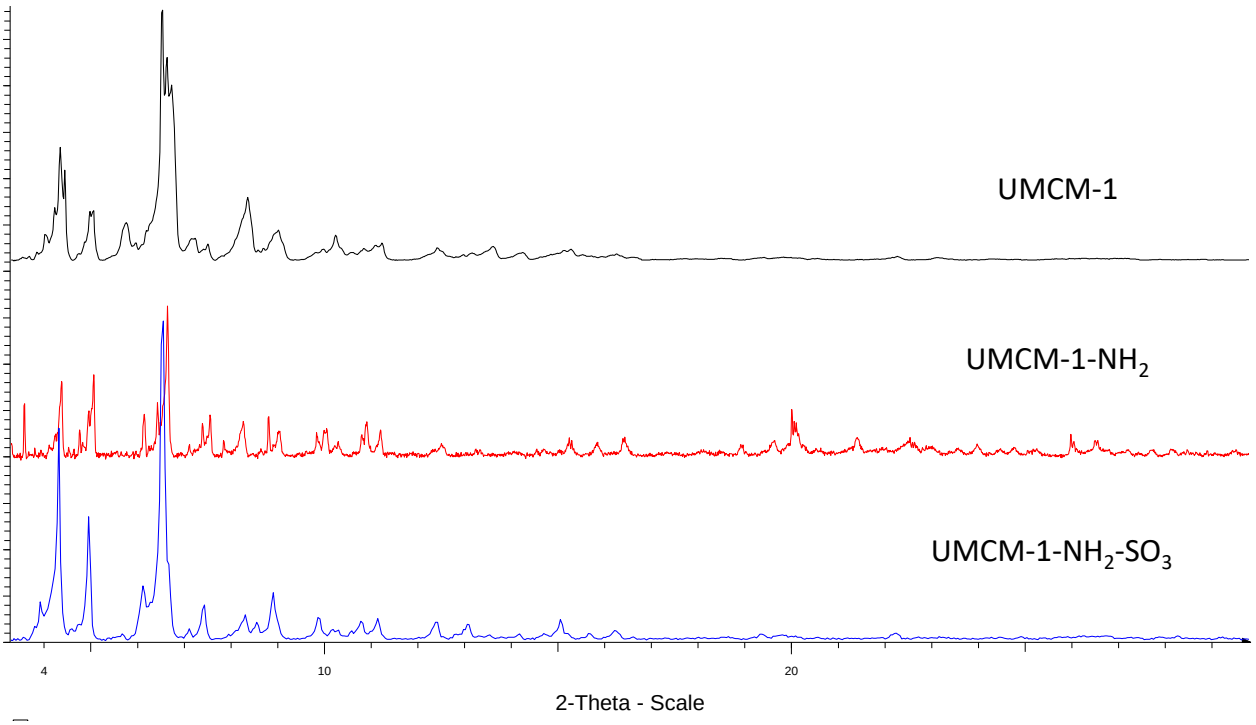

Figure 4.8 PXRD of UMCM-1, UMCM-1-NH_2 and sulfonate functionalized UMCM-1 (UMCM-1-NH_2-SO_3)

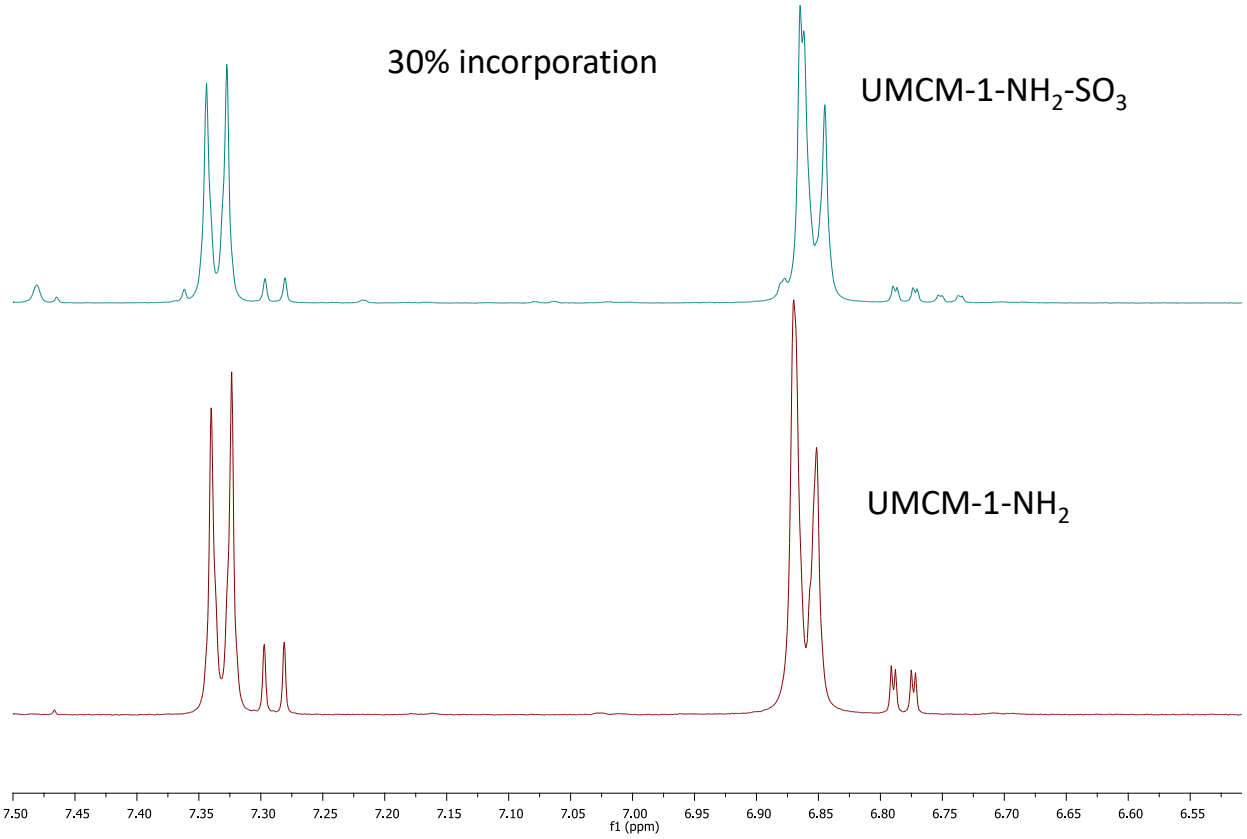

Figure 4.9 ^{1}H NMR of chemically digested UMCM-1-NH_2 and UMCM-1- NH_2-SO_3 highlighting the diagnostic signals in the amino and sulfonate functionalized linker

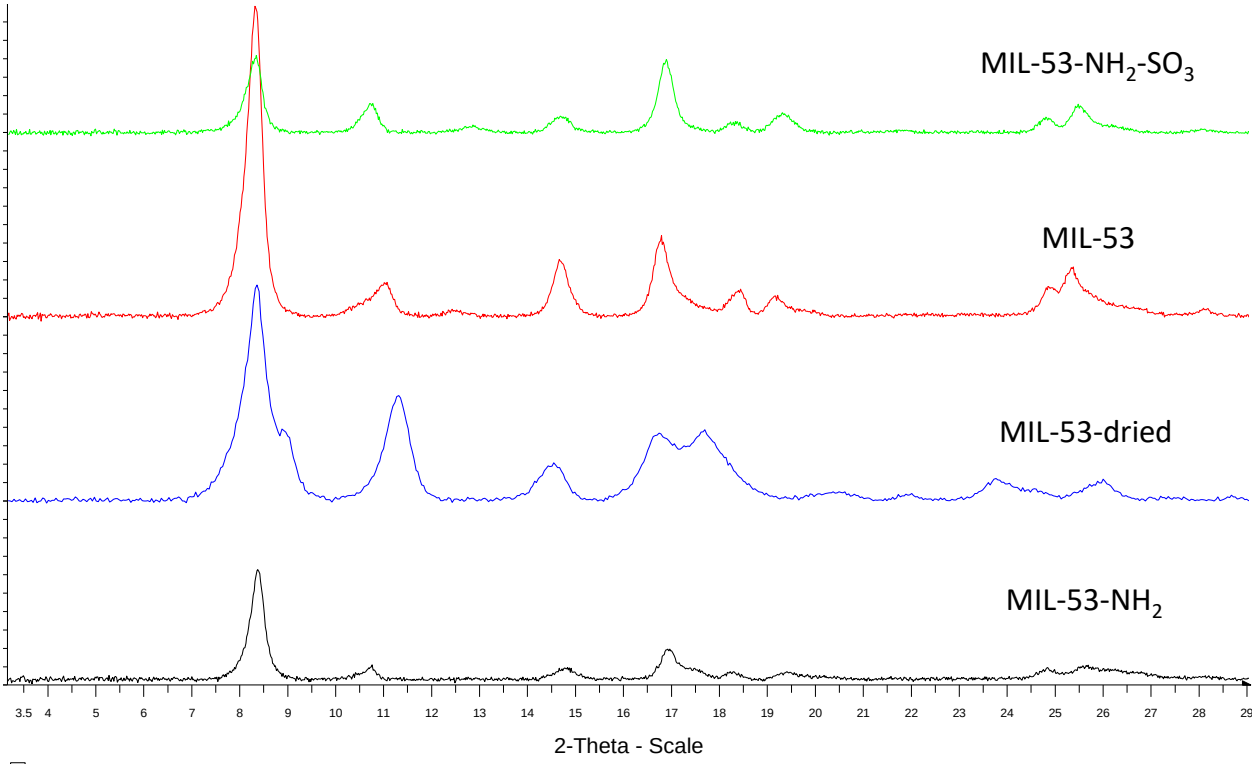

Figure 4.10 PXRD of MIL-53, MIL-53 that has been evacuated under vacuum (MIL-53-dried), MIL-53-NH_2 and sulfonate functionalized MIL-53 (MIL-53-NH_2-SO_3)

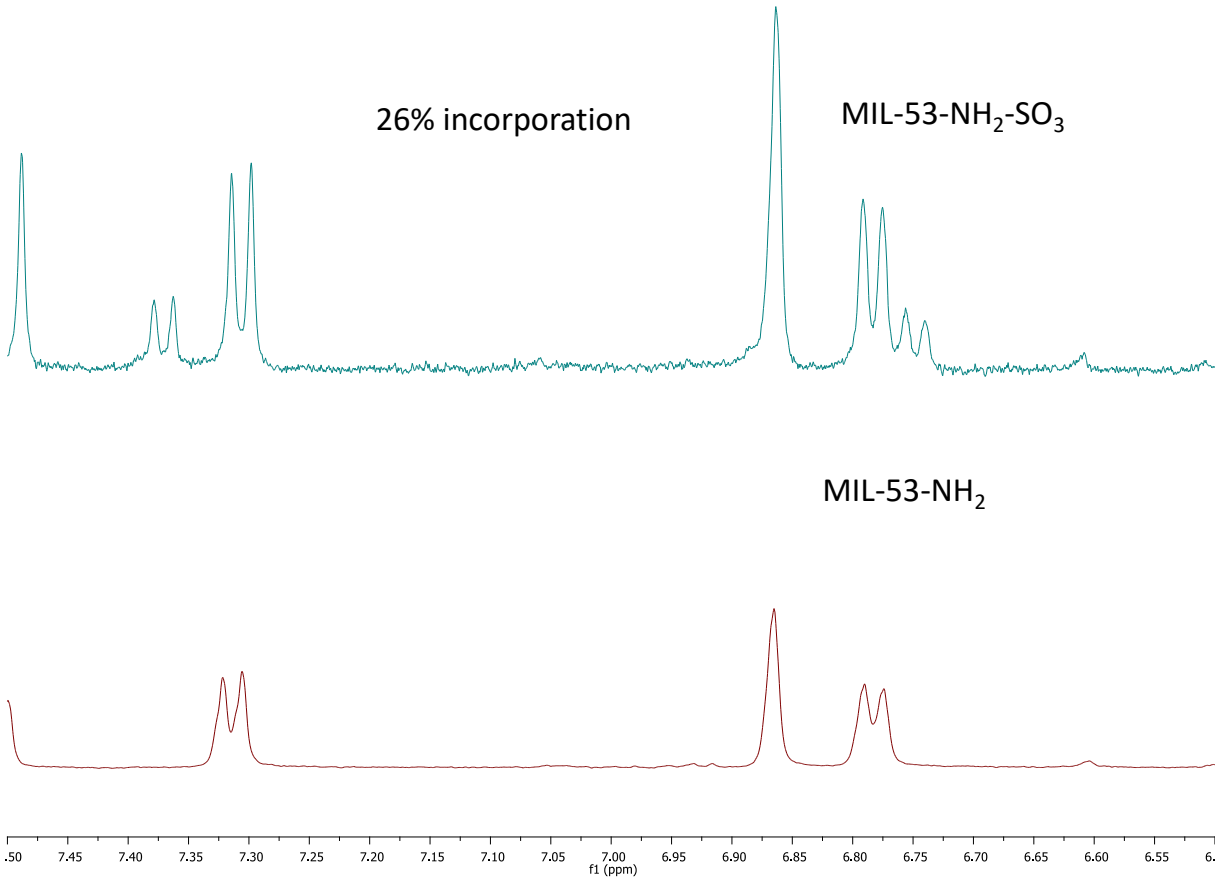

Figure 4.11 ^{1}H NMR of chemically digestedMIL-53-NH_2 and MIL-53-NH_2-SO_3 highlighting the diagnostic signals in the amino and sulfonate functionalized linker

4.4.2 Analysis of MOFs

Powder X-ray Diffraction (PXRD) data were recorded at room temperature on a Bruker AXS D8 Advance powder diffractometer at 40 kV, 40 mA with a CuKα source (λ = 1.5406 Å) between 3 and 30° 2θ with a scan speed of 0.1 s/ step and a step size of 0.04. Samples were measured on a glass microscope slide in an aluminium holder. ICP-OES data was collected on a Perkin-Elmer Nexion 2000. 1-2 mg of MOF was dissolved in 1 ml concentrated ammonium hydroxide then diluted to 10 ml with DI water. Nitrogen sorption data was collected on a Quantachrome Nova 4200e N2 sorption experiments were carried out at 77K. The isotherm was obtained and analysed using the NOVAwin software.All ^{1}H NMR were collected on a Varian Inova 500 (11.7 Tesla, 1H 500 MHz) spectrometer at ambient temperature. 1-2 mg of MOF were chemically digested in NaOD/D_2O prior to analysis. Spectra were processed using Mestrelab MestraNova NMR software.

4.4.3 Catalyst loading of MOFs

A typical MOF loading involved suspending 10 mg MOF in 0.3 ml DMF. 0.0074 mmol catalyst was dissolved in 0.2 ml DMF. The catalyst solution was added to the suspended MOF and the suspension placed on a shaker for 3 days. The solids were collected by centrifugation and washed 3 × 2 ml with DMF, changing solvent daily for 3 days.

4.5 References

1. S. Seth and A. J. Matzger, *Crystal Growth & Design* **2017**, *17*, 4043–4048.
2. D. Britt, C. Lee, F. J. Uribe-Romo, H. Furukawa and O. M. Yaghi, *Inorganic chemistry* **2010**, *49*, 6387-6389.
3. O. K. Farha, I. Eryazici, N. C. Jeong, B. G. Hauser, C. E. Wilmer, A. A. Sarjeant, R. Q. Snurr, S. T. Nguyen, A. Ö. Yazaydın and J. T. Hupp, *Journal of the American Chemical Society* **2012**, *134*, 15016-15021.

4. W. Zhao, L. Luo, H. Wang and M. Fan, *2017* **2017**, *12*, 1246–1262.
5. Y. Kang and F. Wang, *CrystEngComm* **2014**, *16*, 4088.
6. G. Barin, V. Krungleviciute, O. Gutov, J. T. Hupp, T. Yildirim and O. K. Farha, *Inorganic chemistry* **2014**, *53*, 6914-6919.
7. Z. Y. Gu and X. P. Yan, *Angewandte Chemie* **2010**, *49*, 1477-1480.
8. H. Bamdad, K. Hawboldt and S. MacQuarrie, *Renewable and Sustainable Energy Reviews* **2018**, *81*, 1705–1720.
9. P. Falcaro, R. Ricco, C. M. Doherty, K. Liang, A. J. Hill and M. J. Styles, *Chemical Society reviews* **2014**, *43*, 5513–5560.
10. J. Liang, Z. Liang, R. Zou and Y. Zhao, *Advanced Materials* **2017**, *29*, 1701139.
11. O. K. Farha and J. T. Hupp, *Accounts of Chemical Research* **2010**, *43*, 1166–1175.
12. S. Surble, C. Serre, C. Mellot-Draznieks, F. Millange and G. Ferey, *Chemical communications* **2006**, 284-286.
13. G. Ferey, C. Mellot-Draznieks, C. Serre, F. Millange, J. Dutour, S. Surble and I. Margiolaki, *Science* **2005**, *309*, 2040–2042.
14. G. Ferey, C. Serre, C. Mellot-Draznieks, F. Millange, S. Surble, J. Dutour and I. Margiolaki, *Angewandte Chemie* **2004**, *43*, 6296-6301.
15. S. M. Cohen, *Journal of the American Chemical Society* **2017**, *139*, 2855–2863.
16. M. Kim, J. F. Cahill, H. Fei, K. A. Prather and S. M. Cohen, *Journal of the American Chemical Society* **2012**, *134*, 18082-18088.
17. M. Kim, J. F. Cahill, Y. Su, K. A. Prather and S. M. Cohen, *Chemical Science* **2012**, *3*, 126.
18. S. M. Cohen, *Chemical reviews* **2012**, *112*, 970-1000.
19. Z. Wang, K. K. Tanabe and S. M. Cohen, *Inorganic chemistry* **2009**, *48*, 296–306.
20. Y. Luan, N. Zheng, Y. Qi, J. Yu and G. Wang, *European Journal of Inorganic Chemistry* **2014**, n/a-n/a.
21. M. Huang, G. Chang, Y. Su, H. Xing, Z. Zhang, Y. Yang, Q. Ren, Z. Bao and B. Chen, *Chemical communications* **2015**, *51*, 12205-12207.
22. M. Sun, J. Feng, W. Chen, L. Li, H. Duan and C. Luo, *Journal of Separation Science* **2014**, *37*, 1283-1288.
23. M. Zhang and Z. E. Rassi, *ELECTROPHORESIS* **1998**, *19*, 2068-2072.
24. X. Chen, H. Lü, Q. Lin, X. Zhang, D. Chen and Y. Zheng, *Journal of Membrane Science* **2018**, *549*, 12-22.
25. T. Chen, Q. Chen, G. Liu and G. Chen, *Journal of Applied Polymer Science* **2018**, *135*, 45943-n/a.
26. W. Lu, D. Yuan, J. Sculley, D. Zhao, R. Krishna and H.-C. Zhou, *Journal of the American Chemical Society* **2011**, *133*, 18126-18129.
27. Y.-R. Lee, Y.-M. Chung and W.-S. Ahn, *RSC Advances* **2014**, *4*, 23064-23067.
28. J. Ji, G. Zhang, H. Chen, S. Wang, G. Zhang, F. Zhang and X. Fan, *Chemical Science* **2011**, *2*, 484-487.
29. M. M. Islam, S. Bhunia, R. A. Molla, A. Bhaumik and S. M. Islam, *ChemistrySelect* **2016**, *1*, 6079-6085.
30. L. Zhou, Z. Liu, M. Shi, S. Du, Y. Su, X. Yang and J. Xu, *Carbohydrate Polymers* **2013**, *98*, 146-151.
31. F. G. Cirujano, *Catalysis Science & Technology* **2017**, *7*, 5482-5494.

32. H. Liu, F.-G. Xi, W. Sun, N.-N. Yang and E.-Q. Gao, *Inorganic chemistry* **2016**, *55*, 5753-5755.
33. S. Bernt, V. Guillerm, C. Serre and N. Stock, *Chemical communications* **2011**, *47*, 2838-2840.
34. L. A. Buldt and O. S. Wenger, *Chemical Science* **2017**, *8*, 7359-7367.
35. J. Liu, L. Chen, H. Cui, J. Zhang, L. Zhang and C. Y. Su, *Chemical Society reviews* **2014**, *43*, 6011–6061.
36. D. T. Genna, L. Y. Pfund, D. C. Samblanet, A. G. Wong-Foy, A. J. Matzger and M. S. Sanford, *ACS Catalysis* **2016**, *6*, 3569–3574.
37. D. T. Genna, A. G. Wong-Foy, A. J. Matzger and M. S. Sanford, *Journal of the American Chemical Society* **2013**, *135*, 10586–10589.
38. M. Eddaoudi, J. Kim, N. Rosi, D. Vodak, J. Wachter, M. O'Keeffe and O. M. Yaghi, *Science* **2002**, *295*, 469-472.
39. M. J. Katz, Z. J. Brown, Y. J. Colon, P. W. Siu, K. A. Scheidt, R. Q. Snurr, J. T. Hupp and O. K. Farha, *Chemical communications* **2013**, *49*, 9449–9451.
40. J. Gascon, U. Aktay, M. Hernandezalonso, G. Vanklink and F. Kapteijn, *Journal of Catalysis* **2009**, *261*, 75-87.
41. Pore window listed is for unfunctionalized MIL-101(Cr). The actual pore window is expected to be smaller after amine and sulfonate functionalization